ABSTRACT

Title of Dissertation / Thesis: Synthesis of Layered Group IV Nitride Materials by Soft Chemical Anion Metathesis

Chad Alan Stoltz, Doctor of Philosophy, 2005

Dissertation / Thesis Directed By: Professor Bryan W. Eichhorn
Department of Chemistry and Biochemistry

Traditionally, solid state chemistry has been dominated by high temperature methods that only lead to thermodynamically stable products. More recently, soft chemical methods have emerged as a means to new kinetically stable materials that cannot be attained by traditional methods. Ion exchange, or metathesis, has become a powerful soft chemical synthetic tool, especially in oxide chemistry. Although cation exchange has become extremely common in many solid state materials, anion exchange is much more uncommon due to effects such as size and polarizability. This work developes rare anion metathesis as a synthetic tool in the MNX (M = Zr, Hf; X = Cl, Br, I) system, making new materials that cannot be prepared by traditional methods. Topochemical reactions between β-ZrNCl and A_2S (A = Na, K, Rb) in the solid state provide α-Zr_2N_2S (*P*-3*m*1, 800°C), which neatly transforms to β-Zr_2N_2S ($P6_3/mmc$) at elevated (> 850°C) temperatures. At low temperatures (300 - 400 °C), this reaction yields ACl intercalated phases of the formula $A_xZr_2N_2SCl_x$ ($0 < x < \sim 0.15$) that are reversibly hygroscopic. Reactions of ZrNCl with excess A_2S at 400 - 1000 °C gives A_2S

intercalated phases of the formula $A_{2x}Zr_2N_2S_{1+x}$ (*R*-3*m*) where $0< x \leq 0.5$. Recrystallized β-ZrNCl reacts with excess NaF in the solid state via anion exchange to give A_xZrNF_{1+x} (A = Na, K; $x \approx 0.3$), the first fluoride structural analogue ($P6_3/mmc$ crystal symmetry) of the MNX system (M = Zr, Hf; X = Cl, Br, I). Organic/inorganic hybrid materials have also been obtained by chloride for alkoxide exchange. Excess AOR (A = Na, K; OR = OMe, OEt, O*n*-Bu) reacts with ZrNCl solvothermally in THF (200-250^{o}C) yielding a series of ZrN(OR) compounds, which retain the trigonal, lamellar nature of the ZrNCl parent. Full structural and analytical characterization is described for all phases as well as implications of the results.

Synthesis of Layered Group IV Nitride Materials by Soft Chemical Anion Metathesis

By

Chad Alan Stoltz

Dissertation submitted to the Faculty of the Graduate School of the
University of Maryland, College Park, in partial fulfillment
of the requirements for the degree of
Doctor of Philosophy
2005

Advisory Committee:
Professor Bryan W. Eichhorn, Chair
Associate Professor Gregory Jackson
Professor Lawrence Sita
Assistant Professor Andrei Vedernikov
Associate Professor Robert Walker

Dedication

To my wonderful, supportive, loving wife, Jaime, for always standing by me. Throughout our years together, you're always there to help me remember who I really am.

Acknowledgements

I would first and foremost like to thank Professor Bryan Eichhorn for his guidance and also for allowing me the privilege of working with him during my graduate career. I have learned an immeasurable amount from Dr. Eichhorn regarding science and what it really means to be a scientist. (Thanks also for broadening my horizons regarding beer and strong coffee!)

I am extremely grateful to Tim Maugel for extensive help with SEM, TEM, EDAX measurements and many other electron diffraction related questions as well as Phil Piccoli for countless hours of WDS microanalysis, without which the compositional analysis throughout this work would not have been possible. I would also like to thank Dr. Lourdes Salamanca-Riba and Kevin McIlwrath for additional TEM imaging.

I would also like to express gratitude to Dr. Brian Toby of the NIST Center for Neutron Research for extensive help with neutron diffraction measurements/refinements and for providing me with a deeper understanding of diffraction in general. I am also grateful to Dr. Jim Fettinger for help maintaining the powder XRD facilities. Thanks also to Mike Trembly for many emergency glass repairs and good hunting stories.

To all of my lab mates (past and present) and friends, I express my deepest gratitude. To those I've worked with, Dr. Serpil Gonen, Dr. Banu Kesanli, Dr. Scott Sirchio, Dr. Melanie Moses, Emren Nalbant-Esenturk, Oktay Demircan, Selim Alayoglu, Shenghu Zou, Dr. Mary Sukeshini, Captain D'Anne Spence, Dan

Paluchowski, and Jordan Halsig, thanks for memorable years and good times during grad school and for letting me work on your cars!

Thank you to my family and friends for always supporting me. Mom and Dad, Gail and Icha (my other mom and dad), Gayle and Trevor, Kevin and Amy, Gram, and everyone else not mentioned here, you'll never know how much your support means to me.

Last, but certainly not least, to my wonderful wife to whom this thesis is dedicated, words cannot begin to describe what it means to have you in my life. Without you beside me through these past years, I probably would not be writing this. I love you more than anything and now you can finally start thinking about retirement!

Table of Contents

List of Tables

List of Figures

List of Abbreviations

cm	centimeter
mm	millimeter
nm	nanometer
Å	Angstrom
mg	milligram
mmol	millimole
h	hour
min	minute
^{o}C	degrees Celsius
K	Kelvin
eV	Electron volt
XRD	X-ray powder diffraction
ED	Electron diffraction
EDS/EDX	Energy dispersive X-ray spectroscopy
WDS	Wavelength dispersive X-ray spectroscopy
SEM	Scanning Electron Microscopy
TEM	Transmission/Tunneling Electron Microscopy
TGA	Thermo-Gravimetric Analysis
IR	Infrared
sym.	Symmetric
asym.	Asymmetric

R_p	Crystallographic agreement factor
R_{wp}	Weighted crystallographic agreement factor
R_{bragg}	Bragg crystallographic agreement factor
Chi^2	Crystallographic agreement factor
ESD	Estimated Standard Deviation
d	crystallographic inter-plane spacing
eq	equation
JC-PDF	Powder Diffraction File

Chapter 1:
Introduction

1.1. The Solid State Tradition

The term "solid state", when concerning materials synthesis, often invokes ideas of high temperatures and pressures, among other various harsh experimental conditions. However, these methods often fall short when some type of control is desired, such as synthetic control of structure, properties, etc. Traditional ceramic methods have even been cleverly and justifiably referred to as the "shake and bake" approach.[1] When using typical ceramic methods, reactants are simply ground together and heated to extreme temperatures. The work of the solid state chemist is then to determine what reaction (if any) took place, what the products are, what the interesting properties (if any) are, etc. It is well known that the majority of useful and interesting materials are discovered through serendipity.[2] These useful and interesting materials and general understanding of materials obtained by ordinary solid state methods is very extensive, however, this circumstance of having little control is obviously undesirable. Ideally, new materials could be synthesized with particular structures and properties in mind,[3] but is this realistic? Ceramic solid state methods lead to thermodynamic products, or the only stable product or phase of that product under the given reaction conditions. Therefore, if a different product or product phase with different properties is desired, new methods must be used. Many of these new methods are classified as "chimie douce" or soft chemical synthesis.

Soft chemical synthesis allows the formation of alternative, metastable products that are not achievable using typical ceramic methods, such as zeolites, gold nanowhiskers, intercalation compounds, pillared, layered materials, battery electrode materials and microporous oxide solids.[4-6]

Although soft chemical methods have been applied extensively throughout oxide chemistry,[7,8] another very important field within inorganic/materials chemistry is the synthesis, chemistry and properties of transition metal nitride compounds and their derivatives. In particular, group IV transition metal nitrides are important for many reasons, including industrial uses as microelectrical devices, lithium battery electrode materials, magnetic device materials and wear resistant coatings.[9-13] The majority of these materials have traditionally been made using ceramic, high temperature methods.[14,15] These traditional methods have led to many useful nitride materials, however there is much work to be accomplished in this field. As will be discussed later in this introduction, the majority of the nitride materials made with soft chemical methods are binary nitrides.[16,17] In order for new materials discovery and design to take place in nitride chemistry, it is important to explore these soft chemical synthetic methods in this field.

Within the "toolbox" of soft chemical synthetic methods, cation metathesis has become common in solid state oxide materials, while the exchange of anions is very rare in refractory, inorganic materials. The remainder of this introduction will describe a variety of soft chemical methods in detail, including materials prepared with these methods. Nitride materials prepared by soft chemistry will also be discussed, followed by a description of the MNX (M = Zr, Hf; X = Cl, Br, I)

family.[18,19] This family of compounds provides a very interesting material for which a relatively ignored soft chemical method, anion metathesis, can be developed.

1.2. Soft Chemistry (Chimie Douce)

Soft chemistry is defined by the synthetic methods that it encompasses. As previously mentioned, many of the products generated using soft chemistry are kinetically stable (or metastable) phases. Therefore it is important to understand why and how these interesting metastable phases can exist. A more detailed and comprehensive explanation of the following was provided by J. Gopalakrishnan.[4] Metastable phases have a higher free energy than the corresponding stable phase with the same chemical composition,[20] therefore their formation compared to the thermodynamically more stable state is brought into question. The causes of metastability may differ from one case to the next. For example, doped semiconductors and metallic glasses are compositionally metastable; meaning the entropy provided by defects and static intrastructural disorder gives rise to the lower free energy. In certain examples such as some superconducting oxides, metastability may be caused by electronic instabilities (superconducting structure) as well as compositional disorder.[21] Certain microporous solids such as zeolites have structural variations[22] due to the many ways in which the AlO_4, SiO_4 and PO_4 tetrahedra can be assembled; these are known as topologically metastable materials. A final example of variation in metastability is found in oxide material fine particles. The excess free energy associated with fine particle morphology[4] gives rise to metastability in these particles. These examples help illustrate what allows metastable materials to exist,

but concerning synthesis, how and why do these compounds and phases actually form rather than proceeding directly to the thermodynamically most stable phase? Wilhelm Ostwald observed that when possible pathways exist towards both metastable and the most thermodynamically stable phases, systems will generally choose the metastable phase.[20] During synthesis of a solid, several thermodynamically possible pathways are available for structure formation, including the thermodynamically most stable phase as well as metastable phase(s). The structure formation of the kinetically favored (metastable) phase has the smallest correlations of atomic motion and position. Initially, far from equilibrium, nucleation of the kinetically favored phase can possibly be lower in energy and therefore be more favorable than the most thermodynamically stable phase. Hence, Ostwald's rule: the first phase to form is often not the most stable that is thermodynamically accessible.

Why should soft chemical methods be considered as useful pathways to the desired products? In some cases soft chemical methods are the only pathways to the desired products. Many materials that traditionally have been made using ceramic methods have alternate phases that exhibit interesting and unusual properties. Often, these phases are metastable and can only be synthesized using soft methods. Perovskite structured compounds provide good examples[23] because of interesting aspects such as dielectric properties and applications as catalysts. For instance, a metastable, photoconductive layered perovskite, $Nd_2Ti_3O_9$, has been prepared by acid exchange from $K_2Nd_2Ti_3O_{10}$.[24] $Nd_2Ti_3O_9$ (NTO) can so far only be made using soft chemical synthesis, in this case acid exchange, whereas its precursor $K_2Nd_2Ti_3O_{10}$ is

prepared using conventional solid state methods. Also notable is that NTO, the metastable phase, exhibits an interesting photoconductive property that its ceramic made precursor does not.

The majority of soft chemical synthetic routes can be classified as either topochemical or nontopochemical. By definition, a reaction is said to be topochemically controlled when the reactivity of a solid is controlled by the crystal structure, rather than by the chemical constituents of the crystal.[25] Topochemical synthetic methods allow the essential features of the parent structure to be conserved and often yield metastable phases which are not achievable using conventional ceramic methods. Among the noteworthy examples of topochemical methods are: ion exchange/metathesis, reductive intercalation and oxidative deintercalation, layer/chain exfoliation and pillaring.[4,25]

Due to its extreme importance and large range of use, a substantial amount of explanation and examples will be given to ion exchange. Ion exchange, or metathesis, is an extremely widespread phenomenon used frequently throughout solid state chemistry.[26] Metathesis, requiring two precursors, can be accomplished in the liquid, gas or solid state.[27] Metathesis reactions can be a very powerful synthetic route. Some metathesis reactions can self-initiate at room temperature, internally produce enough heat to be self sustaining, and yield pure crystalline products in a matter of seconds. The facile control of crystallinity and ability to prepare both cationic and anionic solid solutions are two significant features of metathesis not typically found in other precursor synthetic methods. Typical metathesis reactions are carried out with metal halide and alkali metal main group starting materials,

which are usually ground separately and then combined. The products will then contain the desired material, containing the metal-main group compound, and an alkali metal-halide salt possibly with other by-products which can then easily be washed away from the desired product. Often, the very favorable formation of the alkali metal-halide is the driving force for the reaction. In some cases, the reactions are self-initiating, in others they are initiated with a hot filament or low temperature heating in an evacuated sealed vessel. The methods used are particular for each reaction and depend on reaction parameters such as activation energy and facility. A typical ion exchange reaction is given by the reactions of transition metal chlorides with lithium sulfide in nonaqueous solvents to give metal disulfides and lithium chloride[27] according to eq. 1.1:

$$MCl_4 + 2Li_2S \rightarrow MS_2 + 4LiCl \qquad (M = Ti, Zr, Hf, \text{and } V) \qquad \text{eq. 1.1.}$$

A simple example of a gas phase metathesis is given by (eq. 1.2.) the synthesis of silicon nitride using ammonia and silicon tetrachloride:

$$3SiCl_4 + NH_3 \rightarrow Si_3N_4 + 12HCl \qquad \text{eq. 1.2.}$$

A discussion of solid state metathesis would be incomplete without mentioning the work of R.B. Kaner. For years, he has been a leading researcher in the realm of metathesis reactions.[27-29] Before Kaner, relatively few examples of solid-state metathesis reactions were known, which included the synthesis of metal ferrites at moderate (eq. 1.3., 400^{o}C to 500^{o}C) temperatures:[30]

$$MCl_2 + Li_2Fe_2O_4 \rightarrow MFe_2O_4 + 2LiCl \qquad \text{eq. 1.3.}$$

And the synthesis of chromites using similar methods.[31]

One of Kaner's earlier reported metathesis syntheses was that of molybdenum disulfide (eq. 1.4.) by the following reaction:[27]

$$MoCl_5 + 5/2Na_2S \rightarrow MoS_2 + 5NaCl + 1/2S \qquad \text{eq. 1.4.}$$

Many other precursors are possible, however $MoCl_5$ and Na_2S are reported to have been the most effective. This reaction self initiates on light mixing at room temperature and was carried out in a helium filled drybox. The reaction time, from initiating to the peak of the reaction, was less than 0.5 seconds after an induction period of approximately 30 seconds. This reaction is highly exothermic and produces a white flash of light along with a small mushroom cloud. The pure, crystalline MoS_2 can be obtained by washing away unreacted $MoCl_5$ with methanol, and washing NaCl and unreacted Na_2S out with water. Any excess sulfur that forms can be washed away, if it has not already boiled off during the reaction, with chloroform or carbon disulfide. The percent yield was 80% of theoretical and the X-ray powder diffraction pattern (showing the high degree of crystallinity) is comparable to that of MoS_2 made using ceramic synthesis of MoS_2 from its elements at 900^{o}C for 5 days, showing the practicality of this method. As mentioned previously, the formation of the metal-halide salt is very favorable in this type of reaction. The formation of the desired phase in a reaction such as this can be controlled by designing metathesis reactions to give favorable by-products. A useful advantage is that the extreme heat generated by these reactions can cause the reaction to become self-propagating, requiring little (if any) energy to initiate. The alkali salts produced can also melt due to the extreme heat given off by the reaction. The molten salt can then form a solution in which the reactants can diffuse, helping to propagate the reaction even further. Yet another

advantage is that in some cases it is possible to control the particle size of the desired phase by including an inert additive such as NaCl in the case of the MoS_2 synthesis.[27]

Kaner's use of solid state metathesis is very broad, to say the least. For example, mixed-transition metal dichalcogenides have been synthesized [32] such as molybdenum-tungsten disulfide solid solutions, (Mo, W)S_2 from rapid, self-propagating reactions with ($MoCl_5$-WCl_6) and Na_2S. Again, note the formation of the metal-halide salt, NaCl, as a product. These early transition metal dichalcogenides have been studied because of their interesting intercalation chemistry,[33] as well as applications such as solid lubricants,[34] cathode materials,[35] hydrodesulfurization catalysts,[36] and photoelectrochemical cells.[37]

A thorough overview of using rapid metathesis reactions to produce refractory ceramics from solid-state precursors was provided[38] by Kaner, as well as the metathecal synthesis of Pnictide (N, P, As, Sb)[14,39] and other "III-V" compounds[39-41] which will be discussed later in more detail.

$LiAlO_2$ provides an important classical example of ion exchange pertaining to structure influence on reactivity.[4,42] When $LiAlO_2$ crystallizes, it can have three different forms: α, β, and γ. The β and γ forms of $LiAlO_2$ have Li occurring in tetrahedral oxygen coordination and do not undergo any ion exchanges. However, α-$LiAlO_2$, which has Li and Al coordinated in an octahedral fashion and a rock salt superstructure, can undergo facile exchange in benzoic acid of Li^+ with H^+ forming spinel-like $HAlO_2$. Another important instance of metastable oxide synthesis using soft chemical methods is the hydrolytic proton exchange of $K_2Ti_4O_9$.[4,43,44] When $K_2Ti_4O_9$ is hydrolyzed, the two main products are: partially hydrolyzed

$K(H_2O)Ti_4O_8(OH)$ and fully hydrolyzed $(H_2O)_2Ti_4O_7(OH)_2$. When both are dehydrated, $K(H_2O)Ti_4O_8(OH)$ yields a novel octatitanate, $K_2Ti_8O_{17}$, and $(H_2O)_2Ti_4O_7(OH)_2$ yields a metastable modified version of TiO_2. This is important because the formation of the octatitanate shows that protonation of $K_2Ti_4O_9$ is selective and occurs first at the most basic corner oxygens. The $LiAlO_2$ and $K_2Ti_4O_9$ systems have been further studied with regards to semiempirical electronic structure calculations.[45,46]

A more recent example of soft chemical metathesis involving oxides is the transformation of the Ruddleson-Popper oxide, $K_2La_2Ti_3O_{10}$ into layered perovskite oxides. [47] Ruddleson-Popper (R-P) phases, given by $A_2[A'_{n-1}B_nO_{3n+1}]$, are one of the several lamellar materials derived from the perovskite structure, widely studied because of properties such as those previously given for perovskites themselves.[23,24] The Ruddleson-Popper oxide undergoes the following (eq. 1.5.-1.7.) metathesis reactions:[47]

$$K_2La_2Ti_3O_{10} + 2BiOCl \rightarrow (Bi_2O_2)La_2Ti_3O_{10} + 2KCl \qquad \text{eq. 1.5.}$$

$$K_2La_2Ti_3O_{10} + MCl_2 \rightarrow MLa_2Ti_3O_{10} + 2KCl \ (M = Ba, Pb, Sr) \qquad \text{eq. 1.6.}$$

$$K_2La_2Ti_3O_{10} + VOSO_4{\cdot}3H_2O \rightarrow (VO)La_2Ti_3O_{10} + K_2SO_4 + 3H_2O \qquad \text{eq. 1.7.}$$

Although ionic exchange metathesis reactions are well known in solid state chemistry,[27] these reactions are unique in that they show interlayer cation replacement in R-P phases of alkali cations, in this case K^+, by structural entities: $(Bi_2O_2)^+$ and $(VO)^{2+}$ and $(PbBiO_2)^+$ (reaction not shown here). The formation of $(VO)La_2Ti_3O_{10}$ is particularly interesting because it occurs in such mild conditions, ~100 ^oC, in aqueous

medium. A similar synthesis has been done of $(CuX)LaNb_2O_7$ by Kodenkandath et al.[48]

Another topical soft chemical method is intercalation, including reductive intercalation and oxidative deintercalation.[4] Intercalation refers to a solid state reaction involving reversible insertion of guest species G into a host structure, [Hs], which provides a system of interconnected and accessible unoccupied sites; represented by eq. 1.8.:

$$xG + [Hs] \leftrightarrow G_x[Hs] \qquad \text{eq. 1.8.}$$

The host matrix retains its relative structure throughout intercalation/deintercalation, therefore making this process topotactic (topochemical).[25] Although the first reported intercalation reaction was as early as 1841, the intercalation of graphite by sulfate, reported by Schauffautl, only within approximately the last 40 years has intercalation chemistry received its due attention. A wide variety of inorganic solid hosts can be intercalated such as transition metal oxides, chalcogenides, halides, oxyhalides, layered silicates, zeolites, fullerenes and metal alloys, to name a few. Guest species can range from hydrogen to alkali metals and halogens to neutral molecules (NH_3, H_2O, amines, etc.) to complex organometallics such as chromocene and cobaltocene.[25,26]

A well known instance is the insertion of lithium into layered TiS_2 to give Li_xTiS_2 where $0 \leq x \leq 1.0$.[4] This intercalation can be accomplished chemically or electrochemically and is used for the development of cathode materials for solid state batteries. Chemically, n-butyllithium dissolved in a hydrocarbon acts as the lithiating agent. Electrochemically, A polycrystalline pellet of TiS_2 serves as the cathode, a

sheet of Li metal or LiAl alloy serves as the anode, and a solution of $LiClO_4$ in a polar organic solvent is the electrolyte. Research of this type[49] has led to the use of aqueous $LiNO_3$ as an electrolyte for the first time, making lithium batteries cost effective as well as safe.[4]

A recent example of oxidative deintercalation is the synthesis of a new nonlinear optical material, $Ba_{1.5}VOSi_2O_7$ by K. Ramesha and J. Gopalakrishnan[50] The parent fresnoite compound, $Ba_2VOSi_2O_7$, was oxidized using either Br_2 in CH_3CN or $CHCl_3$ according to eq. 1.9:

$$Ba_2VOSi_2O_7 + 1/2Br_2 \rightarrow Ba_{1.5}VOSi_2O_7 + 1/2BaBr_2 \qquad \text{eq. 1.9.}$$

The term "oxidative" is used for this type of deintercalation because the vanadium must be oxidized to maintain charge balance when the barium is lost. Magnetic susceptibility was used to show that in going from $Ba_2VOSi_2O_7$ to $Ba_{1.5}VOSi_2O_7$, the oxidation state of vanadium goes from IV to V and x-ray powder diffraction showed that the oxidized structure retained the structure of the parent. Also, this nonlinear optical material, $Ba_{1.5}VOSi_2O_7$ can only be synthesized via chimie douce oxidation; directly reacting $BaCO_3$, V_2O_5, and SiO_2 at elevated temperatures does not give this new material.

Reductive intercalation has been used in conjunction with a wide range of layered (and unlayered) materials to make new materials such as superconductors as well. For example, ß-zirconium nitride chloride, ZrNCl, was first intercalated with lithium and shown to superconduct in 1996.[51] Since this report, there have been many more studies on the intercalation and electronic structures of ZrNCl and its hafnium analogue, HfNCl,[19,52-54] which will be discussed later in more detail.

Many of the compounds that undergo intercalation are lamellar compounds; materials with strong bonds in two dimensions and weak bonds in the third.[55] In many cases lamellar compounds, such as those with layered structures, remain entirely or partially crystalline due to the attractive interactions between the host layers and guest intercalates. In some cases, the host undergoes an extreme version of intercalation, known as exfoliation.

Exfoliation occurs when the attraction between the layers is weakly attractive or even repulsive,[55] which then allows the layers, or sheets, to be separated by solvent molecules. Exfoliation of layered (or chain) materials to yield single layer (or chain) colloidal dispersions and their subsequent restacking in the presence of large guest molecules afford another new strategy to synthesize novel metastable materials.[56] In other words, once the compound layers, or sheets, are exfoliated, they can be restacked or used as precursors to make many other new materials. Exfoliation, even though it requires "pulling apart" of the layers, is still considered as a topochemical reaction because the layer structure itself remains (usually) unchanged.

The first exfoliated dispersions were obtained for certain clays and layered dichalcogenides such as TaS_2 and MoS_2,[57] however, a wide variety of exfoliated single and multiple layers have been made and used as precursors for applications such as polymer-sheet nanocomposites[58] and self-assembled aperiodic multilayers.[59]

A recent study of this sort was performed on the reactions of α-zirconium phosphate.[55] Atomic force microscopy (AFM) studies and transmission electron microscopy (TEM) studies were used to show that when α-ZrP is reacted with tetra(n-butylammonium) hydroxide (TBA^+OH^-), intercalation compounds are initially

formed. The intercalation is then followed by exfoliation into unilamellar colloids. The authors discuss a pillaring effect at the edges of the α-ZrP sheets which leads to the final topochemical soft chemical process that will be discussed, pillaring.

Pillaring is a type of intercalation in which a robust, thermally stable molecular species is intercalated (even exfoliated) into layered hosts to "prop open" the layers in order to convert the two dimensional interlayer space into a porous structure with molecular dimension.[4,25] Examples include pillaring of montmorillonite (a smectite),[60,61] MoO_3, and layered double hydroxides (LDH's) all by ion exchange with polycationic species.[25]

The next major category of soft chemical routes falls under nontopochemical methods. Nontopochemical methods are those in which the structure is not retained from parent to product. Among the notable nontopochemical methods are: sol-gel methods, hydrothermal methods, molten salt usage, and acid leaching.

Sol-gel methods are most likely the oldest of the soft chemical processes.[4,62] This method forms an oxide network directly from a solution by way of hydrolysis and condensation of molecular or ionic precursors.[4] Sol-gel methods are also widely used for the synthesis of a variety of new materials. Metal alkoxides are common molecular precursors for the sol-gel synthesis of many TiO_2, SiO_2, and Al_2O_3 based ceramics. Sol-gel methods have also grown into biological applications. For instance, biomaterials have been produced by encapsulating enzymes and other proteins, such as bacteriorhodopson,[63] in optically transparent, porous silicate glasses.[4]

The next nontopochemical route is the hydrothermal method. The hydrothermal method allows reactions to occur at a lower temperature by utilizing high pressure, usually 1 – 10kbar. Hydrothermal reactions can be carried out in either an open or closed system. In the open system, the solid is in direct contact with the reacting gases, usually fluorine, nitrogen, or oxygen. These reacting gases also help to intensify the pressure. In the closed system, rather than being in direct contact with reacting gases, an additive is used that will decompose or change phase to provide the necessary pressure.[4,25]

Among the many materials that hydrothermal methods are used to synthesize, one example is the calcium silicate hydrate family.[26] These are industrially important because they are components of cement and concrete. In this case, lime, CaO and quartz, SiO_2 and water are heated together at temperatures ranging from 150 – 500^{o}C with pressures of 0.1 to 2.0kbar.

A final, more recent example of the usefulness of hydrothermal methodology involves nonlinear optical (NLO) materials[50] as mentioned earlier. In a similar study,[64] two new NLO structures: batisite, $Na_2Ba(TiO)_2Si_4O_{12}$, and fresnoite, $Ba_2TiOSi_2O_7$ were reported. One of the required starting materials for these reactions is $Na_4Ti_2Si_8O_{22}$, which is prepared hydrothermally.[65]

Now with a general understanding of the varieties of topochemical and nontopochemical soft chemistry methods, a discussion involving target materials and the methods for synthesizing these materials is required.

1.3. Nitrides and Related Materials

Solid state materials such as group III – V compounds and other transition metal nitrides are of extreme importance and interest because of their interesting properties as well as already known industrial uses. For instance the III – V semi-conductors are well known and widely studied for their electronic and optoelectronic properties,[39,66] as well as their magnetic behavior.[67] There is also great interest in many different cubic phase nitride compounds due to: their hardness, 8 to 9 on Moh's scale; high melting points of 2000 to 4000^{o}C;[41,68] impressive chemical resistance to organic solvents and inorganic acids, and low-temperature superconductivity.[9] Another recent speculation[69] is that the future of full-colored, flat panel displays, blue lasers, and optical communication is likely to be based on gallium nitride, GaN. Titanium nitride, TiN, thin films have the above properties, making them ideal for tool coatings, conductive microelectronic coatings, glass solar coatings, barrier materials, and even decorative coatings.[70] Many nitride materials (Si_3N_4, TiN, and BN to name a few) are sought after, and even already in use, to replace steel and other metals as materials for automotive parts.[71] Organometallic complexes containing metal nitrides are also of recent interest because of their functionality.[72]

Ceramic methods have often been utilized in the past for the synthesis of nitrides and other useful pnictide compounds.[15] Many alternative synthetic methods have been invented in order to overcome the problems of high temperature, traditional ceramic synthesis of these compounds. For example, one approach to making III – V phosphide compounds is to start with a metal phosphorus precursor.[73]

(Al, Ga, or In)P was produced upon heating aluminum(gallium or indium) and Zn_3P_2 at 850oC for 5 hours. In this case, the zinc byproduct was removed by vapor transport in a temperature gradient. Another alternative method used a combination of excess metal halides and elemental pnictogens (N, P, As, etc.). The desired compounds could then be made usually in fewer than 12 hours at less than 600^{o}C, removing the excess metal halide via vapor transport.[74] Other alternate synthetic routes for preparing pnictide compounds include precipitating amorphous III – V materials from solution,[75] and decomposing single source precursors to give bulk powders.[39,76]

Hoffman, Fix and Gordon have done pioneering work on thin nitride films, especially relating to chemical vapor deposition.[9,77] Historically, group 4 metal nitride coatings have been made chemically as well as by physical vapor deposition techniques. Chemical vapor deposition (CVD) has been used to prepare cosmetic and tribiological coatings from metal halides, hydrogen, and nitrogen at temperatures above 1000^{o}C.[78] Often, these techniques fall short because the extreme temperatures required for the CVD reactions are too high for the temperature sensitive substrates.[9] Hoffman, Fix and Gordon, however synthesized titanium, zirconium, and hafnium nitride thin films from tetrakis(dialkylamido)-metal(IV) complexes and ammonia at low temperatures (200 – 400^{o}C) with high growth rates by atmospheric pressure CVD.[9] The depositions were carried out on various substrates including: silicon, low-sodium glass, soda lime glass, vitreous carbon, and boron. Polyester and stainless steel were also used as substrates for lower temperature depositions of titanium nitride (below 250^{o}C). All of these deposited thin films show chemical

resistance and good substrate adhesion. Results were also reported for the chemical vapor deposition of vanadium, niobium and tantalum nitride thin films as well.[77]

Other metal nitride deposition work has also been published. Wade and Crooks have utilized anodic dissolution of the corresponding metal in liquid ammonia electrolyte solutions to prepare metal nitride ceramic precursors. These precursors were then deposited onto n-Si substrates by electrophoresis. This method is useful among other coating methods such as chemical vapor deposition (CVD), physical vapor deposition (PVD), and reactive sputtering, because electrophoretic deposition does not require expensive equipment and can potentially coat irregularly shaped objects.[79]

Aside from films and deposition techniques, it has been found that other synthetic methods for preparing pnictides, especially nitride compounds, are proving much more useful than previous ceramic methods. For instance, referring back to previously mentioned work[27,39] by R.B. Kaner, metathesis has greatly influenced how these materials are currently being made. Crystalline powders of the III – V semiconductors have been synthesized [39] via solid state metathesis (eq. 1.10.) by the following scheme:

$$MX_3 + Na_3Pn \rightarrow MPn + 3NaX \qquad \text{eq. 1.10.}$$

where M = Al, Ga, In; X = F, Cl, I; and Pn = pnictogen (P, As, Sb). These reactions are either heated in a sealed tube, or ignited with a hot filament. The byproduct salts are easily removed upon washing with proper solvents. Rare earth pnictide "III – V" type compounds (eq. 1.11.) have also been synthesized with the same type of metathesis reaction:[67]

$GdI_3 + Na_3Pn \rightarrow GdPn + 3NaI$ eq. 1.11.

where Pn = pnictogen (P, As Sb or P_xAs_{1-x}). These particular reactions are initiated with a hot filament, takes place in seconds, and the products are easily isolated by a water/methanol wash. This method is obviously advantageous compared to traditional ceramic synthesis. In order to produce this material from its elements, the starting materials must be heated at 1000°C for 100 hours; undesirable conditions at best.

In addition to previously mentioned work, Kaner has also synthesized other nitride systems using solid state metathesis. One example is the synthesis of refractory group 4 (Ti, Zr, Hf) and group 5 (V, Nb, Ta) nitrides.[14] Metal halides, as expected, are reacted with Li_3N or NaN_3 to produce the following mononitrides: TiN, ZrN, HfN, NbN, and TaN. In certain cases, the high temperatures and pressures achieved by these highly exothermic reactions allow the formation of phases such as cubic NbN and TaN, which are normally only synthesized under extreme ceramic temperature and pressure conditions. Other interesting properties related to these reactions are the abilities of ZrN and NbN to superconduct at 8.5K and 15.5K respectively. GaN, important for already mentioned uses such as flat panel displays, blue lasers, etc., has recently been synthesized showing again the usefulness of metathesis. GaN can be synthesized from metathesis of GaI_3 and Li_3N at 4.5 GPa of pressure[69], therefore a method requiring a much lower pressure was desired. After unsuccessful attempts at using different nitriding agents and inert salt additives, it was found that in the proper ratio, the addition of ammonium chloride to the GaI_3 and Li_3N reaction (eq. 1.12.) under ambient pressures yields crystalline gallium nitride:[40]

$$GaI_3 + Li_3N + NH_4Cl \rightarrow GaN + 3LiI + NH_3 + HCl \qquad \text{eq. 1.12.}$$

The three solid state precursors can be (in an inert Helium atmosphere) weighed out, ground together, and placed in a steel reactor (modeled after a bomb calorimeter) where a resistivity heated nichrome wire is used to initiate the rapidly propagating reaction.

More of Kaner's recent work includes similar, self-propagating metathesis reactions yielding cubic phase, metastable group 4 phosphides (ZrP and HfP).[80] Like previous examples, these materials which took extreme temperatures, pressures, etc. to synthesize from their elements can be made in the cubic phase, in crystalline form, in seconds due to the extreme temperatures and pressures generated as in the other metathesis examples. Finally, Kaner's most recent work shows the rapid solid state synthesis of tantalum, chromium, and molybdenum nitrides.[41] Notable in this work is that direct metathesis, i.e. $TaCl_5 + 5/3Li_3N$, only yields the subnitride, Ta_2N, rather than the mononitride under ambient conditions. However, when 12 moles of sodium azide (NaN_3) is added to the reaction mixture, cubic phase TaN is formed along with Ta_2N. This occurs because of a large nitrogen overpressure created by the excess NaN_3.

Complementary to the synthesis and deposition studies, many other interesting studies have included nitride materials. One such study examines the electronic and geometric structures of TiN, VN and CrN by ab initio MCSCF and multireference configuration interaction (CI) techniques.[81] This study reports the ground state symmetries to be: $^2\Sigma^+$, $^3\Delta$, and $^4\Sigma^-$, respectively. Also reported in this study are pertinent dissociation energies, vibrational frequencies, dipole moments, bond

lengths, and charge distributions and comparisons with experimental results for a variety of electronic states.

1.4. The MNX Family (M = Zr, Hf; X = Cl, Br, I)

Derivative compounds of nitride/pnictide compounds serve as important materials as well. One of the most important examples is the previously mentioned metal nitride halide compounds.[51-53] β-ZrNCl, reported by S. Yamanaka,[82] one of the leading metal nitride halide researchers, is a layer structured material comprised of a hexagonal Zr – N net in the a-b plane (see Figure 1.1). In the c direction, double layers of chlorine atoms are separated by van der Waals interactions between double layers of the Zr – N structure. The unit cell in the c direction contains 3 entire layers of the Zr – N structure with the chlorines in between.

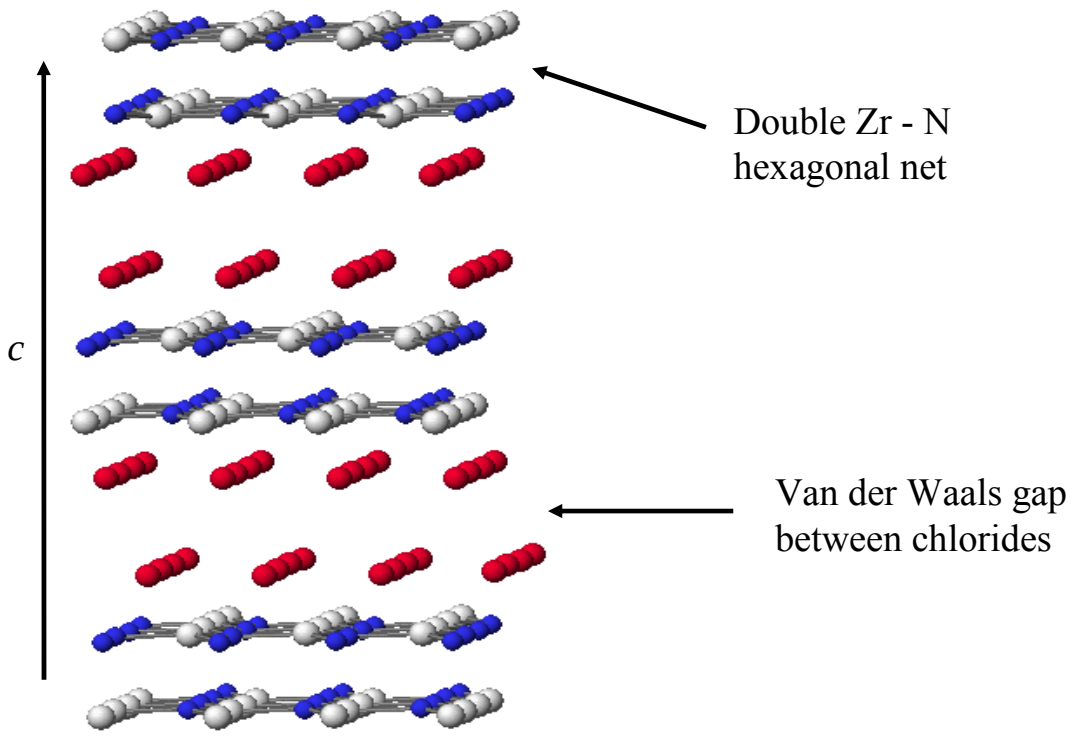

Figure 1.1. Two layers of the β-ZrNCl structure and the Zr coordination sphere. (Zirconium – gray, Nitrogen – blue, Chlorine – red)

β-ZrNCl was originally synthesized by first reacting $ZrCl_4$ with gaseous ammonia at 300 – 400°C to form α-ZrNCl (which has the FeOCl structure),[83] and then heating to approximately 600°C in order to convert it into the β - form. It was then found that β-ZrNCl could be directly prepared by the reaction of zirconium metal or zirconium hydride with ammonium chloride.[82] This chemical transport method, which is still used today, uses two heaters; one to vaporize the ammonium chloride at about 360°C and the other to form β-ZrNCl between 550 – 700°C. The

vaporized ammonium chloride is carried through the reaction vessel, across the zirconium or zirconium hydride, with a stream of gaseous ammonia. It was then reported[83] that the powder form of β-ZrNCl, as prepared, could be vapor transported to a very highly crystalline form which allowed further study by methods such as x-ray diffraction. Major interest in this compound and its hafnium analogue has developed since the report of superconductivity upon electron doping.[51,52] β-HfNCl, upon doping with lithium, as well as other doping agents has been shown to superconduct below 25.5K, a fairly high T_c.[51] Typical lithium intercalations are carried out by dispersing MNCl powders in a lithiating agent such as n-butyllithium in hexane[53] or a lithium naphthalene in THF solution.[52] This provides a good example of the previously mentioned reductive intercalation.[4] In this example Li is intercalated, sometimes including a co-intercalate molecule such as THF, into the parent structure.[51] The relative structure does not change, except for a possible increase in distance between the layers, making this a topochemical soft chemical process. The reduction aspect is also demonstrated by the electron doping that accompanies intercalation. It has also recently been discovered that other doping methods, such as deintercalation of the interlayer chlorides can induce superconductivity as well.[84,85]

Recently, many interesting studies of these superconducting metal nitride halides have been reported. These include studies of electronic structures and instabilities in ZrNCl and HfNCl,[19,54] as well as high resolution electron microscopy structural studies.[86] These electron microscopy studies have verified that the chlorines in between the zirconium nitride layers are in a staggered pattern. Another

example[87] of the recent work done on β-(Zr)HfNCl shows that the superconductivity that occurs in the lithiated/doped compound is quasi-two-dimensional in nature, meaning that the conductivity takes place through the a-b plane, Zr – N hexagonal net, rather than through the chlorine layers in the c direction. Recent high pressure synthetic techniques have also led to single crystals of these materials, even including the lithiated superconducting phases.[88-90]

Although these materials have been studied extensively, they have yet to be utilized as new material precursors. As described earlier, cation exchange has become quite common in solid state materials; however anion metathesis is very rare in refractory, inorganic systems. The MNX (M = Zr, Hf; X = Cl, Br, I) materials described here provide ideal systems for which to explore anion metathesis as a suitable, soft chemical method for new materials design and preparation. The interlayer halides should readily undergo topochemical exchange, giving new group IV nitride materials by anion metathesis in these refractory, inorganic systems.

1.5. Thesis Organization

The focus of this thesis involves the manipulation of the β-ZrNCl system to give novel, new, metastable materials. The synthetic and characterization methods are discussed in conjunction with structural and physical properties. In this work, topochemical anion exchange is utilized to achieve a variety of zirconium nitride based materials, previously unknown and unable to be synthesized using typical solid state methods.

Chapter 2 introduces proof of concept regarding rare anion exchange with a variety of zirconium nitride sulfide materials. These sulfide pseudo-analogues of the zirconium nitride chloride system include α- and β- forms of Zr_2N_2S, as well as an excess sodium sulfide stabilized phase and a hygroscopic sodium chloride stabilized material. Each of these materials can be obtained by slight manipulation of reaction variables, showing extreme kinetic experimental control.

A new, alkali stabilized fluoride analogue is discussed in Chapter 3. This extremely low temperature solid state metathesis reaction gives sodium and potassium stabilized fluoride materials with unique structural properties. The synthetic and structural details and properties are described. Chapter 4 presents organic/inorganic hybrid materials based on the layered ZrNCl system. Chloride for alkoxide exchange is discussed, as well as structural analysis. Implications of results and importance are discussed for each of these systems.

Chapter 2:

Topochemical Synthesis and Characterization of the Zr_2N_2S Phases and the Na_2S and ACl Derivatives

2.1. Introduction

There has been major interest in the MNX (M = Zr, Hf; X = Cl, Br, I) family of compounds especially since the report of superconductivity upon electron doping, yielding a T_c of 25.5K for β-HfNCl.[51,52,87,91] Similar to the A_xMS_2 superconductors (A = alkali, M = early transition metal), the MNX superconducting behavior is relatively unaffected by intercalant variation.[92-94] It is well known, however, that in most solid state systems, anions control many of the structural and physical characteristics. In contrast to systems such as the M_2S derivatives, the halide anions in the MNX compounds can be changed (Cl, Br, I) giving different structure types and slight changes in the superconducting properties.[51,95] Compositionally similar (yet structurally different) compounds such as Zr_2ON_2 have been reported.[96,97] However, until this work no real derivative materials of ZrNCl have been reported other than its MNX analogues (M = Zr, Hf; X = Cl, Br, I).

Metathesis, a soft chemical process, has also been utilized to make many novel, metastable oxide and sulfide materials.[23,27,32,47] R.B. Kaner has shown extensively that certain halide-containing solids can undergo anion exchange by metathesis reactions with alkali metal salts, which drives the reaction by yielding

alkali halide byproducts.[27,39,41,80] Although cation exchange is becoming more common, the exchange of anions in a solid refractory inorganic host is quite rare. The β-MNX materials (M = Zr, Hf; X = Cl, Br, I) comprise double layers of halides in the van der Waals gap between the metal nitride layers as shown in (Chapter 1) Figure 1.1.[83,98,99] Previous studies have shown that intercalation can take place in between these layers, suggesting that atoms, ions, and even small molecules can move through this solid state structure.[51,100] Therefore it seems reasonable that β-ZrNCl should readily undergo anion metathesis, yielding new novel materials.

One such material, Zr_2N_2S, is expected to adopt the La_2O_2S structure type.[101-103] In this structure type, double La – O layers (arranged identically to the Zr – N layers in ZrNCl) are linked together by a single layer of sulfide anions. Preparing Zr_2N_2S from ZrNCl would require a two for one exchange of chloride for sulfide anions. This exchange would link the double ZrN layers together, effectively eliminating the van der Waals gap of the parent material. Although traditional synthetic attempts to prepare this material have failed, a synthetic route to a NaCl-stabilized derivative, $NaZr_2N_2SCl$, was reported by Lissner and Schleid.[102] This compound has a very similar structure to ZrNCl, where a disordered 1:1 mixture of S and Cl reside in the ZrNCl chloride sites and the Na^+ cations fill the octahedral holes in the van der Waals gap. Reported herein is the synthesis and characterization of low and high temperature Zr_2N_2S phases (*P*-3*m*1 and $P6_3/mmc$ crystal symmetries, respectively) by topotactic anion exchange. The synthesis and characterization of a Na_2S excess phase, $Na_{2x}Zr_2N_2S_{1+x}$ ($0 < x < 0.5$) are provided, as well as defect

members of the Lissner and Schleid phase, $A_xZr_2N_2SCl_x$ (A = Na, K, Rb and $0 < x < 0.15$).

2.2. Experimental

Air and moisture sensitive materials were stored and handled in a nitrogen filled Vacuum Atmospheres drybox. A high vacuum line (10^{-5} Torr) used for all glass tube evacuation consisted of a belt driven mechanical pump followed by a glass oil diffusion pump and a liquid nitrogen trap. Evacuated silica tubes were sealed using an oxygen/hydrogen torch. Standard schlenk techniques were used for all air sensitive solution processes. Microanalysis was performed by Atlantic Microlab, Inc.; Norcross, GA.

2.2.1. Synthesis

β-ZrNCl was prepared by two different methods. The first method uses slight modifications of previously reported methods.[82] In a typical reaction, 1.5g of Zr metal (99.7% Cerac, 325 mesh) was placed in a quartz boat in the center of an argon flow through furnace. Approximately 12g of dry NH_4Cl was placed in a second quartz boat approximately 12 cm from the center of the furnace in the direction of the argon inlet. The furnace was purged with argon for 10 hours and then heated at 30°C/min to 650°C for three hours under flowing argon. The ammonium salt boat was heated to approximately 350°C, while the Zr boat at the center of the furnace was heated to 650°C, as determined by external thermocouple readings. After cooling to

room temperature under argon, the center boat containing amorphous β-ZrNCl was removed, and the thin layer of white ZrO_2 which forms on the surface of the product was manually scraped away. The amorphous β-ZrNCl product was pale green in color.

A_2S (A = Na, K, Rb) reagents were prepared by direct, stoichiometric reactions of the alkali metals with sulfur or selenium in liquid ammonia.

α-Zr_2N_2S and β-Zr_2N_2S were prepared by the following methods. In a typical reaction, 91mg (1.0mmol) ZrNCl and 39mg (0.5mmol) Na_2S or 55mg (0.5mmol) K_2S were ground and intimately mixed. The mixtures were loaded into silica tubes in the drybox and subsequently evacuated and sealed. During evacuation, a heat gun was used to warm the reaction mixtures to *ca.* 200 °C in order to drive off any residual moisture. α-Zr_2N_2S was prepared by heating the samples at 1 °C per minute until a temperature of 800 °C was reached. The reaction mixture was held at this temperature for 2 days. β-Zr_2N_2S was prepared by heating 1 °C per minute to 900 °C, and kept at that temperature for 3 days. α-Zr_2N_2S is brown whereas β-Zr_2N_2S is dark brownish-green in color.

$A_{2x}Zr_2N_2S_{1+x}$ was prepared according to the above procedure, using appropriate stoichiometric amounts of ZrNCl and Na_2S. The mixture was then heated at 1 ^oC per minute to 800 – 1000 °C, and kept at that temperature for 3 days. The title compounds are yellow-brown in color. A less crystalline product is obtained between 400-800 °C.

$A_xZr_2N_2SCl_x$ was also prepared by a similar procedure. In a typical reaction, 91mg (1.0mmol) ZrNCl and 39mg (0.5mmol) Na_2S were heated (3^oC per minute) to 350^oC and held at that temperature for 7 days yielding a tan product. In all reactions, excess alkali halide salt byproducts were washed away by sonicating with 10mL

distilled water 4 times, followed by a final acetone wash. For the $A_xZr_2N_2SCl_x$ compounds, washing and/or exposure to air resulted in the formation of the hydrated $A_xZr_2N_2SCl_x(H_2O)$ phases. The hydrates are quantitatively converted back to the anhydrous form by heating the samples under dynamic vacuum at 200 °C. XRD data for the anhydrous material were recorded using sealed, anaerobic sample holders.

2.2.2. Characterization

X-ray diffraction (XRD) patterns were recorded using a Bruker C2 Discover X-ray Powder Diffractometer with an area detector and CuK_α radiation. Typically, six frames were collected and merged to give 2θ scans from 4° to 90°. Unit cell indexing and Reitveld refinements were performed using MDI Jade and TOPAS software packages, respectively.[104,105] The simulation of α-Zr_2N_2S was also carried out using TOPAS. Errors for all crystallographic data (positions, bond lengths, etc.) were calculated within the TOPAS refinement software.

Energy Dispersive X-ray analysis (EDX) was performed with an AMRAY 1820K Scanning Electron Microscope with an acceleration potential of 20 kV. Wavelength Dispersive Spectroscopy (WDS) was performed with the JXA-8900 Superprobe, using ZrNCl as a Zr and Cl standard, Molybdenite as a S standard, Albite as a Na standard, and $K_2La_2Ti_3O_{10}$ as a K standard. Samples and standards were mounted into casting resin epoxy plugs. EDX and WDS measurements were carried out by analyzing 10 spots per sample.

Compound formulas were calculated from WDS data and microanalysis data. The nitrogen content was calculated by charge balance. The reported errors are

generated from propagated counting statistics associated with the WDS analysis. Hydration-TGA analysis was carried out in a series of 3 runs by heating the sample in a small Pt boat at 200^{o}C, starting with initial product masses of approximately 300mg. WDS data was obtained with the assistance of Dr. Phil Piccoli of the UMCP Department of Geology.

High-resolution transmission electron micrographs (HRTEM) were recorded using a JEOL 4000 FX transmission electron microscope operated at 300 KV. All TEM images were taken by Dr. Riba-Salamanca of the University of Maryland Department of Materials Engineering. A 200 mesh copper grid with a formvar/carbon film was introduced in the vial containing the powder of the sample to get some of the nanoparticles attached to the film. Electron diffraction patterns and high resolution lattice images were obtained from several nanoparticles to get statistical information on the structure of the powder.

2.3 Results

2.3.1. Synthesis

Metathesis reactions of β-ZrNCl with A_2S (A = Na, K, Rb) at various temperatures and in different stoichiometries have yielded a family of previously unknown zirconium nitride sulfide materials described below.

β-ZrNCl reacts with A_2S (A = Na, K, Rb) in a 2:1 ratio at 800^{o}C (*in vacuo*) for 48 hours giving α-Zr_2N_2S along with ACl (eq. 2.1). The ACl byproduct, observed

by powder X-ray diffraction (XRD), is washed away with distilled water leaving the brown α-Zr_2N_2S product.

$$2\ ZrNCl + A_2S \rightarrow \alpha\text{-}Zr_2N_2S + 2\ ACl \quad (A = Na, K, Rb) \qquad \text{eq. 2.1.}$$

XRD analysis shows trace amounts or ZrO_2 (Figure 2.1), due to a slight impurity in the ZrNCl precursor. Energy dispersive X-ray spectroscopy (EDX) analysis, after accounting for the ZrO_2 impurity, shows a Zr/S ratio of 2:1. Further XRD analysis shows that the compound crystallizes with *P*-3*m*1 crystal symmetry, having the expected La_2O_2S structure type, which will be discussed in the next section with TEM and ED studies.

When ZrNCl reacts with A_2S at temperatures greater than 850°C or when α-Zr_2N_2S is heated above 850°C for 48 hours, a different polymorph, β-Zr_2N_2S, forms that is dark greenish brown in color. This compound represents a new structure type and possesses $P6_3/mmc$ crystal symmetry. As in the alpha form, EDX and microanalysis give a 2:1 Zr/S ratio after accounting for the ZrO_2 impurity. This phase is stable in the absence of air up to 1050°C. Powder XRD analysis (Rietveld refinement) will be discussed in the next section. Neither Zr_2N_2S polymorph is hygroscopic and both are stable in air at room temperature.

ZrNCl reacts with excess A_2S (A = Na, K) between 400-1000°C to give a yellow-brown sodium sulfide excess phase, $A_{2x}Zr_2N_2S_{1+x}$ (eq. 2.2), a highly-defective form of the $NaZr_2N_2SCl$ structure type.[102]

$$2\ ZrNCl + 1{+}x\ A_2S \rightarrow A_{2x}Zr_2N_2S_{1+x} + 2\ ACl \quad (A = Na, K) \qquad \text{eq. 2.2.}$$

This phase exists in the range $0 < x \leq 5$, and data suggest that x increases with temperature. Two members of this series, $Na_{0.5}Zr_2N_2S_{1.25}$ (x = 0.25) and $Na_{0.95}Zr_2N_2S_{1.84}$ (x = 0.5) have been characterized in detail. While the sodium containing materials could be obtained as single phase, the potassium analogues $K_{2x}Zr_2N_2S_{1+x}$ are formed competitively with Zr_2N_2S and could not be prepared in pure form. Rb_2S reactions give Zr_2N_2S exclusively. Reactions below 800°C result in a 25% maximum Na_2S incorporation, regardless of stoichiometry. Wavelength dispersive spectroscopy (WDS) and elemental analysis performed on the x = 0.25 and x = 0.5 phases gave the formulas $Na_{0.49(3)}Zr_{2.00(7)}N_2S_{1.28(4)}$ and $Na_{0.90(3)}Zr_{2.0(2)}N_2S_{1.85(1)}$, respectively, with Zr normalized to 2 and N assumed to be 2. These compound formulas will herein be referred to as $Na_{0.5}Zr_2N_2S_{1.25}$ and $Na_{0.95}Zr_2N_2S_{1.84}$.

A highly defect, hygroscopic $A_xZr_2N_2SCl_x$ phase, where $0 < x \leq \sim 0.15$ (A = Na, K, Rb) also forms when eq. 1 or eq. 2 are carried out at lower temperatures (300-400°C) as shown by EDX and WDS analysis. Excess Na_2S with regrinding and refiring does not reduce the residual chloride amount in this temperature regime. The $NaZr_2N_2SCl$ (x = 1 end member) described by Lissner and Schleid cannot be prepared by the synthetic methods reported here. The compounds are poorly crystalline due to low reaction temperatures and hygroscopic instabilities, but the prominent [0 0 l] low angle reflections in the XRD profile show that the unit cell c-lattice parameter increases with alkali ion size (see Table 1). Unlike the former sulfide phases in this work that are very stable in air, these phases are extremely

hygroscopic and reversibly hydrate to form $A_x(H_2O)Zr_2N_2SCl_x$ (monohydrates) according to TGA analysis. The c-lattice parameters of the hydrated materials (~33-34 Å) are presumably dictated by the size of the H_2O intercalant and are relatively unaffected by the size of the alkali ions. The alkali chloride stabilized compounds have highly variable compositions based on analytical data. WDS and EDS analyses show 5 - 15 % ACl contents, with Cl often having a higher concentration than the alkali. The data indicate that the reaction products are mostly heterogeneous with various $A_xZr_2N_2SCl_x$ solid solution members, as well as corresponding hydrates and potential incomplete metathesis products. This heterogeneity makes the exact hydration level difficult to determine.

2.3.2. Structural Studies

Table 2.1 provides a summary of the structural data while each compound is decribed individually below.

α-Zr_2N_2S: On the basis of the powder XRD, TEM and ED studies, the crystal symmetry is assigned to be *P*-3*m*1 where a = 3.605(1) Å and c = 6.412(3) Å. Although the XRD pattern could not be refined by Rietveld analysis due to poor crystallinity, the simulated pattern obtained by adjusting the expected La_2O_2S (predicted by Lissner and Schleid)[101-103] structural parameters to reflect proper Zr-N bond distances gives a near perfect match (Figure 2.1). The trace amount of ZrO_2 impurity is likely from the ZrNCl starting material. Figure 2.2 shows an idealized ball and stick drawing of the α-Zr_2N_2S structure.

Table 2.1. Crystallographic and Compositional Data

Empirical Formula	$Na_xZr_2N_2SCl_x$[a]	$K_xZr_2N_2SCl_x$[a]	$Rb_xZr_2N_2SCl_x$[a]	$Na_xZr_2N_2S_{1+x/2}$[b]	α-Zr_2N_2S[a]	β-Zr_2N_2S[b]
Space Group	*R*-3*m*	*R*-3*m*	*R*-3*m*	*R*-3*m*	*P*-3*m*1	$P6_3/mmc$
a/Å	3.63	3.61	3.57	3.637(1)	3.605(2) from Na_2S	3.611(1) from K_2S
c/ Å	28.4	28.9	30.5	29.490(7)	6.412(3) from Na_2S	12.818(1) from K_2S
c/ Å hydrated	32.5	33.9	33.3	----	----	----
Chemical Composition						
Reaction Temperature	300-350°C	300-350°C	300-350°C	400-1000°C	700-800°C	850-1050°C

[a]Room temperature data from MDI Jade cell refinement
[b]Room temperature data from Rietveld analysis of powder XRD data

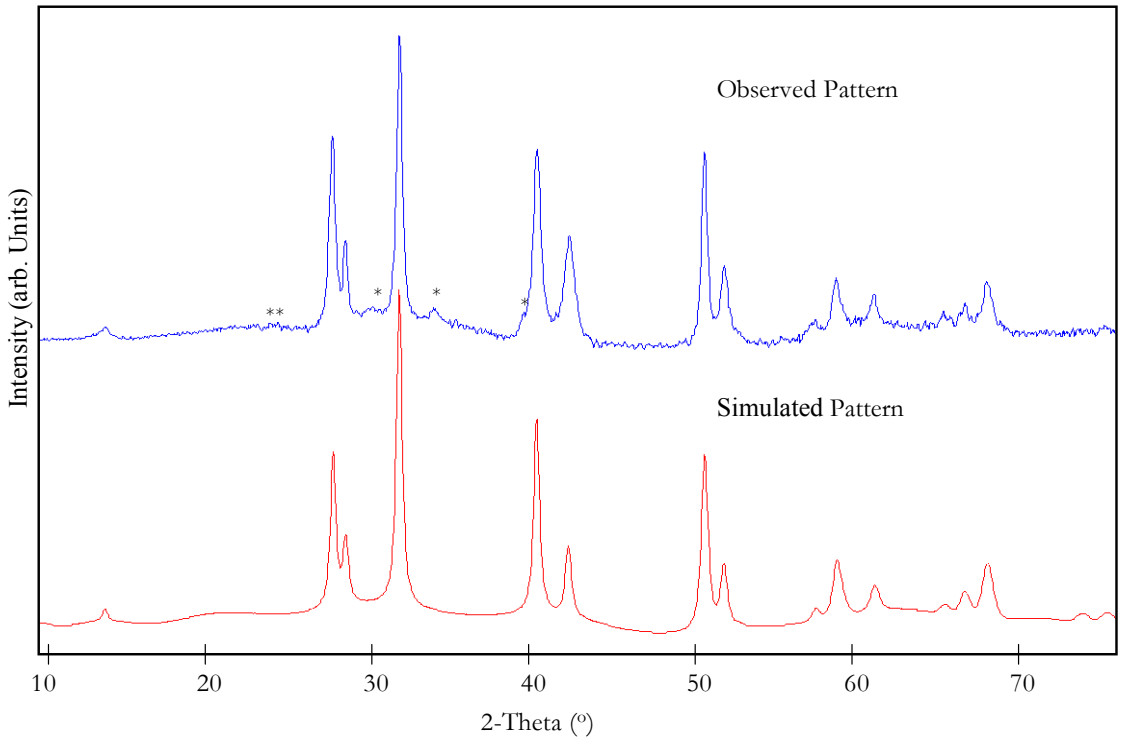

Figure 2.1. Simulated and Observed α-Zr_2N_2S powder XRD patterns. The ZrO2 impurity is denoted with asterisks.

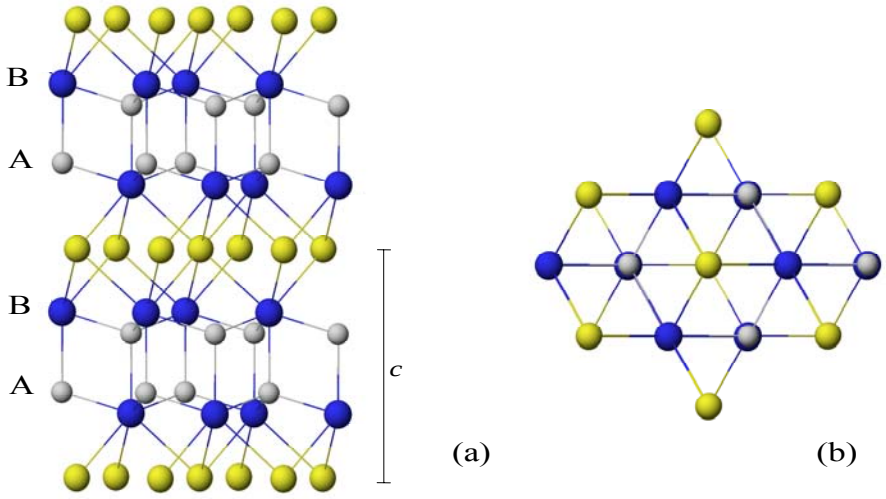

Figure 2.2. Ball and stick drawing of the α-Zr_2N_2S structure. Coloring scheme: zirconium-blue, nitrogen-light gray, sulfur-yellow.

The transmission electron microscopy (TEM) image (Figure 2.3) shows the 6.4 Å *c* lattice parameter as well as the structure's layered nature. The Figure 2.3 inset, the 0 0 1 zone axis Electron Diffraction (ED) image, shows no superstructure reflections and illustrates the hexagonal crystal symmetry.

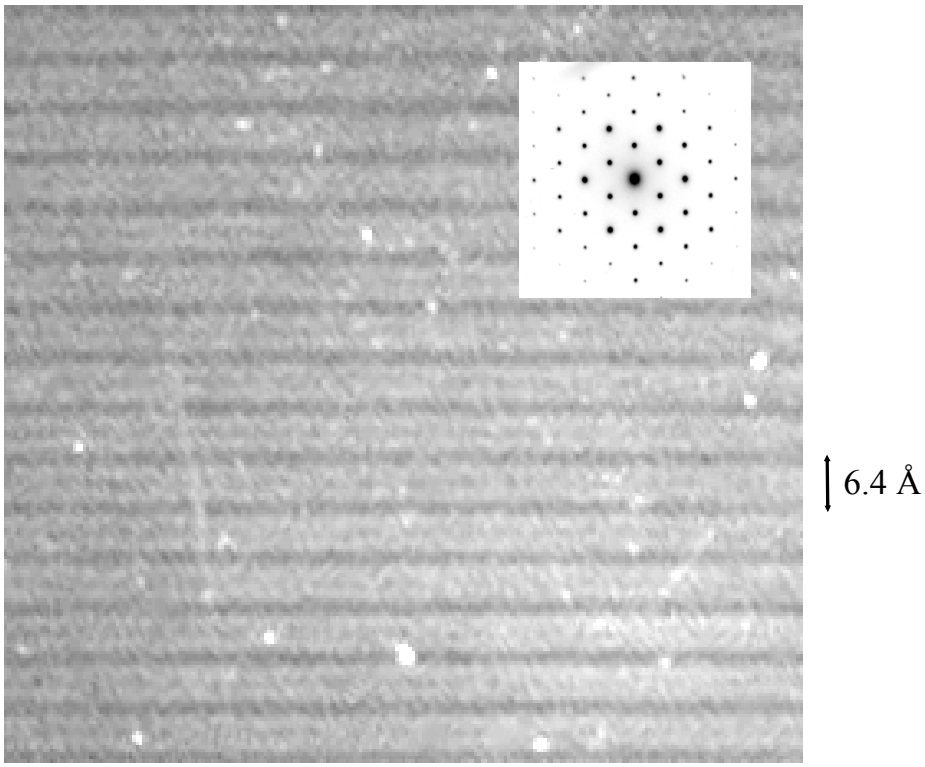

Figure 2.3. TEM image of α-Zr_2N_2S showing the 6.4 Å *c* parameter with inset showing ED pattern.

In this compound, the repeating Zr_2N_2 layers are retained as in β-ZrNCl, and each sulfide replaces two chloride ions in between the layers. In contrast to ZrNCl, the layers have shifted so that stacking occurs in an AB···AB repeat pattern, with the sulfides linking the Zr_2N_2 layers, eliminating the van der Waals gap. In this idealized La_2O_2S structure type, Zr is 7 coordinate while each sulfide is six coordinate, residing in octahedral SZr_6 units as shown in Figure 2.4. From the simulated pattern, the optimized Zr-S distances are 2.74 Å. In the $NaZr_2S_3$ and $Ba_{n+1}Zr_nS_{3n+1}$ perovskites,

the Zr-S distances are on average 2.5 – 2.6 Å, respectively, however the zirconium and sulfur coordination spheres are lower in these materials.[106,107]

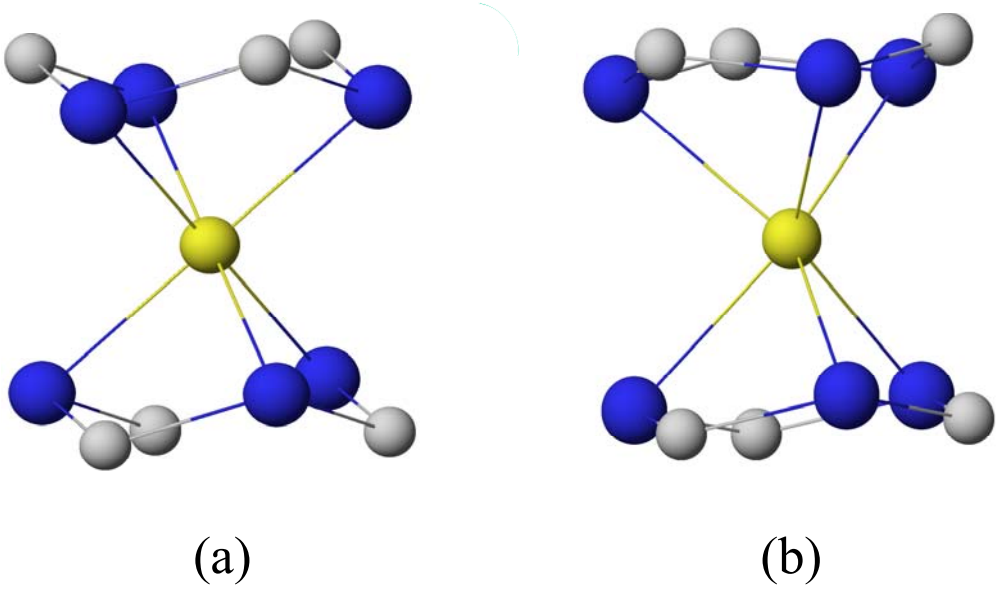

Figure 2.4. Octahedral (a) and trigonal prismatic (b) SZr_6 units of α- and β-Zr_2N_2S, respectively.

β-Zr_2N_2S: This high temperature phase, representing a new structure type, has $P6_3/mmc$ crystal symmetry where a = 3.602(1)Å and c = 12.817(1)Å as determined by Rietveld analysis (Figure 2.5). ZrO_2 impurities were accounted for by a multiphase refinement. A ball and stick drawing of the β-Zr_2N_2S structure is given in Figure 2.6.

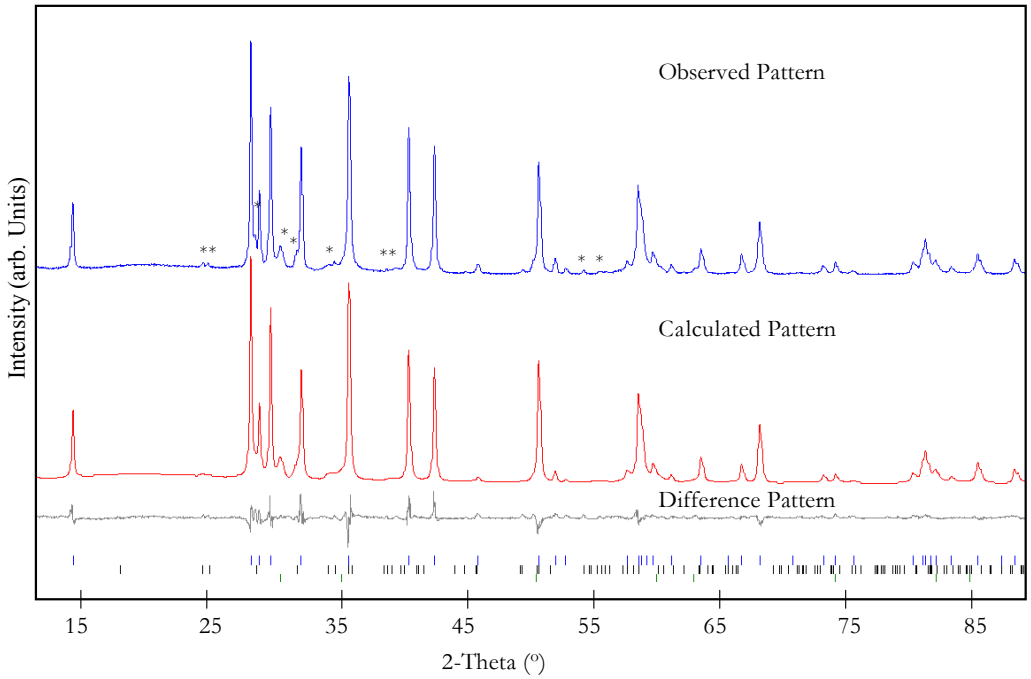

Figure 2.5. Observed, calculated and difference XRD patterns (Rietveld analysis) of β-Zr_2N_2S. The ZrO_2 impurity is denoted with asterisks.

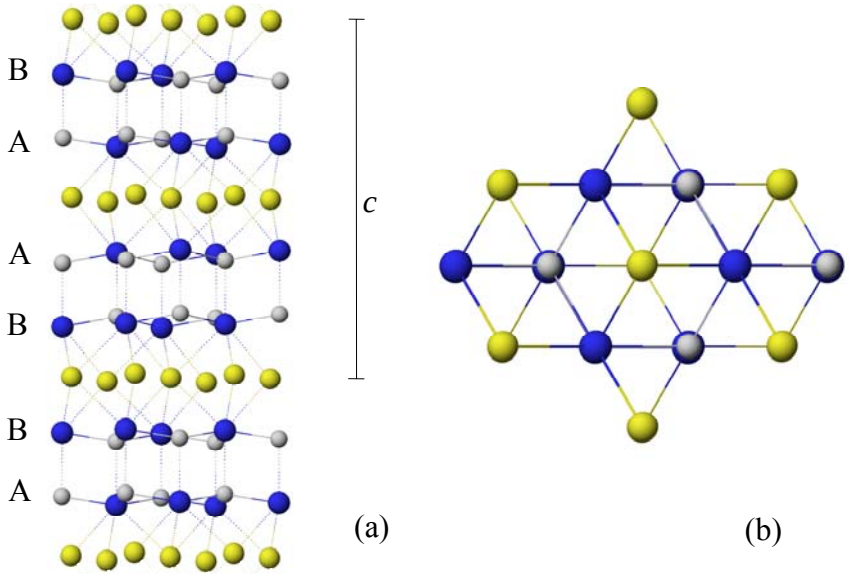

Figure 2.6. Ball and stick drawing of the β-Zr_2N_2S structure. (a) shows the 1 0 0 projection and (b) shows the 0 0 1 projection. Coloring scheme: zirconium-blue, nitrogen-gray, sulfur-yellow.

Table 2.2 provides a summary of the Rietveld refinement data and crystallographic information and selected bond distances and angles are given in Table 2.3.

Table 2.2. XRD Rietveld Refinement Data

		β-Zr_2N_2S	$Na_xZr_2N_2S_{1+x/2}$
Crystal System		Hexagonal	Trigonal
Space Group		$P6_3/mmc$	R-3m
a/Å		3.611(1)	3.637(1)
c/Å		12.818(1)	29.490(7)
R_{wp}		7.8	9.5
R_p		5.9	6.1
R_{bragg}		4.1	4.1
Zr	x	1/3	0
	y	2/3	0
	z	0.8975(1)	0.2135(3)
	beq	0.21(8)	0.46(6)
	occ	1.0	1.0
N	x	1/3	0
	y	2/3	0
	z	0.0809(5)	0.1430(3)
	beq	0.1	0.2
	occ	1.0	1.0
S	x	0	0
	y	0	0
	z	1/4	0.3975(1)
	beq	1.0(1)	0.3(2)
	occ	1.0	0.918(5)
Na	x	---	0
	y	---	0
	z	---	0
	beq	---	2.0(2)
	occ	---	0.95(2)

Table 2.3. Selected Bond Lengths (Å) and Angles (°)

	β-Zr_2N_2S	$NaZr_2N_2S_{1.5}$
Zr – N	2.103(1)	2.078(12)
Zr – N	2.35(1)	2.208(4)
Zr – S	2.814(1)	2.671(2)
Na – S	---	2.822(2)
N – Zr – N	118.3(2)	110.9(3)
N – Zr – N	82.4(2)	72.0(3)
Zr – N – Zr	97.6(2)	108.0(3)
Zr – S – Zr	82.4(2)	85.8(1)
S – Zr – S	79.81(1)	---
S – Na – S	---	99.7(1)
S – Na – S	---	80.3(1)

In this structure, sequential Zr_2N_2 layers are shifted by *a*/2 relative to the α-form. This shifting causes the *c* lattice parameter to double in comparison to the α-form and places the sulfide ions in trigonal prismatic SZr_6 units rather than octahedral units as in α-Zr_2N_2S (Figure 2.4b). This shift changes the Zr_2N_2 double layer stacking to an AB···BA···AB repeat sequence (Figure 2.6) which doubles the c lattice parameter relative to the α-Zr_2N_2S structure. This stacking sequence also aligns Zr atoms from adjacent layers along the c-axis, although the ZrN layers remain the same in both Zr_2N_2S polymorphs. As in the alpha form, the refined Zr – S bond distaces (2.814(1)Å) are long relative to previously reported zirconium sulfide materials,[101,106] again reflecting the high coordination numbers of sulfur (CN = 6) and zirconium (CN = 7). The refined Zr – N bond distances (2.10, 2.35 Å) are quite reasonable.

$Na_{2x}Zr_2N_2S_{1+x}$: This phase crystallizes with *R*-3*m* (rhombohedral) crystal symmetry with $a \approx 3.6$Å and $c \approx 29.4$Å and is closely related structurally to β-ZrNCl

and $NaZr_2N_2SCl$. Although several structurally identical phases have been obtained in this temperature range, Rietveld analysis was performed on the phase made at 1000 ^oC (x = 0.5) giving *a* = 3.6359(1)Å and *c* = 29.4820(6)Å. Calculated, observed and difference profiles are shown in Figure 2.7 and refinement results and selected bond distances and angles are given in Table 2.2 and Table 2.3, respectively. Analytical data (WDS) give a formula of $Na_{0.90(3)}Zr_{2.0(2)}N_2S_{1.85(1)}$, which agree quite well with the refined occupancies from the Rietveld analysis – $Na_{0.95(2)}Zr_2N_2S_{1.84(3)}$.

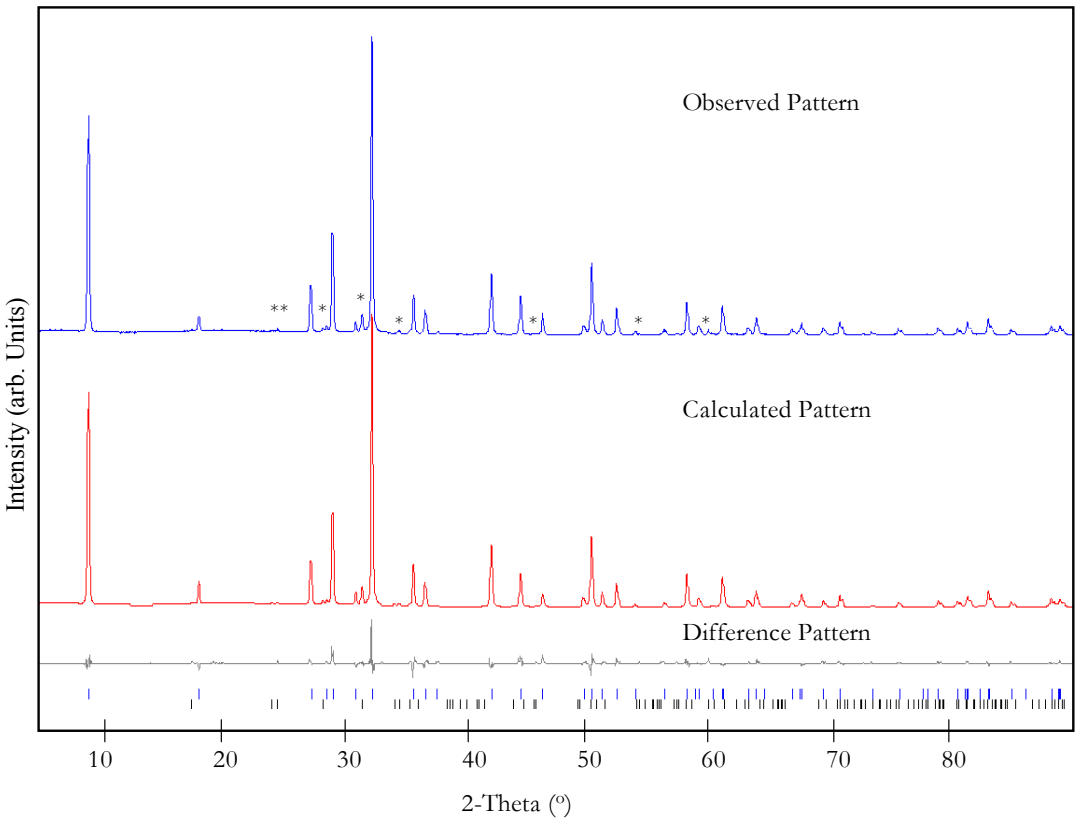

Figure 2.7. Observed, calculated and difference XRD patterns (Rietveld analysis) of $NaZr_2N_2S_{1.5}$. The ZrO_2 impurity is denoted with asterisks.

This compound essentially adopts the $NaZr_2N_2SCl$ structure type, with some exceptions. Excess sulfide in the above formula presumably arises from disulfide units in the sulfide layers. Instabilities associated with large vacancy concentrations would be alleviated by the formation of these disulfide units, which is a common phenomenon. In the $Na_{0.95}Zr_2N_2S_{1.84}$ sulfide layers, approximately 15% randomly distributed vacancies still exist, while the vacancies approach 50% for lower x members in the $Na_xZr_2N_2S_{1+x}$ series. In this structure, the sulfide ions sit in the partially vacated sites where the chlorides appear in ZrNCl.

The sodium ions sit in octahedral holes in the van der Waals (vdW) gaps between the sulfide layers. Rather than shrinking the *c* parameter and changing the crystal symmetry by linking the Zr_2N_2 layers as in the Zr_2N_2S phases, the layers are slightly "propped open" by the sodium ions. These sodium ions are intercalated between the sulfide layers, retaining the basic parent ZrNCl structure. The sodium sites in the vdW gaps can be fully occupied or virtually empty as x approaches zero in the $Na_{2x}Zr_2N_2S_{1+x}$ compounds, which is very similar behavior to the A_xMS_2 compounds (A = alkali, M = early transition metal).[92-94]

The Zr – S refined bond lengths for this compound, 2.671(2) Å, are shorter than those of the Zr_2N_2S phases and more similar to those of other zirconium sulfide compounds, [101,106] reflecting the lower coordination numbers of zirconium and sulfur in this structure. The refined Zr – N and Na – S distances (Table 2.3) are typical.[102,108] Attempts at the K and Rb versions of this compound have been unsuccessful thus far.

$A_xZr_2N_2SCl_x$ (and hydrates): These compounds are rhombohedral, space group *R*-3*m*, with alkali dependent lattice parameters of a = 3.6 Å and c = 28.5 Å (Na), 28.9 Å (K), and 30.5 Å (Rb). The $A_xZr_2N_2SCl_x$ phases are also isostructural with the Lissner and Schleid compound $NaZr_2N_2SCl$ but have vacancies on both the Na and S/Cl sites. The XRD profiles are characteristically broad in appearance, as shown in Figure 2.8, and are virtually superimposable with that of ZrNCl. The *c*-lattice constants were estimated from the low angle 0 0 l reflections and the TEM images whereas the *a*-lattice constants were estimated from the electron diffraction data and the higher angle diffraction data. Cell constants and structures could not be refined due to the poor diffraction data quality.

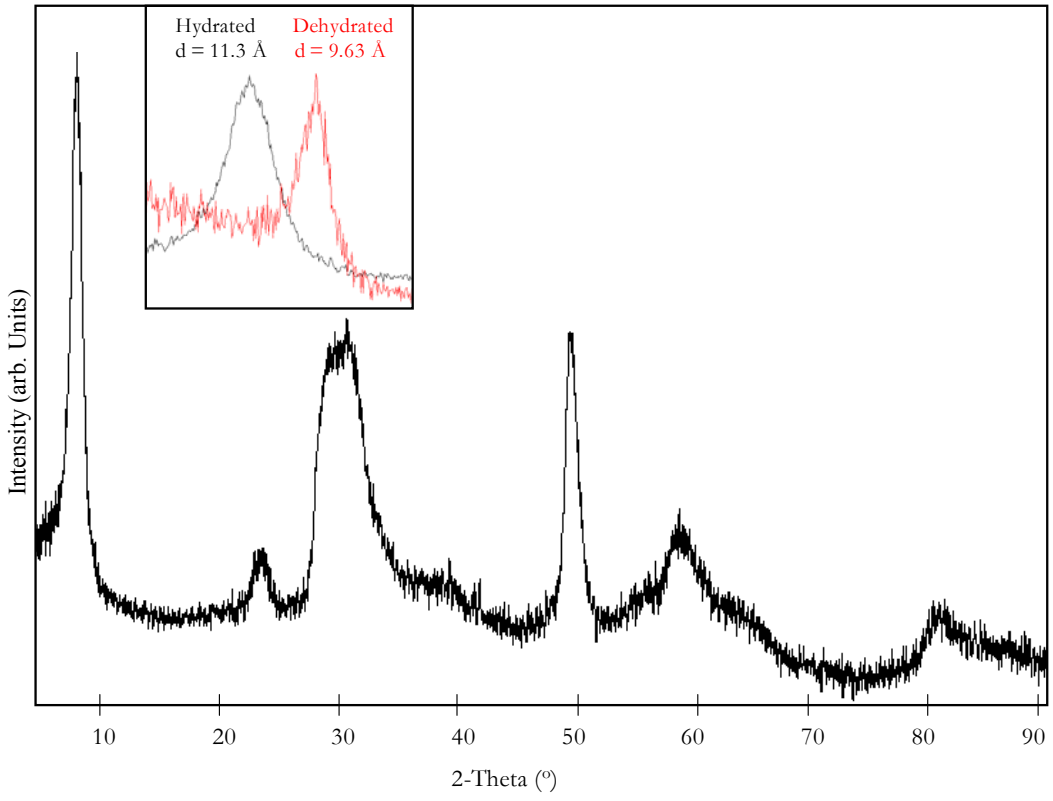

Figure 2.8. $K_xZr_2N_2SCl_x$ powder XRD profile with inset showing hydration effect.

All of the $A_xZr_2N_2SCl_x$ compounds (A = Na, K, Rb) reversibly hydrate, increasing c-lattice parameters to ~33 – 34 Å (see Table 2.1 and Figure 2.8 inset). TEM images of of $K_xZr_2N_2SCl_x$ where x ~ 0.15, (Figure 2.9) also confirm the reversible hydration in accordance with XRD, showing *c* lattice spacings for both dehydrated and hydrated structures.

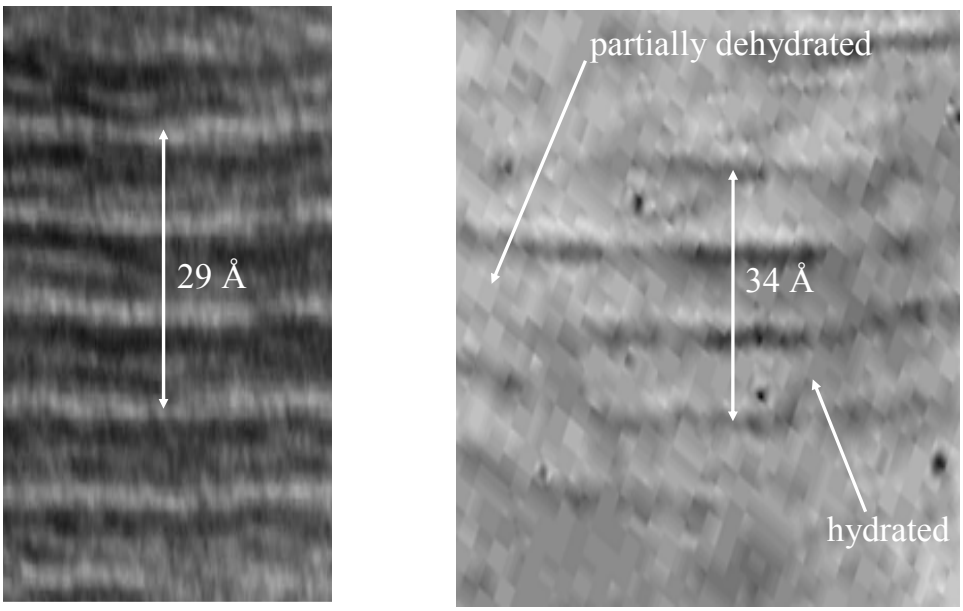

Figure 2.9. TEM image of $K_xZr_2N_2SCl_x$ showing (a) dehydrated and (b) hydrated and dehydrated regions.

Notably, the dehydrated and hydrated regions in the TEM images are from the same crystallite, indicating the reversible nature of the hydration process. XRD data

shows that the c-lattice parameter for the hydrated materials does not depend on the nature of the alkali metal, indicating that the inter-layer spacing is dictated by the water molecule size. Presumably, the water molecules are hydrogen bonded to the interlayer sulfide and chloride anions, however the exact crystal symmetries of these hydrated phases are unknown.

2.4 Discussion

Noteworthy in this work is that topotactic anion exchange has provided a means to both Zr_2N_2S phases as well as the Na_2S and NaCl excess compounds. To date, other possible synthetic routes to these materials are not known. Also, lower reaction temperatures afford the lower temperature α-Zr_2N_2S phase due to the metathesis pathway. After the alpha phase is converted to the higher temperature beta phase, it cannot be forced to revert back to the original alpha phase. Therefore, the alpha phase can potentially be described as metastable. The structural differences between the alpha and beta forms of Zr_2N_2S are interesting also. Intuitively one might speculate that the alpha phase, having sulfur in an octahedral SZr_6 unit (rather than the trigonal prismatic SZr_6 in the beta phase) should be more stable. However, for reasons that are unclear, we see that this phase is only metastable and higher temperatures lead to the higher symmetry (hexagonal rather than trigonal) beta phase.

The excess sodium sulfide stabilized phase shows intriguing compositional stability. Once prepared, the Na_2S content in the $Na_{2x}Zr_2N_2S_{1+x}$ phase does not change, even with further heating with or without excess Na_2S. The $Na_{2x}Zr_2N_2S_{1+x}$ and Zr_2N_2S compounds are formed competitively, and cannot be interconverted.

Notable as well is that reacting either Zr_2N_2S polymorph with NaCl or Na_2S does not yield the corresponding $Na_xZr_2N_2SCl_x$ or $Na_{2x}Zr_2N_2S_{1+x}$ compounds. It should also be noted that very precise control over stoichiometry is important in these reactions. These compounds provide very good examples of how kinetic control can take precedence, even in the solid state. A variety of materials were prepared from the same precursors, only by varying reaction conditions. Often during synthesis, if reactant stoichiometries and temperatures were not monitored closely, mixtures of the reported compounds were obtained. Success in these experiments is likely due to the topotactic nature of the reaction, retaining the basic parent structure of ZrNCl, rather than the combinatorial type approach taken by Lissner and Schleid.[101,102] The motivation behind this type of chemistry is important also. Unlike cation exchange which is well documented and studied in many systems such as perovskites,[109,110] the idea of solid state anion metathesis (which compounds such as ZrNCl are well suited) is infrequently utilized. An entire array of new and unknown rationally designed materials may be possible by using anion metathesis on precursor materials such as ZrNCl.

Chapter 3:

Synthesis and Characterization of the Alkali Stabilized ZrNX Fluoride Phases (X = Cl, Br, I)

3.1. Introduction

The MNX (M = Zr, Hf; X = Cl, Br, I) family of compounds has become well known, showing interesting structural and physical properties.[54,84,85] These materials are lamellar, comprising M-N hexagonal net layers in the a-b plane (see Figure 1.1, Introduction).[82,90] In the c direction, double layers of chloride ions are separated by van der Waals interactions and sandwich double M-N layers. Depending on the group IV metal and the halide, the stacking sequences vary slightly, giving either the SmSI or YOF structure types.[90,111]

Superconductivity has been the most widely studied feature of these materials since a T_c of 25 K was found for Li–doped HfNCl.[91,112] Typically, alkali metal radicals can be intercalated into the van der Waals gap by vapor transport or solution methods, effectively reducing the group IV metal and adding charge to the M-N layers.[53,113] Intercalation of organometallics as well as deintercalation of the interlayer halides to induce superconductivity has also been reported.[85,100,114] Novel structure-property relationships in this system range from optoelectronic properties to potential zirconium nitride nanotube precursors.[115,116] Properties such as these often show anion dependence in solid state materials and therefore could be controlled by anion variation.

Fluoride anions are especially well known for dictating interesting and unusual properties in materials. Properties such as low phonon energies (relative to oxides), resistance to short wavelength radiation, and low non-linear refractive indices have attracted interest to alkali rare-earth fluorides as laser materials.[117,118] Naturally occurring and synthetic perovskite structured fluorides have also been the subject of recent structural investigations.[119,120] It is possible that the MNX fluoride structural analogue may provide novel properties, such as a higher superconducting T_c in these materials.

Although the fluoride MNX (M = Zr, Hf; X = Cl, Br, I) structural analogue is unknown, a zirconium nitride fluoride phase, ZrN_xF_{4-3x}, has been reported by Jung and Juza.[121] This phase is orthorhombic, having many superstructure modifications that vary with composition. One particular composition, $ZrN_{0.906}F_{1.28}$ was characterized with a 27-fold a-axis superstructure (space group *Cm*2*a*) with a fluorite-type subcell. This fluorite type cell is expected due to the tendency of N-F pairs to chemically resemble two O^{2-} units. Although this phase was synthesized by ammonolysis of ZrF_4 at 580 ^oC, another study claims that ammonolysis of β-ZrF_4 or $ZrF_4 \bullet NH_3$ at similar temperatures yields ZrNF and $Zr_4ON_3F_5$.[122] In this case, ZrNF crystallizes in the $P2_1/c$ space group, isotypically to baddeleyite ZrO_2. This study suggested that the 27-fold superstructure described by Jung and Juza was actually an oxygen containing, coherent intergrowth of $Zr_5ON_4F_6$ and $Zr_6ON_5F_7$, two members of a Vernier type M_nX_{2n+1} homologous series. After reporting a composite modulated structure approach toward the structural description of the ZrN_xF_{4-3x} system, Schmid, et. al. thoroughly studied the compositional range of this phase.[123,124] Although their

findings indicate structural features similar to that reported by Jung and Juza,[121] the purity (oxygen free) of the nitride fluoride is questionable. Their description of this phase is "an incommensurate, compositely modulated structure, with a continuously variable, composition-dependent, primary modulation wave-vector."[123] Regardless, the reported ZrNF and oxynitride fluoride phases all have ZrO_2 or related structures due to the thermodynamic stability of this structure type. Importantly, none of these resemble the MNX lamellar phases where M = Hf, Zr and X = Cl, Br, I.

It is known that β-ZrNCl can be obtained by ammonolysis of $ZrCl_4$ at 300-400°C followed by heating to 600°C, as well as directly reacting Zr or ZrH_2 with sublimed NH_4Cl.[18,83] However, these synthetic routes do not lead to the isostructural fluoride member of the MNX family. Previously, chloride for sulfide exchange was achieved, giving new sulfide derivative phases of ZrNCl, showing this method to be a successful means to exchange the anions in this system without drastically changing the parent host structure.[125] Described herein is the topochemical synthesis of $A_{0.3}ZrNF_{1.3}$ (A = Na, K) by anion exchange, a new sodium stabilized zirconium nitride fluoride phase which retains the MNCl Zr-N host matrix.

3.2. Experimental

A nitrogen filled Vacuum Atmospheres glovebox was utilized for storage and handling of air and moisture sensitive materials. A high vacuum line (10^{-5} Torr) used for all glass tube evacuation consisted of a belt driven mechanical pump followed by a glass oil diffusion pump and a liquid nitrogen trap. Evacuated silica tubes were sealed using an oxygen/hydrogen torch.

3.2.1. Synthesis

β-ZrNCl was prepared by flowing sublimed NH_4Cl over Zr metal (99.7% Cerac, 325 mesh) in an argon flow through furnace as previously reported.[82,125] Recrystallized ZrNCl (Figure 3.1) was prepared for the metathesis reactions via vapor transport by first grinding and intimately mixing 250mg (1.78mmol) of "as prepared" ZrNCl and 50mg (0.935mmol) of dry, sublimed NH_4Cl. This mixture was then loaded into 12mm x 25cm silica tubes in the glovebox and then evacuated and sealed. After heating 1^oC per minute to 800^oC and holding at that temperature for two days, the tube was opened in the glove box. The crystalline material, which had been transported to the center of the tube (the hottest zone of the furnace), was scraped from the inside walls of the tube.

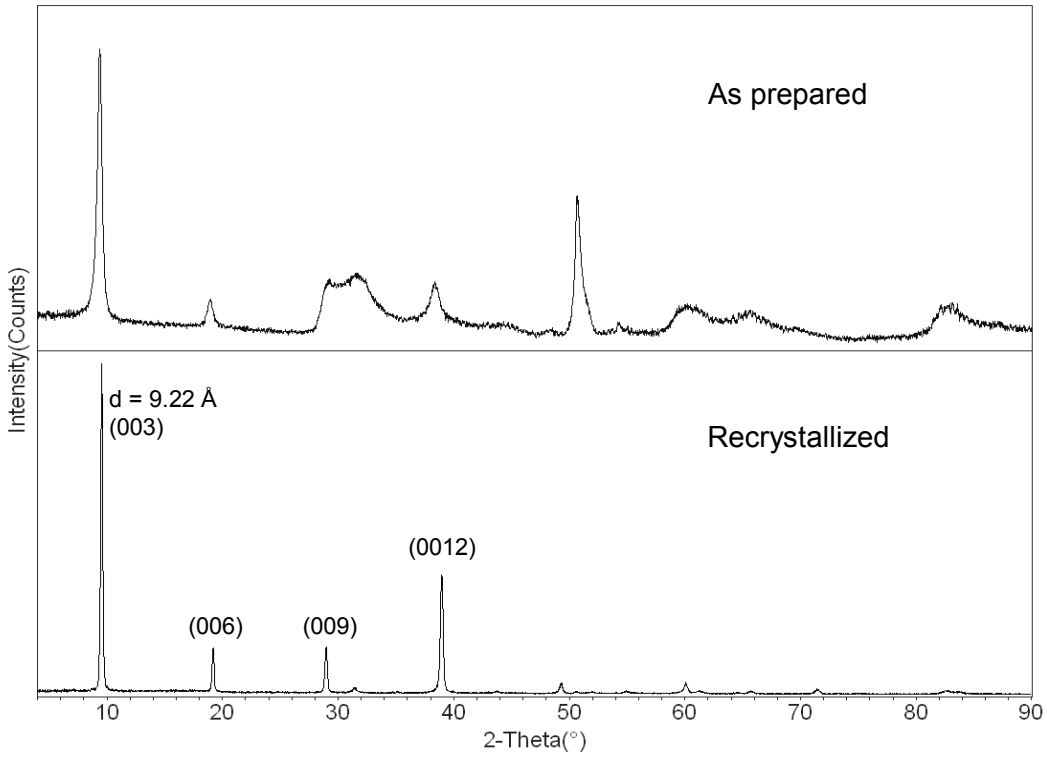

Figure 3.1. Powder XRD profiles of as prepared (top) and recrystallized β-ZrNCl starting materials showing selected [00l] reflections.

Typical batches of Na_xZrNF_{1+x} were prepared by grinding and intimately mixing 200mg (1.42mmol) of amorphous or recrystallized ZrNCl and 119mg (2.84mmol) of dry NaF. The mixtures were loaded into 9mm x 15cm silica tubes in the glovebox and then evacuated and sealed. A heat gun (approximately 150°C) was used during evacuation to remove any residual moisture. After heating at 5°C per minute to 275°C or 350°C (for amorphous and recrystallized ZrNCl reactions, respectively) and holding at that temperature for 5 days, the tube was oven cooled to room temperature and opened in the glove box. For samples made with the amorphous ZrNCl, the contents were washed and dried as described below. For

samples made with recrystallized ZrNCl, the contents were once again ground and intimately mixed with 119mg (2.84mmol) of pre-dried NaF in the glovebox. After firing in a silica tube at 350°C for 5 days a second time, the excess sodium halide byproducts were washed away by sonicating with 10mL distilled water five times. The product was dried in a 150°C oven, and stored on the benchtop.

K_xZrNF_{1+x} was prepared in a similar fashion to the Na analogue. In this reaction, 176mg (1.25mmol) of recrystallized ZrNCl was ground and intimately mixed with 145mg (2.50mmol) of dry KF. This reaction mixture was fired in an evacuated, sealed, silica tube at 275°C for 5 days. Two additional grinding/heating cycles (275°C for 5 days) were completed before washing the product with distilled water and oven drying as described above. Before each of the two additional heating cycles, 145mg of dry KF was ground and mixed with the product mixture in the nitrogen filled glovebox. After washing and drying as described previously, the powder product was stored on the benchtop.

3.2.2. Characterization

X-ray diffraction (XRD) patterns were recorded using a Bruker C2 Discover X-ray Powder Diffractometer with an HiStar area detector and CuK_α radiation. Six frames were collected with the area detector and merged to give 2θ scan ranges from 4° to 90°. Powder XRD profiles used for unit cell refinements were taken with a Bruker D8 Advance X-ray Powder Diffractometer with a Sol-X detector and CuK_α radiation from 4° to 140° in 2-theta. High temperature powder XRD measurements were taken using an Anton Parr heating stage.

Powder neutron diffraction data were collected using the BT-1 32 detector neutron powder diffractometer at the NCNR, NBSR by Dr. Brian Toby. A Cu(311) monochromator with a 90^{o} take off angle, *lambda* = 1.5402(2) Å, and in-pile collimation of 15 minutes of arc were used. Data were collected over the range of 3-168^{o} *2-Theta* with a step size of 0.05^{o}. The instrument is described in the NCNR internet web site (http://www.ncnr.nist.gov/). The sample was loaded in a vanadium can sample container of length 50 mm and diameter 6.0 mm. Data were collected under ambient conditions. Unit cell indexing and Rietveld refinements were carried out using MDI Jade, GSAS, and EXPGUI software packages respectively.[104,126,127] Rietveld analysis included usable powder neutron diffraction data in the range of 8-105^{o} *2-theta*, excluding the other data due to a very poor background associated with air scattering.

Energy Dispersive X-ray spectrometry (EDX) was performed with an AMRAY 1820K Scanning Electron Microscope with an acceleration potential of 20 kV. Wavelength Dispersive Spectrometry (WDS) was carried out with a JXA-8900 Superprobe, using calcium fluoride and zircon (ZrO_2) standards. All WDS data was obtained by Dr. Phil Piccoli of the UMCP Department of Geology. Samples and standards were mounted into casting resin epoxy plugs. Compound formulas were calculated from WDS data with reported errors generated from propagated counting statistics. Seven data spots were obtained for each sample. Zirconium values were normalized to 1.0 for final sample formulas.

Transmission electron micrographs (TEM) and Electron Diffraction patterns were recorded with a Zeiss EM 10CA Transmission Electron Microscope at 80kV

and a Hitachi Model H-7600 at 110kV. Samples were loaded onto copper grids by dispersion in water followed by placing a drop of water containing the suspended sample onto the grid and evaporating to dryness. TEM images were taken by Tim Maugel (UMCP) and Kevin McIlwrath (Hitachi).

3.3. Results

3.3.1. Synthesis

Recrystallized β-ZrNCl reacts with excess NaF at 350-400 ^{o}C for 10 days (*in vacuo* with intermediate grinding) to give a sodium fluoride excess phase of the formula Na_xZrNF_{1+x} ($x \approx 0.3$) according to eq. 3.1.

$$ZrNCl + xs\ NaF \rightarrow Na_xZrNF_{1+x} + NaCl \qquad (350\text{-}400^{o}C) \qquad \text{eq. 3.1.}$$

"As prepared" ZrNCl undergoes the same reaction, but at lower synthesis temperatures (275^{o}C) resulting in a much less crystalline product. The salt byproducts were removed by washing with distilled water, leaving the tan product. The product was characterized by powder XRD, EDS, WDS, TEM, and neutron diffraction studies.

Powder XRD analysis of the unwashed material verifies the formation of NaCl and the loss of NaF, indicating that the reaction has occurred. The product shows an expected hexagonal, lamellar (c = 18.27 Å) structure type with $P6_3/mmc$ crystal symmetry, which will be discussed in detail in the next section. EDX and WDS analysis give a Na:Zr ratio of 0.3 while WDS shows a F:Zr ratio of 1.1.

Because fluoride analysis is traditionally difficult,[128,129] this value presumably has the largest associated error and therefore a molecular formula of $Na_{0.3}ZrNF_{1.3}$ was assigned. This formula is obtained when normalizing the zirconium content to 1 compared with the sodium analysis. The fluoride content therefore must be 1.3 by charge balance, assuming that the Zr:N ratio remains 1 to 1 in the double layer Zr_2N_2 backbone of the structure (verified by Rietveld analysis in the next section). TEM images provide 5-10 nm particle sizes as well as expected 00l lattice fringes that will be discussed further in the next section. This Na_xZrNF_{1+x} phase exists in a very narrow range of x (~ 0.3) as seen by compositional analysis of several batches of the material.

Above 500 ^oC, the washed Na_xZrNF_{1+x} product slowly begins to convert to a mixture of known sodium fluorozirconate phases (Na_2ZrF_6, Na_3ZrF_7) and zirconium nitride, as verified by XRD. Reactions at lower temperatures or smaller NaF to ZrNCl ratios give only the sodium fluoride excess product and unreacted ZrNCl and do not lead to mixed Cl/F phases. If the unwashed reaction mixture is allowed to reach higher temperatures (above 500 ^oC) or if the as prepared ZrNCl is used (as in eq. 3.1) above 300 ^oC, the Jung and Juza phase is obtained.

Similar reactions between excess KF and recrystallized ZrNCl give a less crystalline product. Multiple grinding and heating cycles at 275^oC appear to give K_xZrNF_{1+x}., the excess potassium fluoride analogue, according to eq. 3.2. The salt byproducts are washed away with distilled water, as in the sodium fluoride excess case, leaving the dark green powder. Although complete analysis is not possible due

to structural uncertainty, this material has been characterized by powder XRD, EDS, and WDS.

$$ZrNCl + xs\ KF \rightarrow K_xZrNF_{1+x} + KCl \qquad (275^oC) \qquad \text{eq. 3.2.}$$

Powder XRD reveals loss of KF and verifies KCl formation, both of which wash away with distilled water (similar to the sodium analogue). The XRD structural analysis suggests a lamellar structure with an increased interlayer d-spacing ($d \approx 9.75$ Å) relative to the sodium analogue ($d \approx 9.13$) and will be discussed in the next section. EDX analysis provides an approximate 0.3 K:Zr ratio while WDS analysis gives a 1.1 F:Zr ratio. A formula of $K_{0.3}ZrNF_{1.3}$ is assigned based on charge balance as described above for the sodium analogue. Upon heating the washed product above the reported reaction temperatures, known potassium fluorozirconate phases (K_2ZrF_6, K_3ZrF_7) begin to form. It is even likely that these phases begin to form in the same temperature regime as the product, contributing to the structural ambiguity. Lower temperatures or different stoichiometries only lead to unreacted starting materials and not mixed Cl/F phases.

Additional reactions not described here between ZrNCl and CsF were attempted. Although extensive attempts were made using varying reaction conditions, the results were unclear. No product suitable for structural analysis could be obtained. EDS analysis showed no cesium in this washed product, indicating a completely different and unclear reaction mechanism than in the sodium and potassium cases.

3.3.2. Structural Studies

$Na_{0.3}ZrNF_{1.3}$: The $Na_{0.3}ZrNF_{1.3}$ phase has a double layer hexagonal unit cell with $P6_3/mmc$ crystal symmetry. Figure 3.2 shows the powder XRD profile and refined peak positions for the product made with recrystallized ZrNCl. The unit cell refinement of the powder XRD data gives $P6_3/mmc$ crystal symmetry with a = 3.660(4) Å and c = 18.14(2) Å.

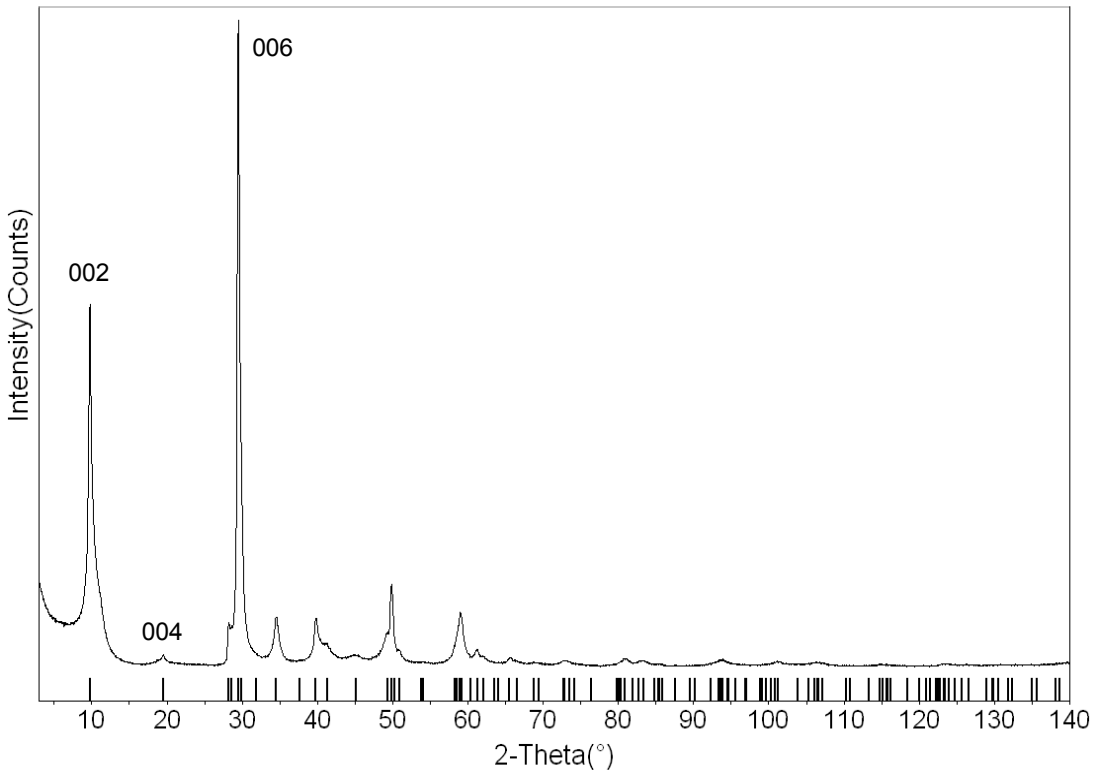

Figure 3.2. Powder XRD profile for Na_xZrNF_{1+x} with selected [00l] reflections marked. The tick marks represent calculated Bragg reflections associated with the refined unit cell.

The powder XRD profile is dominated by [00l] reflections, due to severe preferred orientation in the powder sample. Unit cell refinement data obtained from powder XRD is given in Table 3.1. Although unit cell refinements were completed with XRD, full Rietveld structural analysis could only be accomplished with neutron diffraction data. Figure 3.3 shows calculated, observed, background and difference neutron diffraction profiles. An idealized ball and stick structural drawing is given in Figure 3.4 and will be discussed later.

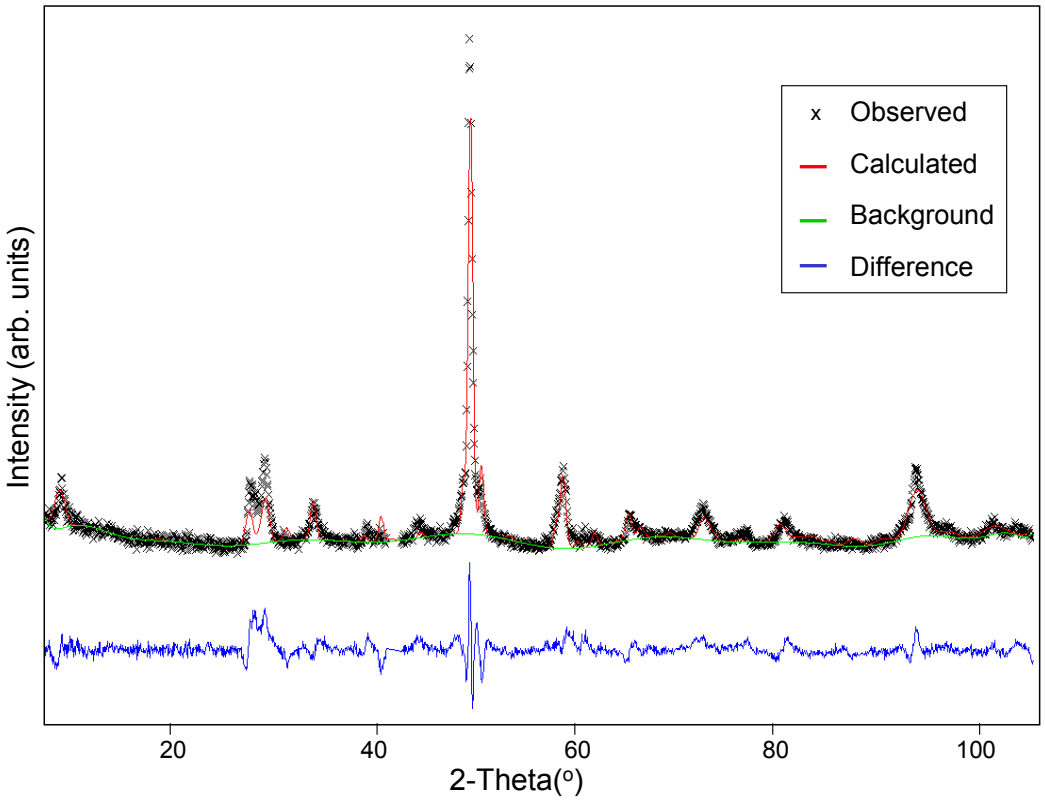

Figure 3.3. Calculated, observed, background and difference powder neutron diffraction profiles (Rietveld analysis, GSAS) for $Na_{0.3}ZrNF_{1.3}$.

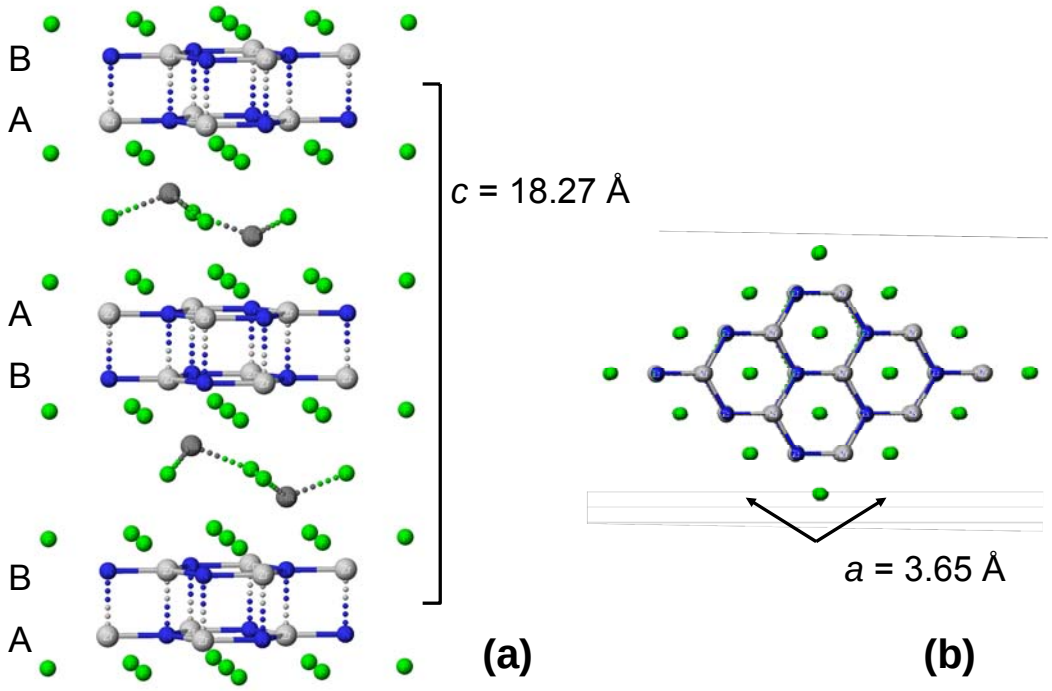

Figure 3.4. Ball and stick drawing of the layered Na_xZrNF_{1+x} structure perpendicular (a) and normal (b) to the [001] zone axis. Selected Na sites have been removed for clarity. The color scheme is as follows: zirconium – gray, nitrogen – blue, sodium – dark gray, fluoride – green.

Rietveld refinement parameters and selected bond distances and angles are listed in Table 3.1 and Table 3.2, respectively. The occupancies were fixed to match the analytical data which gave a formula of $Na_{0.3}ZrNF_{1.3}$. Minor discrepancies arise in the calculated and observed profiles, especially in the region just before 30^o (2-theta), however the overall fit is quite good considering the very poor crystallinity of the sample. Preferred orientation along the [001] vector was introduced into the neutron model to add calculated intensity to the prevalent [00l] reflections in the

powder neutron diffraction profile. This strong preferred orientation is likely due to the thin, plate-like nature of the particles (TEM, Figure 3.5). Fourier difference maps were utilitized at several points throughout the structural refinement in order to locate proper regions of nuclear density, assisting in atomic position assignment.

Table 3.1. Neutron Diffraction Rietveld Refinement Data.

Diffraction Data		Neutron	X-ray
Refinement Type		Rietveld	Unit Cell
Crystal System		Hexagonal	Hexagonal
Space Group		$P6_3/mmc$	$P6_3/mmc$
a/Å		3.654(1)	3.660(4)
c/Å		18.266(8)	18.14(2)
Preferred Orientation		0 0 1	---
ESD of fit		---	0.055
Chi ^{2}		3.628	---
R_{wp}		0.0998	---
R_p		0.0795	---
Na	x	1/3	
	y	2/3	
	z	0.703(4)	
	Beq	0.001(1)	
	occ.	0.3	
Zr	x	1/3	
	y	2/3	
	z	0.435(1)	
	Beq	0.036(4)	
	occ.	1	
N	x	1/3	
	y	2/3	
	z	0.9384(7)	
	Beq	0.020(2)	
	occ	1	
F(1)	x	0	
	y	0	
	z	0.3729((9)	
	Beq	0.064(4)	
	occ.	1	
F(2)	x	2/3	
	y	1/3	
	z	1/4	
	Beq	0.005(1)	
	occ.	0.6	

Table 3.2. Selected Bond Lengths (Å) and Angles (^{o})

Zr – N	2.112(1)
Zr – N	2.30(2)
Zr – F(1)	2.40(1)
Na – F(1)	2.52(4)
Na – F(2)	2.28(3)
N – Zr – N	119.9(1)
N – Zr – N	88.6(7)
Zr – F(1) – Zr	99.1(7)
F – Na – F(2)	79.7(4)
F(2) – Na – F(2)	107(2)

The TEM images show that Na_xZrNF_{1+x} forms as approximately 7 nm hexagonal platelet particles (Figure 3.5), further indicating the hexagonal nature of this material. High resolution imaging (Figure 3.6) shows the appropriate ~ 9 Å interlayer spacing which agrees with the XRD and neutron structural data.

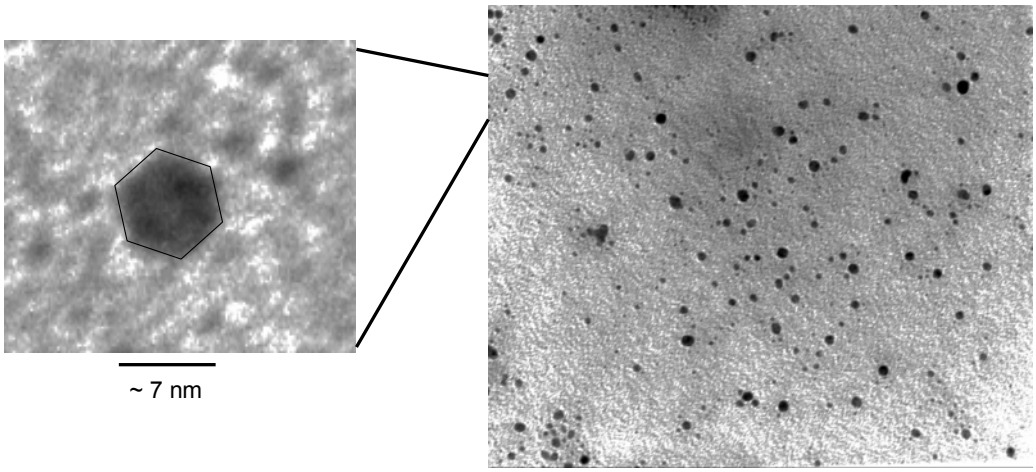

Figure 3.5. Bright field TEM image of Na_xZrNF_{1+x} with expanded area showing the approximate 7 nm particle size (hexagon outline drawn for clarity).

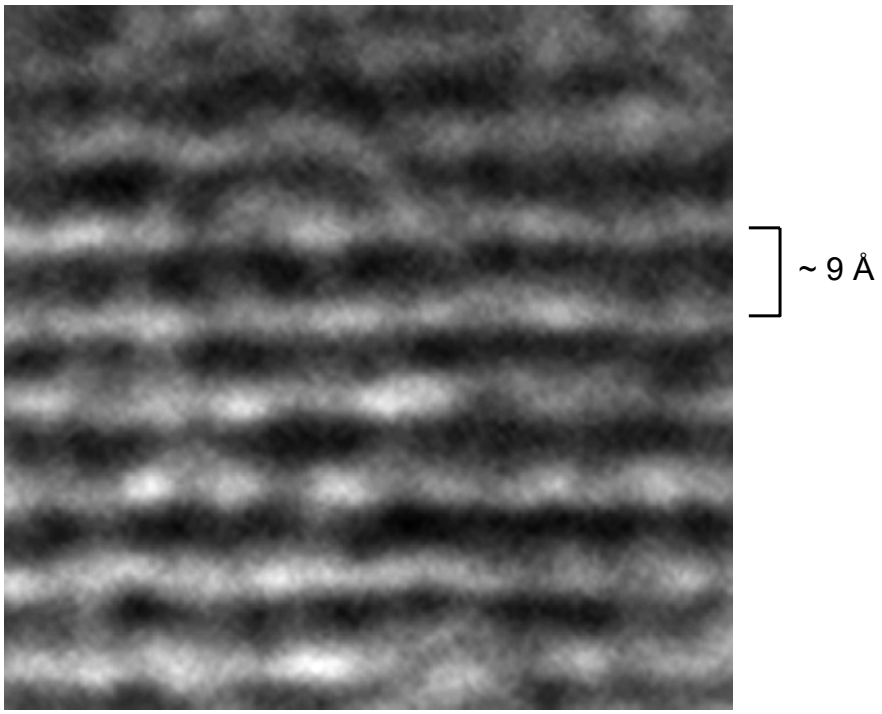

Figure 3.6. High Resolution TEM image of Na_xZrNF_{1+x} showing the appropriate interlayer spacing.

The Na_xZrNF_{1+x} structure is similar to that of β-ZrNCl (refer to Figures 3.4 and 1.1 for comparison). A slight a/b layer shift changes the ZrN layer stacking to an AB···BA···AB stacking sequence, giving a two layer repeat unit as opposed to the three layer repeat unit in ZrNCl. As in the ZrNCl structure, three fluorides are bound to each zirconium giving sequential F – Zr_2N_2 – F layers (directly replacing the chlorides of ZrNCl). In between these layers, extra sodium and fluoride ions reside in partially occupied sites as shown in Figure 3.4. These sodium sites occupy pseudo-octahedral holes between sequential fluoride layers. If the extra fluoride layer sites were fully occupied, each Na would have a pseudo-octahedral NaF_6 coordination sphere as shown in Figure 3.7.

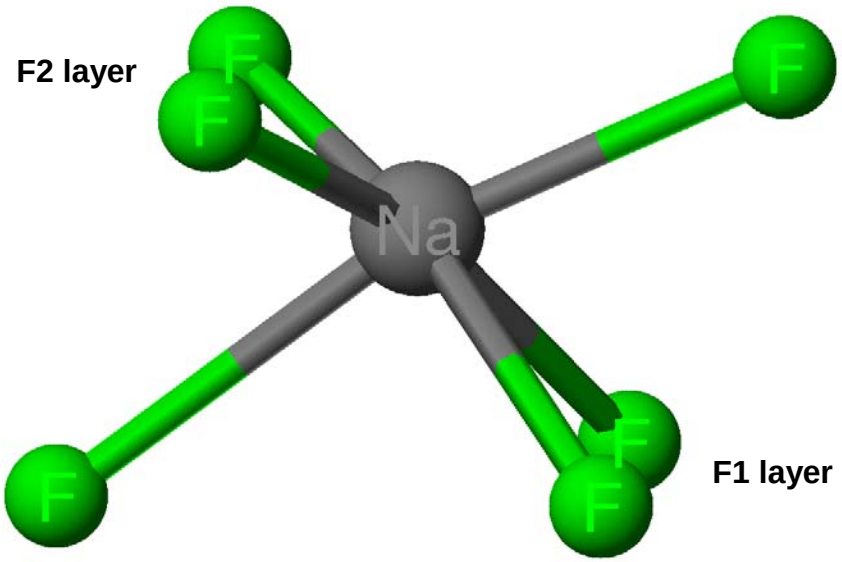

Figure 3.7. Ball and stick drawing of the NaF_6 coordination sphere of Na_xZrNF_{1+x}. The coloring scheme is as follows: sodium – dark gray, fluoride – green.

As the analytical data suggests, the interlayer Na and F sites are only partially occupied. The Na-F intercalates likely cluster in a non-ordered fashion to maximize Na coordination. The refined Zr – F (2.4 Å) and Na – F (2.28 Å) distances are typical compared to similar zirconium fluoride materials and known sodium fluorozirconates, while the 2.52 Å Na – F distance seems slightly long in this coordination.[120,122]

Bond valence calculations were carried out according to eq. 3.3 to examine this sodium coordination sphere.

$$v_{ij} = \exp[(R_{ij} - d_{ij})/b] \qquad \text{eq. 3.3.}$$

In this commonly adopted[130] empirical bond valence expression, R_{ij} is the bond valence parameter. d_{ij} represents respective bond distances between atoms *i* and *j*, while *b* is taken to be a "universal" constant (0.37) for these calculations.[131] The total bond valence (*V*) for an atom is given by the sum of each contributing valence (v_{ij}). A summary of bond valence values calculated for the Na_xZrNF_{1+x} phase are give in Table 3.3.

Table 3.3. Bond Valence Calculation Values

Atom	Coordination Sphere	Bond Valence
Zr	ZrN_4F_3	4.2
Na	NaF_6	0.9
Na	$NaNF_6$	1.07
Na	$NaNF_5$	0.87

Bond valence analysis of the zirconium coordination sphere uses the bond valence parameters of $R_{ZrN} = 2.11$ and $R_{ZrF} = 1.854$.[130] These values, along with the refined Zr – N and Zr – F bond distances (Table 3.2) give a bond valence of $V_{Zr} = 4.2$. Considering the complexity of this structure, this is a very reasonable approximation compared to the expected oxidation state (+4).

When examining the sodium bond valence using the bond valence parameter (R_{NaF}) of 1.677, we can compare several cases.[130] In the case where a NaF_6 octahedron exists, using only Na-F bonding, we obtain a bond valence of $V_{Na} = 0.90$. If we include the contribution from the next closest bound atom (nitrogen) a total of $V_{Na} = 1.07$ is calculated. If we account for the presence of vacancies by excluding an interlayer fluoride , $V_{Na} = 0.87$ for a $NaNF_5$ coordination sphere. This simple analysis

shows that the extra interlayer Na and F ions likely reside in clusters of higher occupancy to maintain a higher Na coordination rather than being completely randomly distributed throughout the layers. This vacancy-clustering phenomenon is common in many metal halide materials[132,133].

With this poorly crystalline material, the powder neutron diffraction data did not provide enough information to locate the exact interlayer sodium and fluoride sites without a certain amount of chemical intuition. The possible interlayer Na and F sites found by fourier mapping during the Rietveld refinement created several possibilities of where the extra Na – F units may be found. Of the possible sites, the most chemically reasonable places an additional fluoride layer directly between the consecutive F – Zr_2N_2 – F layers with sodium ions in the afore mentioned octahedral holes. Several sites were attempted giving various sodium and fluoride coordinations, none of which had dramatic impacts on the Rietveld model. One of these alternate structural models placed NaF_5 trigonal bipyramidal units in between the F - Zr_2N_2 - F host. Another structural possibility placed the sodium in the same plane as the F(2) layer in the reported model, giving a pseudo 9-coordinate sodium coordination sphere. However, in both of these alternate models, the bond valence analysis and calculated bond lengths (not reported here) clearly indicated that these models were improbable. Therefore in this case, the most reasonable model was chosen and refined accordingly.

As described in the previous section an amorphous Na_xZrNF_{1+x} phase is obtained from "as prepared" ZrNCl according to eq. 3.1. This amorphous material is not amenable to complete structural data due to poor crystallinity, therefore only the

product synthesized from recrystallized ZrNCl starting material was used for complete analysis and characterization. Figure 3.8 displays the amorphous nature of the unwashed product obtained from "as prepared" ZrNCl starting material and shows reflections for the NaCl byproduct and unwashed NaF. Also notable is that the [00l] reflections do not shift upon washing with water, indicating that these materials do not intercalate water as the alkali chloride sulfide materials in Chapter 2.

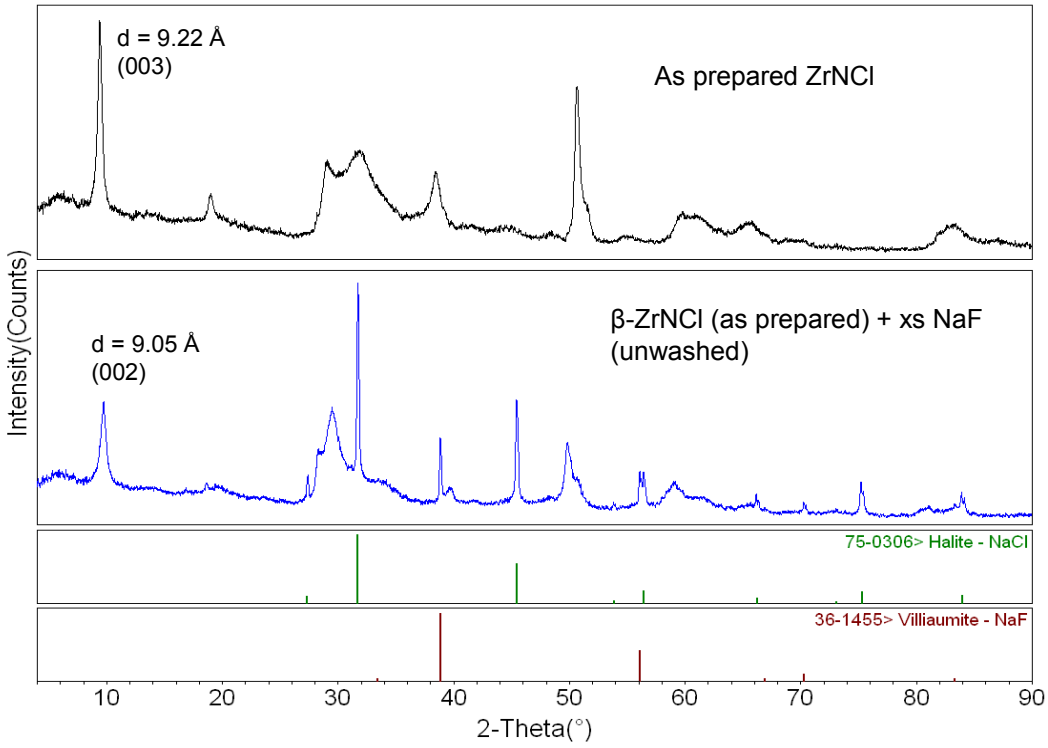

Figure 3.8. Powder XRD profiles of as prepared ZrNCl (top) and the amorphous Na_xZrNF_{1+x} phase (bottom) obtained from as prepared starting material. The green and red tick marks indicate Bragg reflections for NaCl (JCPDF 75-0306) and NaF (JCPDF 36-1455), respectively.

$K_{0.3}ZrNF_{1.3}$: The $K_{0.3}ZrNF_{1.3}$ phase is most likely a structural analogue of the sodium phase, having $P6_3/mmc$ crystal symmetry with the same unit cell *a* lattice parameter (~ 3.6 Å). Although complete structural analysis is not possible due to lack of crystallinity, powder X-ray diffraction suggests a lamellar structure (Figure 3.9) with an increase in the interlayer spacing compared to the $Na_{0.3}ZrNF_{1.3}$ phase.

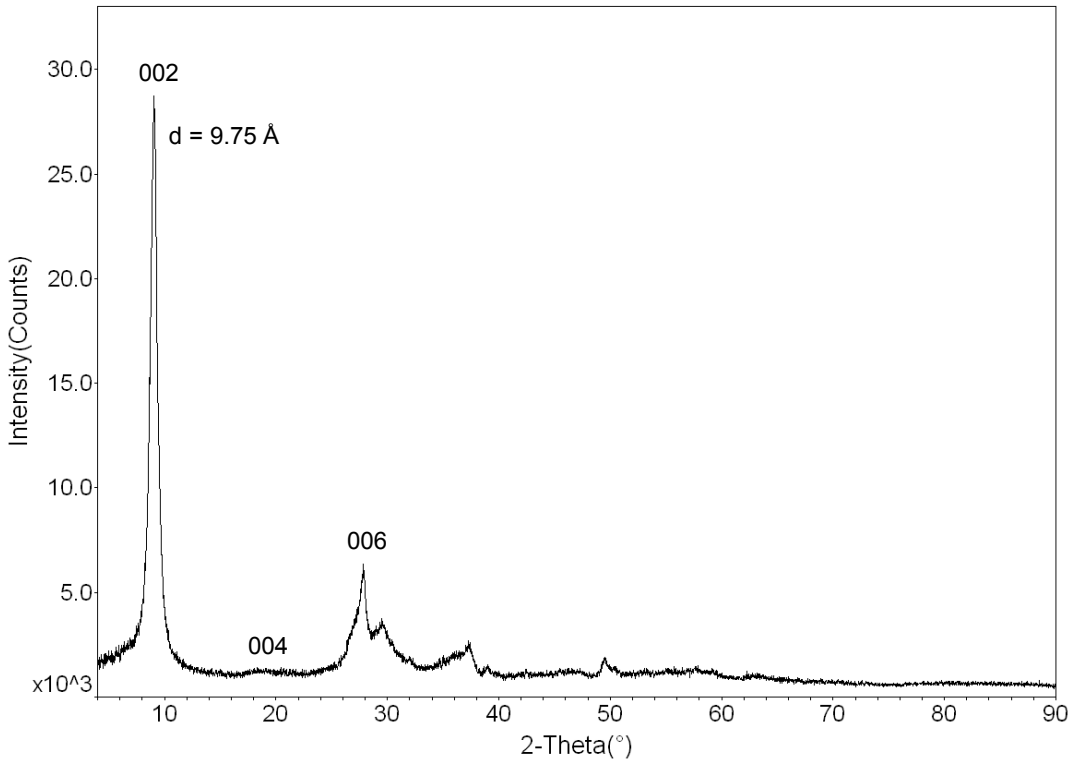

Figure 3.9. Powder XRD profile of $K_{0.3}ZrNF_{1.3}$ showing the increased low angle [00l] reflection.

The *c* lattice parameter was estimated from prominent powder X-ray diffraction [00l] reflections. The XRD profile is characteristically broad and could possibly contain reflections from impurity phases. Rietveld and unit cell refinements

could not be obtained for this material, therefore the structural analysis is speculative. However, comparisons can be made by using the crystal symmetry and relative atomic positions of the sodium analogue. Retaining the Zr – N and Zr – F bond distances from $Na_{0.3}ZrNF_{1.3}$ and expanding the unit cell *c* lattice parameter to 9.75 Å (value obtained from powder XRD) leads to K – F distances of 2.34 Å and 2.63 Å within the structure, which are reasonable when considering the multiple coordination sphere. Bond valence analysis using these calculated bond lengths provides bond valence values of 0.8 (KF_6), 1.1 (KNF_6) and 0.9 (KNF_5). As in the sodium case, these values indicate the likelihood of clustering to occur, maintaining an alkali bond valence close to one.

3.4. Discussion

Cation metathesis has become a well-known topochemical method for materials design, especially in solid state oxide chemistry.[134-136] Cations can be exchanged in and out of inorganic hosts having little or no effect on the bulk material properties.[4] Conversely, anions often account for many of the structural and physical properties of a material. For example, the structure type and stacking sequence of the MNX family (M = Zr, Hf; X = I, Br, Cl, F) depends mostly on the anion present in the host. [90,111].

Notably, a topochemical method such as anion metathesis was necessary to obtain a fluoride analogue to the MNX family that traditional synthetic methods could not provide. ZrNF (with the ZrNCl structrure) was the target phase, but it was not accessible without an AF (A = Na, K) intercalant. It appears that the excess,

interlayer alkali fluoride plays a major role in stabilizing this structure. Excess sodium fluoride provides a material that is well characterized, structurally and analytically. In the reactions between ZrNCl and KF, XRD analysis shows the expected increase in the interlayer d-spacing while preliminary EDX analysis shows a K:Zr ratio similar to the sodium analogue. Although these initial data were promising, full analysis of this material is not feasible due to the extremely poor crystallinity which makes complete structural characterization impossible. Many heat and regrind cycles are necessary to obtain chloride free product, making it very difficult to obtain clean, pure samples for any additional characterization as well. As previously mentioned, cesium fluoride reactions do not follow this same reaction pathway. The decreasing ability to make these alkali fluoride excess phases with increasing alkali size suggests a structural stability dependence on the alkali metal. This fact can possibly be explained by comparing the favorable alkali – fluoride stabilization and the alkali crystallographic sites. Although the alkali metal stabilizes the structure, larger alkali metals may disrupt this stabilization, most likely by creating structure defects due to size even to the point of preventing formation of this structure type in the cesium case.

Similar reasons may explain why pure ZrNF may not be attainable. Since fluoride is such a highly electronegative anion, interlayer cation stabilization is likely necessary to maintain this layered structure type. In this case, F – F repulsions are possibly too large to allow a stable structure, requiring Na^+ ions to mediate this repulsion. One might expect that sodium can go into the layered structure because of its small size and that larger cations (i.e. cesium) should give alkali free, layered

ZrNF. However, as shown here, this is not the case. The stability of these kinetically stable fluoride MNX analogues likely relies on a balance between interlayer cation stabilization and small cation size.

The structural analysis, specifically the Rietveld refinement, proved to be a complicated task. The powder XRD profile is severely dominated by [00l] reflections, due to the strong preferred orientation, making Rietveld analysis impossible with XRD data. Therefore, powder neutron data was obtained for Rietveld analysis. The possibility of a very small amount of oxide contamination also exists in the phases reported here. Fluoride readily reacts at elevated temperatures with glass, such as the tubes used in these experiments. Although no sign of glass etching was evident, it is possible that some of the fluoride sites are occupied by oxides, which could further explain the minor discrepancies in the WDS data. This contamination could also impact the Rietveld refinement results, decreasing the quality of the fit.

Chapter 4:

Two Dimensional Alkoxide/ZrN Hybrids from ZrNCl

4.1. Introduction

Organic/inorganic hybrid materials have become a central focus in materials chemistry. Combining organic functionalities and inorganic rigidity has provided many interesting properties and new materials. This is especially true regarding oxide chemistry. For example, flat TiO_2 – polythiophene arrays, synthesized by sol-gel techniques, are being investigated as photovoltaic (PV) cells.[137] Sol-gel methods have also been used to prepare silicate based solid state lasers based on organic/inorganic hybrids.[138,139] Integrating nanosized oxide clusters into a conducting polymer matrix has been suggested as a means to solid state electrochemical supercapacitors.[140] Hybrid oxide nanocomposites also show many interesting optical characteristics including photochromic, nonlinear optical (NLO), photorefractivity, sensing properties, etc.[141,142]

Adding functionality to an inorganic host can provide interesting morphology as well. For example, Mallouk has shown that layered, perovskite oxides can be exfoliated into individual layers by protonating the layers, followed by reacting with bulky bases.[143,144] The layers are effectively pealed apart and can be recombined into films or other novel structures such as nanoscrolls.[110,145] Hydrophilic/hydrophobic interactions between the layers and solvent systems are responsible for exfoliation

and scrolling, showing morphology control by adjusting functionality within the parent structure.

Inorganic oxides comprise the majority of the previously mentioned novel structures made by controlling interlayer functionality. However, another interesting example may be provided by the MNX family of compounds (M = Zr, Hf; X = Cl, Br, I).[82,90,146] Although well known for properties such as superconductivity (T_c = 25K for HfNCl),[51,52] this material is rarely considered as a functional inorganic host. Literature studies have suggested structural and electronic properties of ZrNCl based nanotubes, if they were to be synthesized.[115] This study shows interesting electronic features, however the authors have overlooked the likelihood of these layered compounds to form oxide-like nanoscrolls rather than nanotubes structures.[110]

Recently, chloride for alkoxide exchange has been reported in the layered zirconium phosphate materials.[147] In this zirconium phosphate system, the number of carbons in the alkoxide chain is directly proportional with the interlayer spacing. The alkoxide chains are held by Zr – O bonding as we might expect for alkoxide for chloride exchange in the ZrNCl system. Although alkoxide exchange in the zirconium phosphate materials can be achieved via mild molecular (in solution) routes, we expect that similar exchange in a true refractory material such as ZrNCl would be much more challenging.

We have shown that ZrNCl can undergo rare anion exchange, due to its layered nature, that is similar to the cation for proton exchange used to achieve many of the exfoliated oxide structures.[125,148] Successful chloride-for-sulfide and chloride-for-fluoride exchange has provided a variety of new, metastable materials that can

only be prepared by anion exchange in the ZrNCl system. As previously shown, it is likely that the chlorides can be exchanged for other anions, leaving the zirconium nitride backbone relatively unchanged. Reported here is the exchange of chlorides for alkoxides (methoxide, ethoxide, *n*-butoxide) by solvothermal-assisted anion metathesis, providing a new class of zirconium based organic/inorganic hybrid materials which may pave the way to future zirconium nitride nanoscrolls/tubes.

4.2. Experimental

A nitrogen filled Vacuum Atmospheres glovebox was utilized for storage and handling of air and moisture sensitive materials. All air sensitive solution processes were carried out using standard Schlenk techniques. The high vacuum line used for all glass tube evacuations consisted of a belt driven mechanical pump followed by a glass oil diffusion pump and a liquid nitrogen trap. Evacuated pyrex tubes were sealed using an oxygen/methane torch. The alkoxide starting materials were used as purchased from Sigma-Aldrich. The THF was distilled from sodium benzophenone ketyl. All alcohol solvents were treated with activated molecular sieves, followed by degassing with a nitrogen purge and storing under nitrogen.

4.2.1. Synthesis

Dry NH_4Cl was sublimed over Zr metal (99.7% Cerac, 325 mesh) at 600^{o}C for 3 hours in order to prepare β-ZrNCl as previously reported. [82,125] β-ZrNCl was recrystallized for use in metathesis reactions by ammonium chloride assisted vapor transport. First, 250mg (1.78mmol) of as prepared ZrNCl and 50mg (0.935mmol) of

dry, sublimed NH_4Cl were ground and intimately mixed. This mixture was then loaded into a 12mm x 25cm silica tube in the nitrogen atmosphere glovebox. The tube was then evacuated on the high vacuum line and torch sealed. After heating 1^oC per minute to 800^oC and holding at that temperature for two days, the tube was allowed to cool to room temperature and opened in the glove box. The crystalline material, which had been transported to the center of the tube (the hottest zone of the furnace), was scraped from the inside walls of the tube. CAUTION: Sealed tubes should be treated with care due to pressure created by gas formation within the reaction tube.

ZrN(OR) (R = Me, Et, *n*-Bu) compounds were prepared by solvothermal methods. For example, the ZrN(OEt) compound (OEt = OC_2H_5) was prepared as follows. 180mg (1.28mmol) of recrystallized ZrNCl was ground and intimately mixed with 215mg (2.56mmol) of potassium ethoxide in the glovebox. This mixture, along with 1mL of distilled THF (tetrahydrofuran) was added to a thick walled 9mm x 15cm pyrex tube. The reactant/THF mixture was then degassed (freeze-pump-thaw cycles) using the high vacuum line and liquid nitrogen a minimum of three times. The tube was then frozen with liquid nitrogen and sealed with a methane/oxygen torch *in vacuo*. The reaction tube was then placed into the steel solvothermal pressure vessel which was filled with distilled water. The pressure vessel cap was tightened and the vessel was attached to the solvothermal reactor. After purging the solvothermal system of air, the preheated furnace (200^oC) was raised to engulf the pressure vessel. The furnace was shut off after 1 week and lowered away from the pressure vessel. Upon cooling to room temperature, the vessel was opened and the reaction tube was removed. The tube was opened after freezing with liquid nitrogen

and quickly placed on the Schlenk line under flowing nitrogen. The tan product mixture was dried under flowing nitrogen, followed by vacuum. The product was washed on the Schlenk line with ethanol five times, leaving the white powder product.

ZrN(OMe) was prepared (OMe = OCH_3) by similar solvothermal methods as well as methanol exchange with the zirconium nitride ethoxide material. For the solvothermal synthesis, 151mg (1.07mmol) of recrystallized ZrNCl was ground and intimately mixed with 450mg (6.42mmol) of potassium methoxide in the nitrogen atmosphere glovebox. This mixture was added to a thick walled 9mm x 15cm pyrex tube along with 1mL of distilled THF. The contents of the tube were then degassed and sealed as described above. The tube was loaded into the solvothermal reactor which had been preheated to 225^{o}C, and allowed to heat for 1 week. Upon removing the furnace and cooling to room temperature, the tan product was washed five times with methanol and dried on the Schlenk line as describe above, leaving a white powder.

To obtain the zirconium nitride methoxide product by ethoxide for methoxide exchange, approximately 100mg of zirconium nitride ethoxide was placed in a flask on the nitrogen Schlenk line. 30 mL of absolute methanol was added and the mixture stirred for 24 hours. After removing the methanol washing with a syringe, the product was dried under vacuum and stored in the glovebox.

ZrN(O*n*-Bu) was prepared (O*n*-Bu = O*n*-C_4H_9) by similar solvothermal methods. In this reaction, 167mg (1.19mmol) of recrystallized ZrNCl was ground and mixed with 450mg (4.68mmol) sodium *n*-butoxide and then transferred to a thick

walled pyrex tube with 1 mL of distilled THF. The remaining portion of the reaction was carried out as described for the ethoxide case with some changes. This reaction required two subsequent heating cycles at 250^{o}C for 8 days each, adding 340mg (3.54mmol) sodium *n*-butoxide to the reaction mixture before the second cycle. The final product was washed five times with 1-butanol and dried on the Schlenk line under vaccuum.

4.2.2. Characterization

A Bruker C2 Discover X-ray Powder Diffractometer with an HiStar area detector and CuK_{α} radiation was used for all powder X-ray diffraction (XRD) data. Typically, six frames were recorded with the area detector and merged to give scan ranges of 4 – 90^{o} in 2–theta. XRD sample holders for air/moisture sensitive materials were covered with polyethylene wrapping and sealed with vacuum grease. All powder XRD data analysis was carried out using MDI Jade software.[104]

An AMRAY 1820K Scanning Electron Microscope with an EDAX detector and an acceleration potential of 20 kV was used to perform all Energy Dispersive X-ray spectrometry (EDX) measurements. Washing with the respective alcohols only removes all of the unreacted alkali alkoxide starting materials, therefore the zirconium nitride alkoxide compounds were washed with distilled water before analyzing chloride content. Although water washing destroys the ZrNOR (R = Me, Et, O*n*-Bu) product, this analysis is only to show complete loss of chloride from ZrNCl, which does not react with or dissolve in water. Powder samples were placed

on carbon tape covered aluminum sample holders before loading into the EDX chamber.

Thermo-Gravimetric Analysis (TGA) was carried out with a TA Instruments TGA Q500 system with air sample purge and nitrogen balance purge gases. All samples were taken from the nitrogen glovebox in nitrogen filled vials and quickly loaded into platinum pans immediately prior to starting the temperature program. Typical heating cycles ran from room temperature at $2^{o}C$ per minute to $1000^{o}C$, followed by cooling to room temperature before unloading the samples. Powder X-ray diffraction was performed on each of the samples after the TGA runs to confirm the decomposition products. Weight loss percentages were taken from the point just prior to alkali halide salt loss, when applicable. The loss of alkali halide byproducts was verified by powder XRD and EDX. Expected weight loss values were calculated assuming total decomposition to ZrO_2 in each case, which was verified by XRD analysis.

Infrared (IR) Spectroscopy measurements were carried out with a ThermoNicolet Nexus 670 FTIR Spectrometer with a tungsten source. Each spectrum consists of 32 scans. All reported spectra have been corrected for background features arising from air. Measurements were obtained using standard KBr pellet methods. Approximately 5mg of each sample was ground and mixed with approximately 100 mg of dry KBr using a mortar and pestle before compressing each mixture into pellets. The pellets were kept under a nitrogen atmosphere before loading into the IR spectrometer.

4.3. Results

4.3.1. Synthesis

Recrystallized β-ZrNCl reacts with 2 equivalents of KOC_2H_5 at 200°C (solvothermally – THF) *in vacuo*, providing $ZrN(OC_2H_5)$ after 1week according to eq. 4.1. The white powdery product is obtained upon removing the excess KOC_2H_5 with ethanol. The product has been characterized by powder XRD, EDX, TGA, and IR spectroscopy studies.

$$ZrNCl + xs\ KOC_2H_5 \rightarrow ZrNOC_2H_5 + KCl + xs\ KOC_2H_5 \quad (200^oC) \qquad \text{eq. 4.1.}$$

Powder XRD analysis of the white product (ethanol washed) indicates a complete conversion of the ZrNCl starting material but shows retention of some KCl byproduct, that was not washed away with ethanol. Upon washing with distilled H_2O, EDX analysis confirms the presence of zirconium and shows a total loss of chloride. Although washing with distilled water decomposes the product, the total loss of chloride indicates that all of the ZrNCl had reacted. The compound retains a layered structure, comprising zirconium – nitrogen double layers and interlayer ethoxide groups which will be shortly discussed in detail in terms of TGA, XRD, and IR spectroscopy studies.

Recrystallized β-ZrNCl reacts with (excess) $KOCH_3$ at 225°C (solvothermally – THF) *in vacuo* to give $ZrN(OCH_3)$ after 1week according to eq. 4.2. The white

powder product is obtained upon washing out the excess $KOCH_3$ and KCl byproducts with absolute methanol.

$ZrNCl + xs\ KOCH_3 \rightarrow ZrNOCH_3 + KCl + xs\ KOCH_3$ (225°C) eq. 4.2.

Upon washing with methanol or distilled water, a total loss of potassium and chloride was observed showing removal of the excess $KOCH_3$ and KCl byproduct. K_2CO_3 was also observed in the XRD profile of the unwashed material, likely due to decomposition of $KOCH_3$ under these synthetic conditions. The absence of chloride indicates that all of the ZrNCl starting material has reacted. This product also retains a layered structure according to XRD, in this case containing methoxide groups between the zirconium nitride double layers. Although this product does appear to form, it is not likely a single phase product as indicated by TGA and XRD. The TGA, XRD, and IR spectroscopy characterization will be discussed in the next section.

Recrystallized β-ZrNCl reacts with a excess NaO*n*-Bu at 250°C (solvothermally – THF) *in vacuo* to give ZrNO*n*-Bu according to eq. 4.3. Two grinding and heating cycles (8 days each) with intermediate addition of sodium *n*-butoxide is required to obtain a complete reaction. The product is obtained upon washing with 1-butanol.

$ZrNCl + xs\ NaOn\text{-}Bu \rightarrow ZrNOn\text{-}Bu + NaCl + xs\ NaOn\text{-}Bu$ (250°C) eq. 4.3.

Upon washing with distilled water, EDX analysis confirms the presence of zirconium and the absence of sodium, indicating removal of the excess NaO*n*-Bu and NaCl byproduct. A complete loss of chloride is observed as well, signifying that all of the ZrNCl starting material has reacted. As in the ethoxide material, water washing decomposes this phase, however, this water washed material is only used to verify complete conversion of the ZrNCl starting material.

β-ZrNCl reacts with a series of alkoxide compounds with varying reaction temperatures, durations, and stoichiometries. All of these phases are extremely unstable in air and immediately begin to decompose when removed from an inert atmosphere. As-prepared zirconium nitride chloride (without recrystallizing) also appears to react in a similar fashion, however, due to lack of product crystallinity only products obtained from recrystallized ZrNCl starting material will be further discussed. TGA, powder XRD and IR spectroscopy characterization are described below for each phase in addition to THF insertion and methoxy exchange studies illustrating the functionality of these compounds.

4.3.2. Characterization

TGA Studies: After accounting for unwashed KCl, the TGA of ZrN(OEt) shows a 14% weight loss which agrees quite well with the expected 15% loss. This expected loss is calculated by assuming complete conversion of the alkoxide product to zirconium oxide (verified by XRD). While less defined transitions are present, an immediate and steady weight loss is observed throughout the TGA run (Figure 4.1), indicating the instability of this material in the presence of air. The final major

transition (starting near 650°C) represents the sublimation of the KCl byproduct upon heating, which has been verified by powder XRD and EDX.

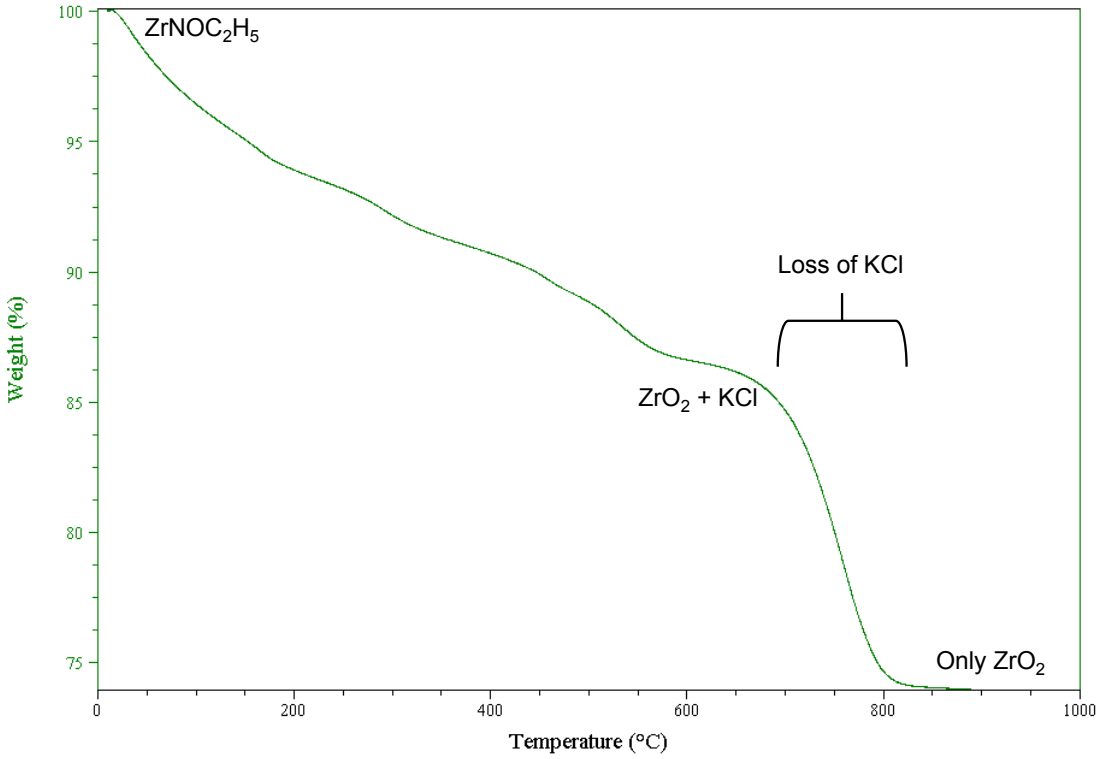

Figure 4.1. TGA weight % vs. temperature curve for ZrN(OEt).

As in the ethoxide product, TGA of ZrN(OMe) (Figure 4.2) indicates the tendency of these materials to quickly and steadily decompose in the presence of air in addition to illustrating a more defined transition.

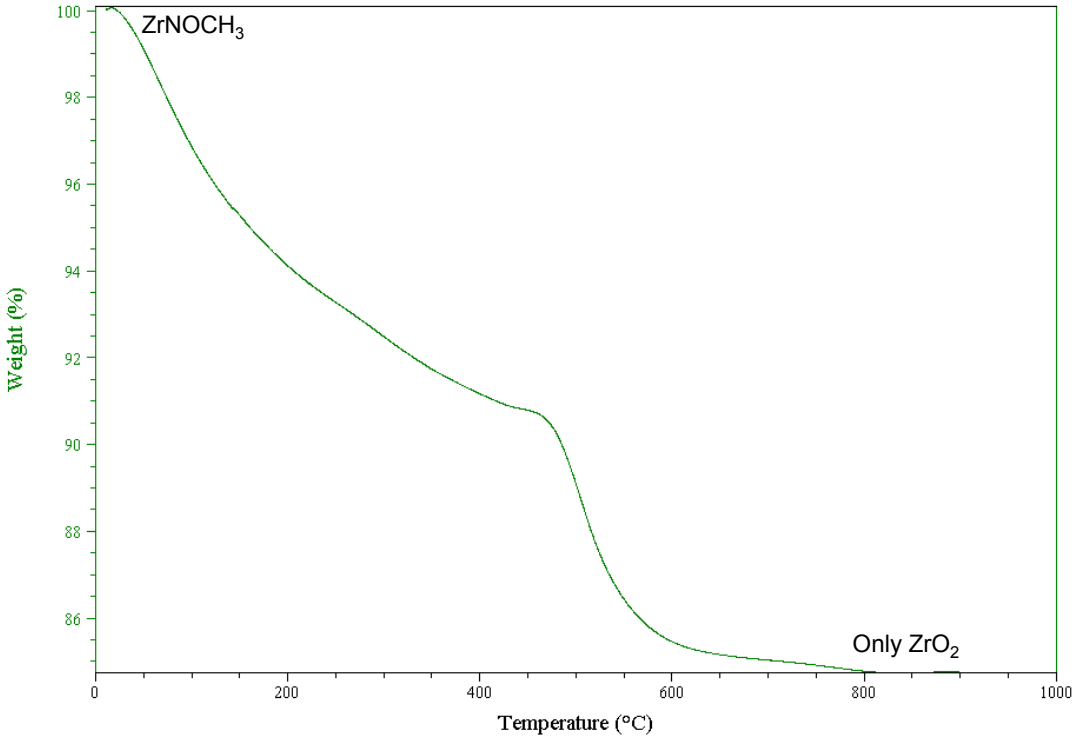

Figure 4.2. TGA weight % vs. temperature curve for ZrN(OMe).

The ZrO_2 final decomposition product from TGA was confirmed by powder XRD. The observed weight loss in this material is approximately 15%, although only 10 % is expected when converting $ZrOCH_3$ to ZrO_2, directly indicating an impure (or solvated) product.

The TGA of ZrN(O*n*-Bu) (Figure 4.3) shows similar air sensitivity. Steady decomposition in air is indicated by mass reduction even at ambient temperatures near the start of the TGA temperature program. Sharper TGA transitions are also observed, in addition to the NaCl loss transition (near 650^{o}C), verified by XRD and EDX.

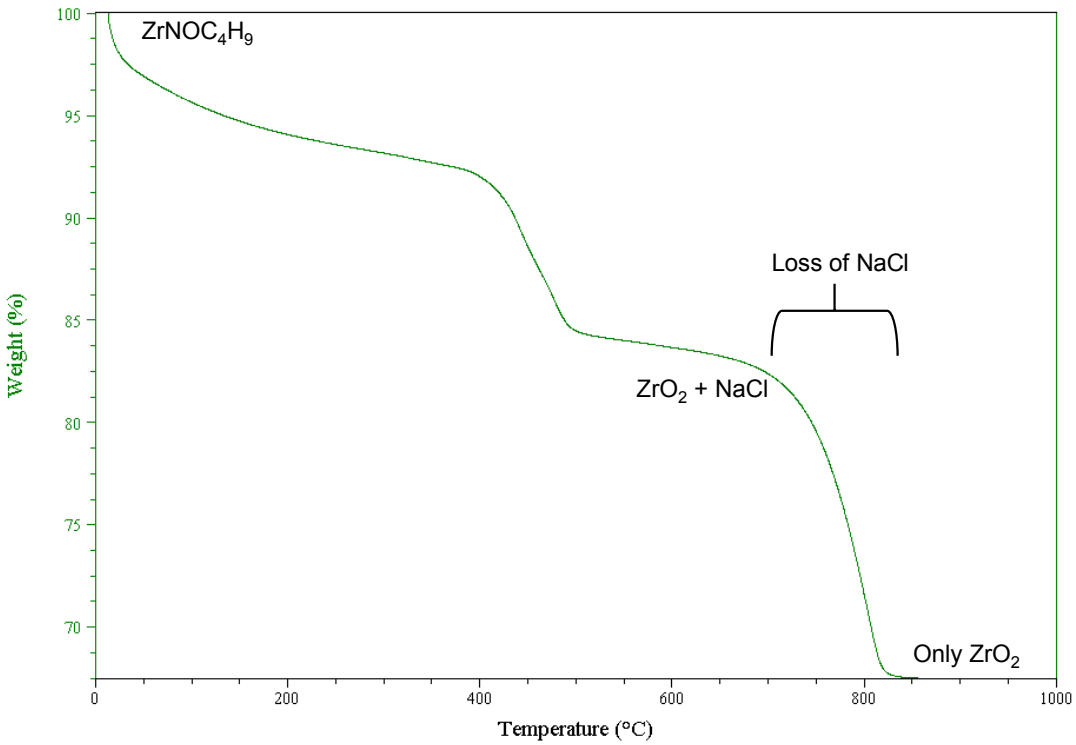

Figure 4.3. TGA weight % vs. temperature curve for ZrN(O*n*-Bu).

In this material, a weight loss of 22% is expected after accounting for the NaCl byproduct present in the material. An 18% loss is actually observed, however this minor discrepancy can easily be explained by observing the beginning stages of the TGA run. The rapid weight loss at the beginning of the experiment indicates that some decomposition occurs during sample loading giving a lower than expected weight loss. The IR spectroscopy and XRD structural details are discussed in the next section.

Infrared (IR) Spectroscopy: The Infrared (IR) Spectrum of ZrN(OEt) (Figure 4.4) confirms the presence of the (-OC_2H_5) ethoxide groups within the

structure. The C-H, C-C and C-O stretching regions are indicated in addition to the Zr-O and Zr-N modes. For comparison, infrared spectra of KOC_2H_5, ZrNCl and ZrO_2 are given in Figures 4.5 and 4.6, respectively. Strong O-H bands rapidly grow into each spectrum as the samples are exposed to air and begin to decompose.

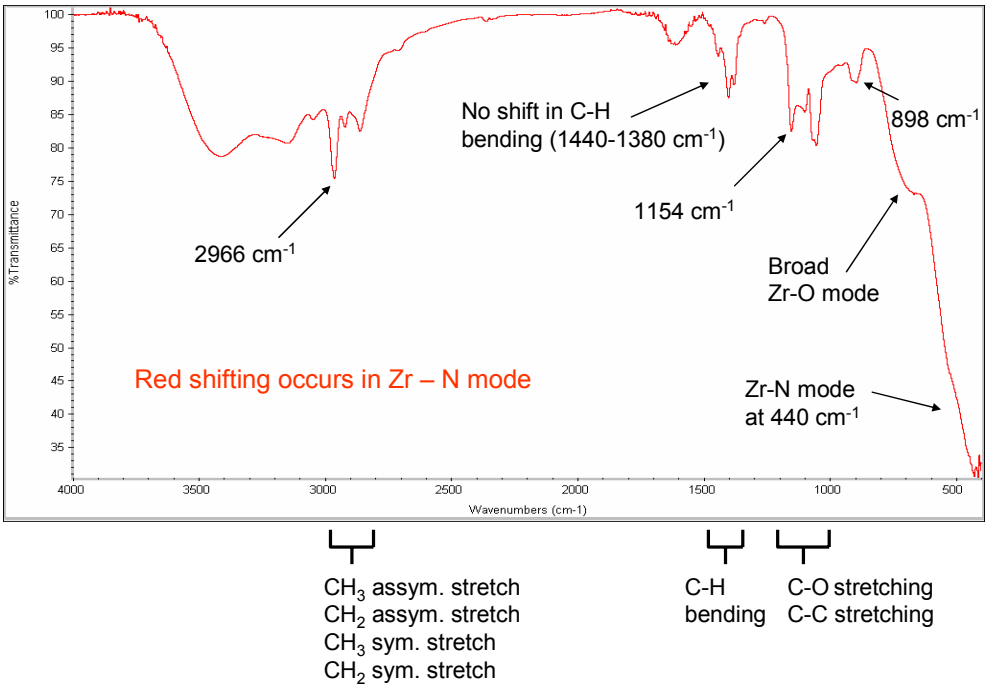

Figure 4.4. Infrared Spectrum of ZrN(OEt).

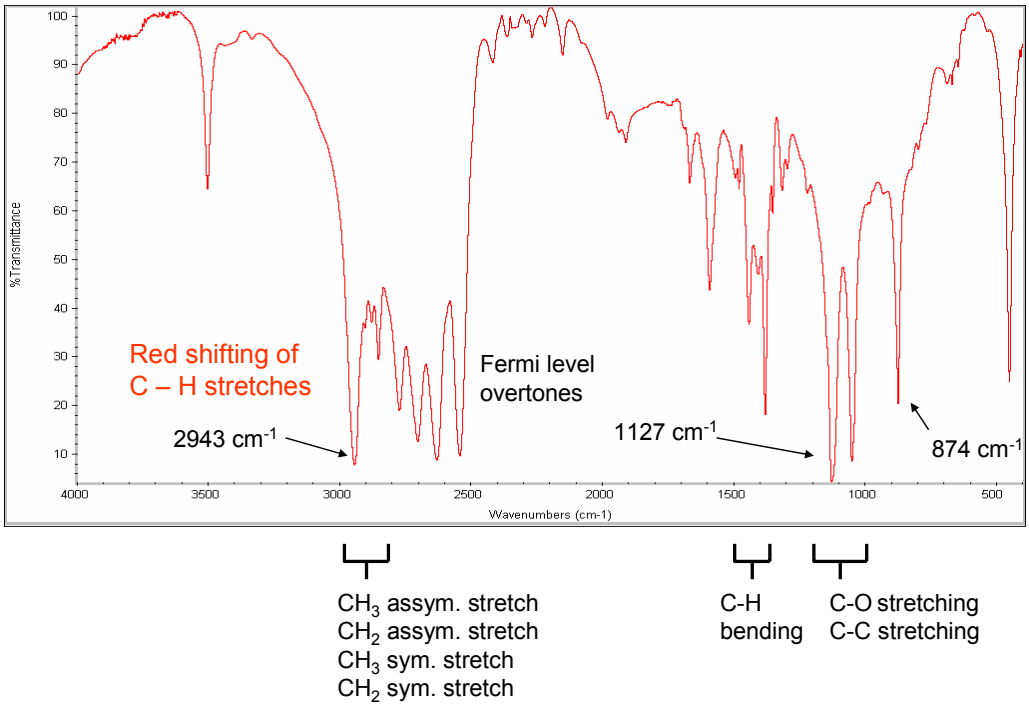

Figure 4.5. Infrared Spectrum of KOC_2H_5.

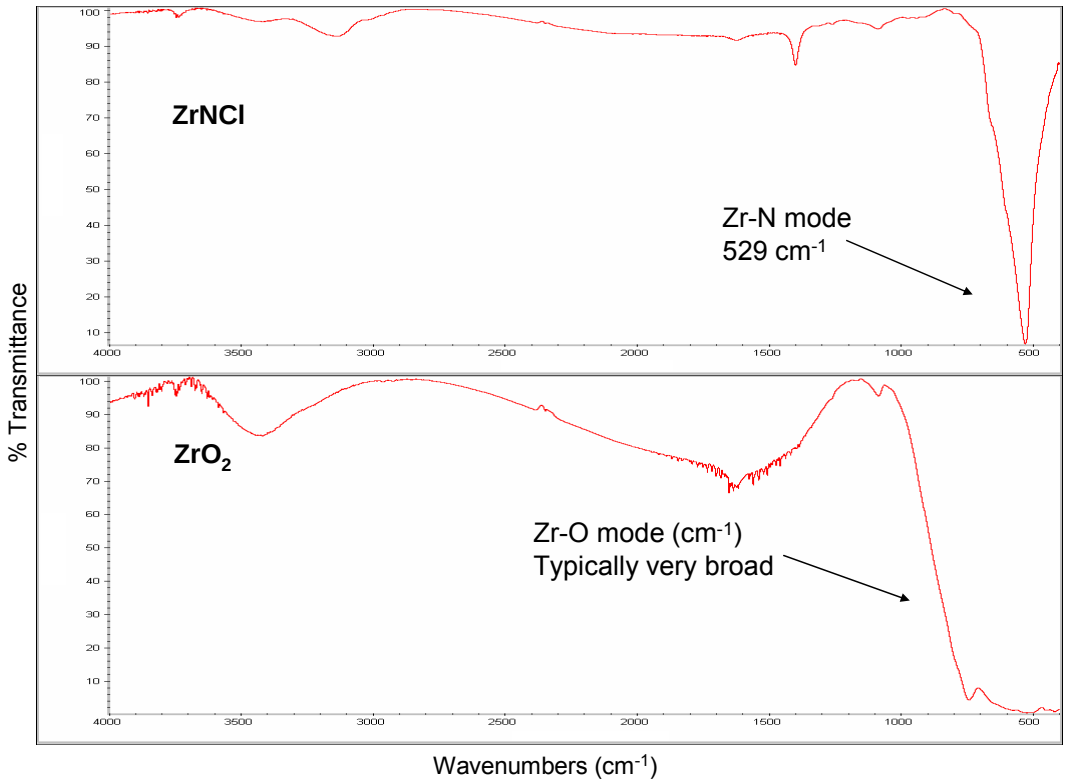

Figure 4.6. Infrared Spectra of ZrNCl (top) and ZrO_2 (bottom).

The IR spectrum very effectively demonstrates the presence of the expected stretching modes for ZrN(OEt). For example, the C-H symmetric/asymmetric stretching region of the ZrN(OEt) (2862 – 2966 cm^{-1}) matches that of the KOC_2H_5 starting material (2851 – 2944 cm^{-1}) quite well. This particular C-H stretching profile is indicative of ethoxy containing compounds. The product –OEt υ(C-H) modes are blue shifted compared to KOC_2H_5 due the more covalent nature of the ethoxy groups in the product compared to the more ionic starting material. The fermi overtones are lost in the product spectrum as well, likely due to the less ionic nature of the product. The Zr-N mode in this product is red shifted compared to that of ZrNCl, while the Zr-O mode remains characteristically broad.

In a similar fashion to the zirconium nitride ethoxide phase, the IR spectrum of ZrN(OMe) shows the expected methoxy, Zr-N, and Zr-O modes (Figure 4.7). The C-H stretching region (2822 - 2954 cm^{-1}) pattern in this material is virtually identical to that of the $KOCH_3$ starting material (Figure 4.8), with the exception of being slightly blue shifted due to a more covalent environment compared to $KOCH_3$. Although part of the C-H stretching region of $KOCH_3$ is obscured by fermi overtone bands, the higher wavenumber C-H asymmetric stretches (2906 - 2933 cm^{-1}) are visible for comparison. Again, this methoxy C-H stretching pattern is typical of methoxy group containing materials and virtually identical in shape to that of methanol (although shifted). The Zr-N stretching mode, also red shifted compared to ZrNCl, as well as the typically broad Zr-O modes are also observed.

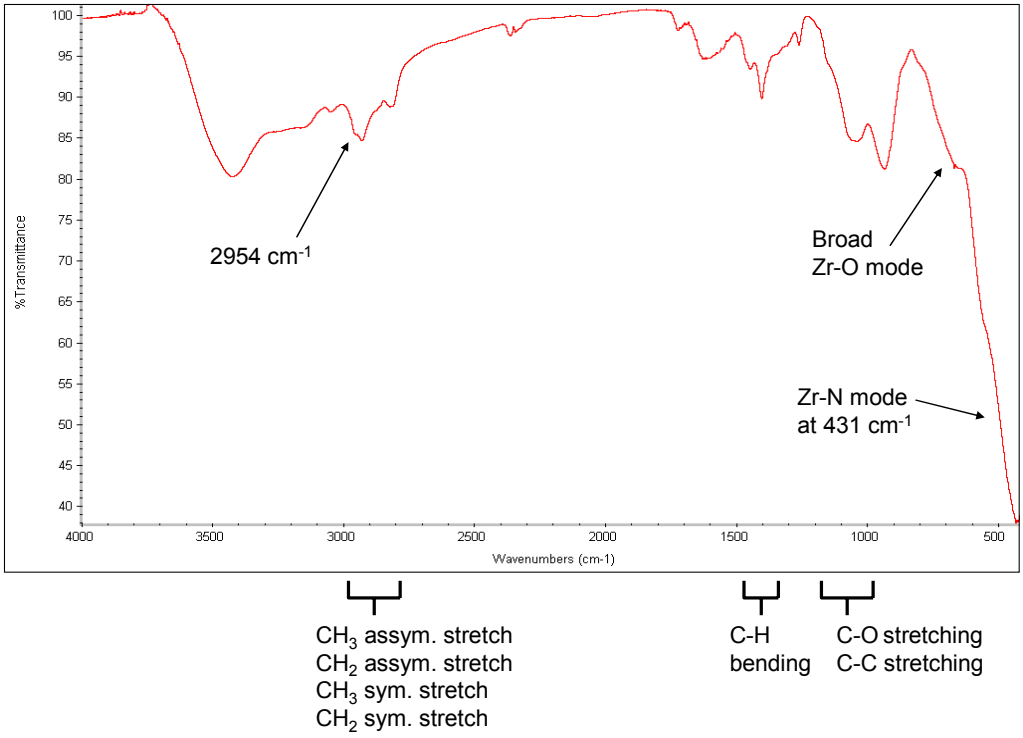

Figure 4.7. Infrared Spectrum of ZrN(OMe).

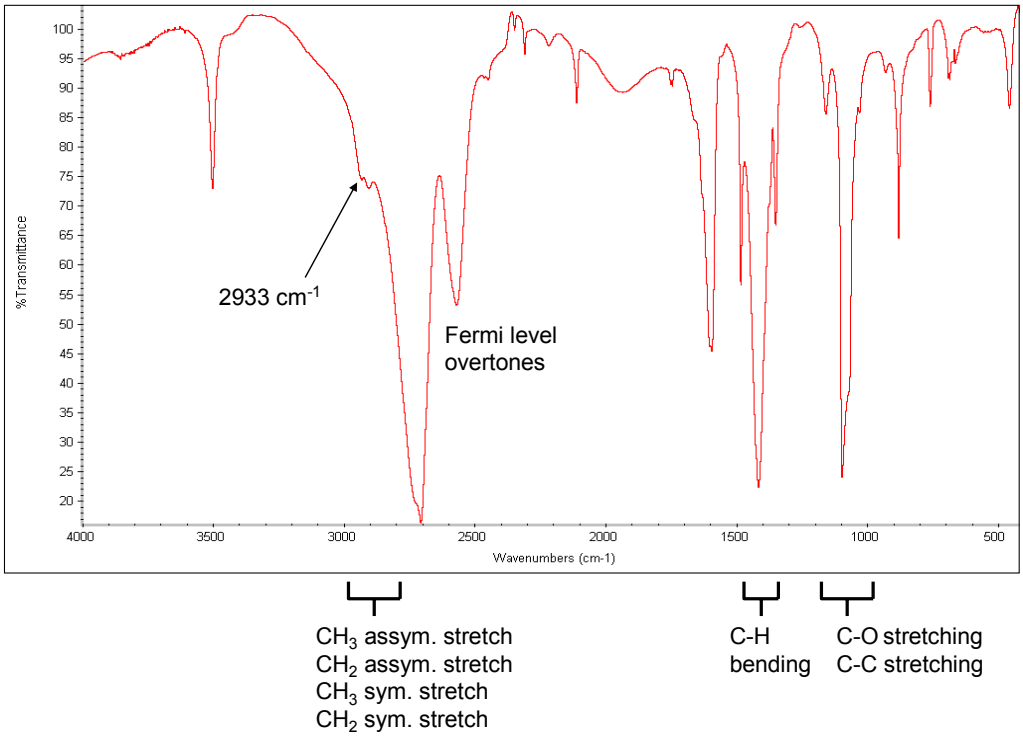

Figure 4.8. Infrared Spectrum of $KOCH_3$ starting material.

The IR spectrum of ZrN(O*n*-Bu) also shows the appropriate butoxide C-H stretching modes in Figure 4.9. The IR spectrum of NaO*n*-Bu is provided in Figure 4.10 for comparison. The highest wavenumber asymmetric stretches for the product and the starting material are 2960 and 2958 cm^{-1}, respectively. As expected, a slightly red shifted Zr-N mode and a broad Zr-O mode are observed, similar to the previous alkoxide products.

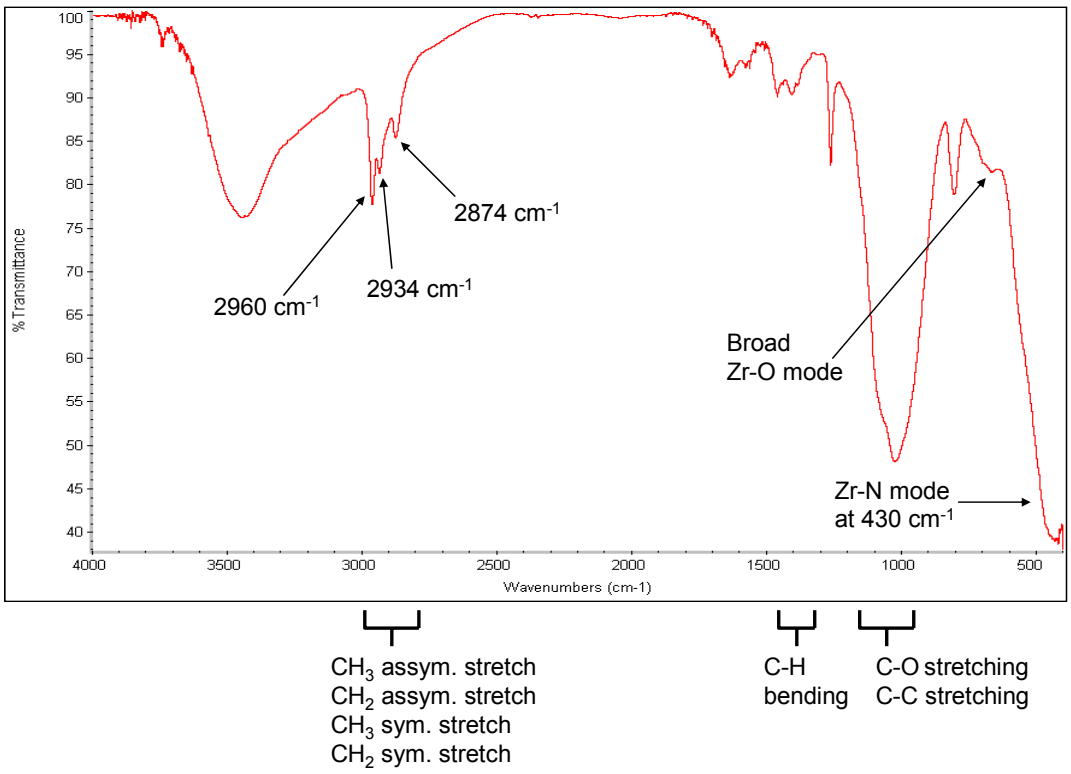

Figure 4.9. Infrared Spectrum of ZrN(O*n*-Bu)**.**

Although there is not a profound shift in the C-H stretching regions when comparing ZrN(O*n*-Bu) and NaO*n*-Bu, there is a loss of the fermi overtone bands as

well as a change in the C-O / C-C stretching profile. The broad mode present in the NaO*n*-Bu IR spectrum is due to the CaF_2 windows used as sample holders.

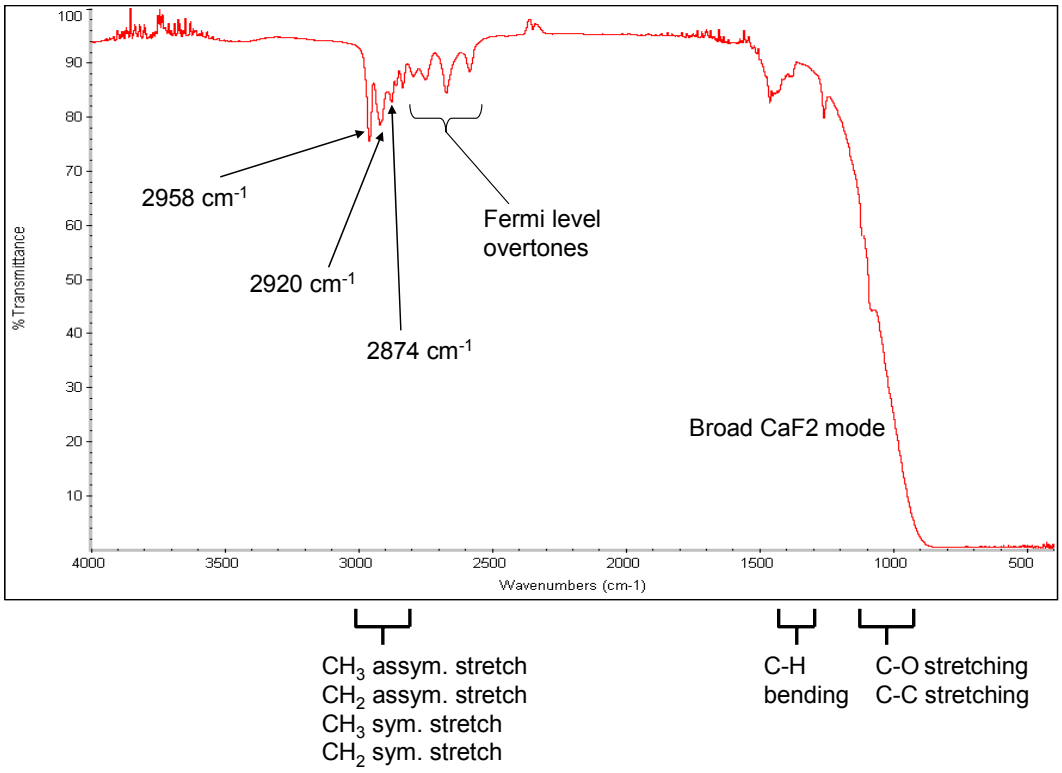

Figure 4.10. Infrared Spectrum of NaOn-Bu.

Powder XRD Analysis: Table 4.1 provides a comparison of the interlayer distances of the zirconium nitride alkoxide compounds according to the powder XRD data, while the XRD results for each phase are described individually below. Although complete (XRD) structural analysis of these phases is not possible due to poor crystallinity, they are presumably layered and trigonal as in the ZrNCl parent.

Table 4.1. Interlayer Distance Comparison

	ZrNCl	ZrN(OMe) solvothermal	ZrN(OMe) exchange	ZrN(OEt)	ZrN(O*n*-Bu)
c lattice parameter (Å)	9.22	14.2	15.1	16.4	20.9

XRD analysis of the ZrN(OEt) compound indicates retention of a layered structure (Figure 4.11). The interlayer spacing expands from ~ 9.2 Å in ZrNCl to 16.4 Å to accommodate the chloride for ethoxide exchange. Sequential [00l] reflections at 16.4 Å and 8.2 Å indicate the layered nature of this material.

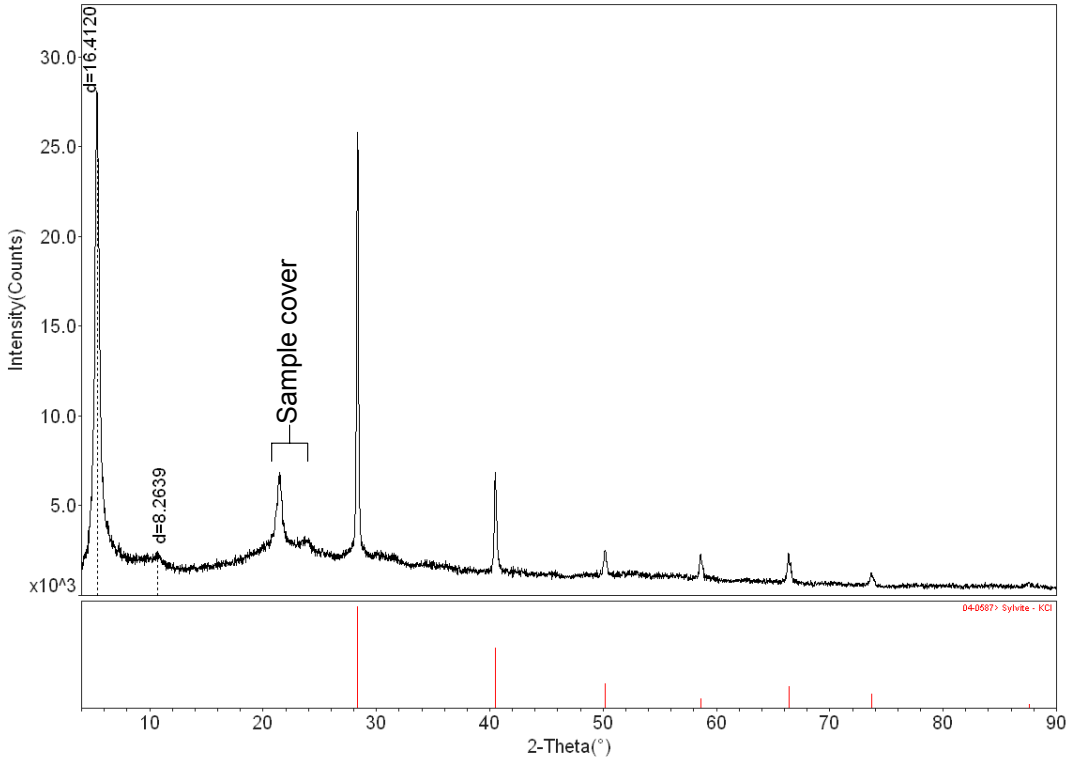

Figure 4.11. Powder XRD profile of ZrN(OEt) after ethanol washing. The sample cover is indicated in addition to the KCl byproduct (JC-PDF: 04-0587).

The powder XRD profile (Figure 4.12) for ZrN(OMe) indicates that the interlayer spacing has increased to 14.2 Å allowing chloride for methoxide exchange.

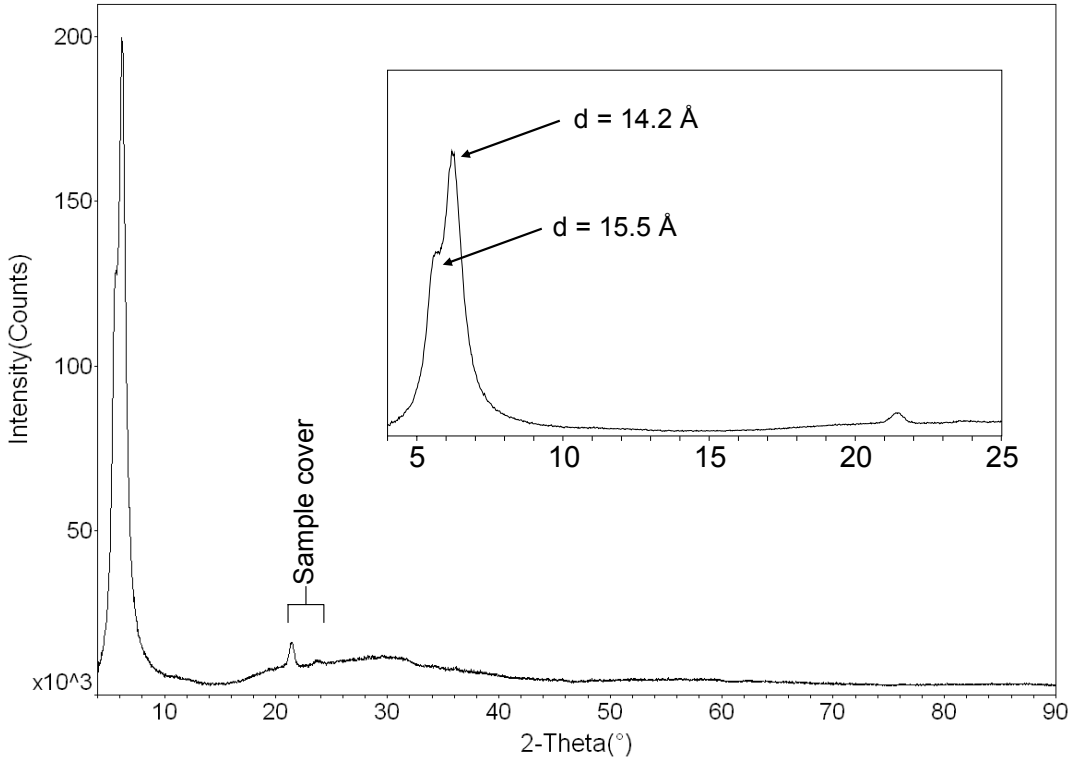

Figure 4.12. Powder XRD Profile of ZrN(OMe) with sample cover indicated. Inset shows a close up of the two overlapping low angle peaks.

As seen in the XRD profile inset, there are two low angle peaks, suggesting two phases with different interlayer distances. The 14.2 Å peak is assigned to the ZrN(OMe) product based on structural models which are discussed in the next section. The larger 15.5 Å d-spacing is likely due to an impurity phase formed during synthesis (as indicated with the TGA analysis). It is possible that the larger d-spacing is caused by a MeOH intercalated material. As previously mentioned, a K_2CO_3

byproduct is apparent by XRD of unwashed material. It is also possible that the phase with the larger d-spacing is due to a carbonate exchange impurity.

The XRD profile (Figure 4.13) of the (butanol washed) ZrNO*n*-Bu product shows retention of the layered structure in which the interlayer spacing increases to 20.9 Å. The NaCl byproduct, not washed away by 1-butanol, is also shown. This phase is even less crystalline than the previous zirconium nitride alkoxide materials, as evident by the rolling background in the XRD profile.

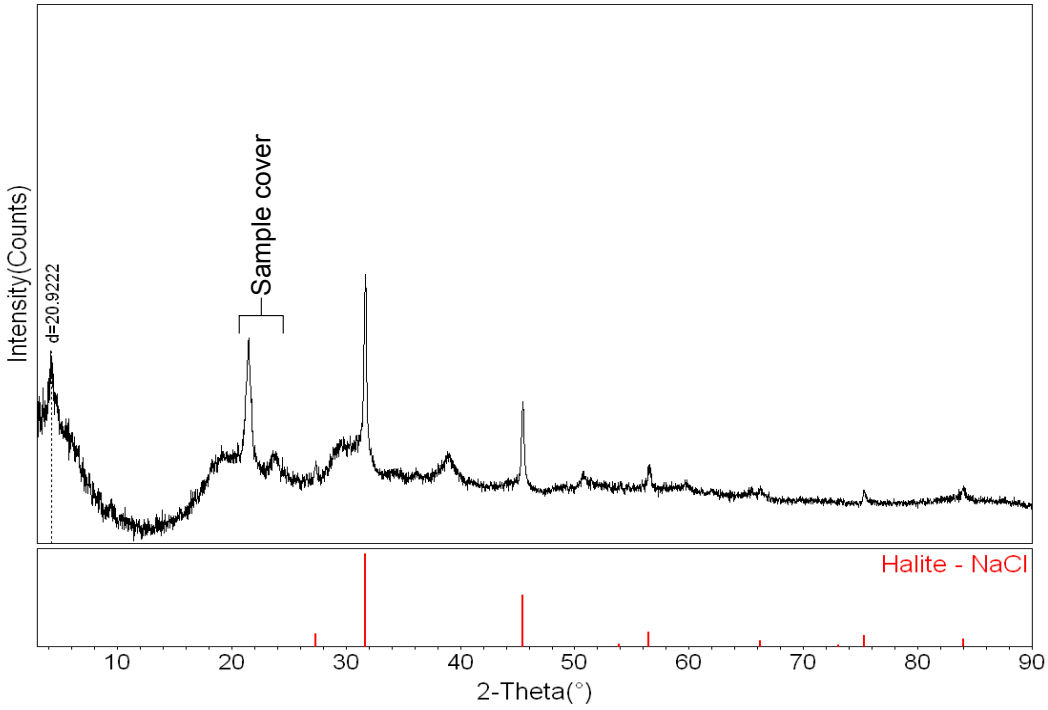

Figure 4.13. Powder XRD Profile of ZrN(O*n*-Bu). The NaCl byproduct is indicated (JC-PDF: 75-0306) with red tick marks.

The structural models for the ZrN(OR) phases are very similar. In each case, oxygen atoms from the alkoxy chains replace the chloride sites from the ZrNCl parent structure. The Zr_2N_2 double layers are also retained, with increased interlayer spacings to accommodate the alkoxy chains. Figure 4.14 provides the proposed structural model of the ZrN(OEt) compound. This structure can be modeled using typical Zr-N bond lengths of 2.13 Å and 2.17 Å,[149] a standard Zr-O 2.3 Å bond distance,[150] and a calculated O-CH_2-CH_3 chain length of 3.0 Å.

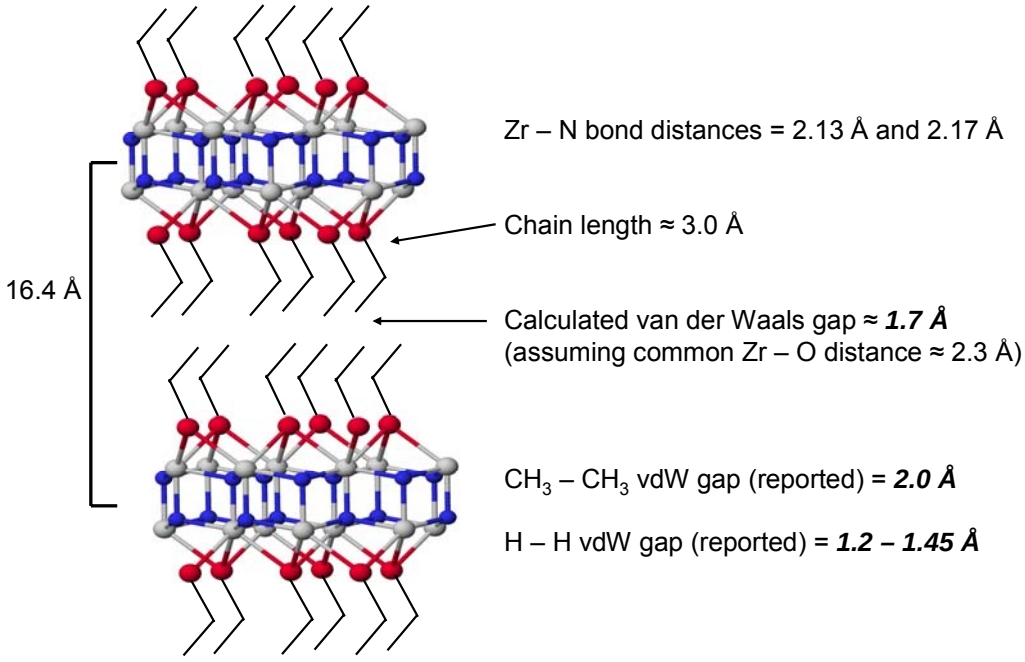

Figure 4.14. Structural Model of ZrN(OEt). Color scheme: zirconium – gray, nitrogen – blue, oxygen – red.

This structural model was constructed with idealized bond lengths and angles for the respective atoms. In such a model, the van der Waals gap is calculated to be

1.7 Å when using the ZrN(OEt) interlayer distance (16.4 Å) obtained from powder XRD. This vdW gap is quite reasonable compared to reported $CH_3 – CH_3$ and H – H vdW gaps of 2.0 Å and 1.45 Å, respectively.[150]

Recently, a thorough study of chloride for alkoxide exchange in layered zirconium phosphates has shown a very similar trend in interlayer spacings relative to the number of carbons in the alkoxide chain.[147] Assuming an all-trans conformation of the alkoxide carbon chains, interlayer distances should show linear dependence to the number of carbons according to equation 4.4.

$$d\ (Å) = mn_c 1.27 \sin \alpha + B \qquad \text{eq. 4.4.}$$

In this equation, 1.27 Å represents the reported increment in chain length for an all-trans alkyl chain per each additional carbon atom in the chain.[151] Regarding the materials reported here, m (the number of chain layers) is determined to be 2 based on direct exchange with 2 layers of chlorides between each double zirconium nitride layer. The interlayer spacing (d) is dependent on the number of carbons (n_c) and the relative angle (α) of the alkoxide chain to the host compound layers. For comparison, the interlayer distances (obtained from XRD) in these zirconium nitride alkoxide compounds follow a linear trend (Figure 4.15) represented by equation 4.5.

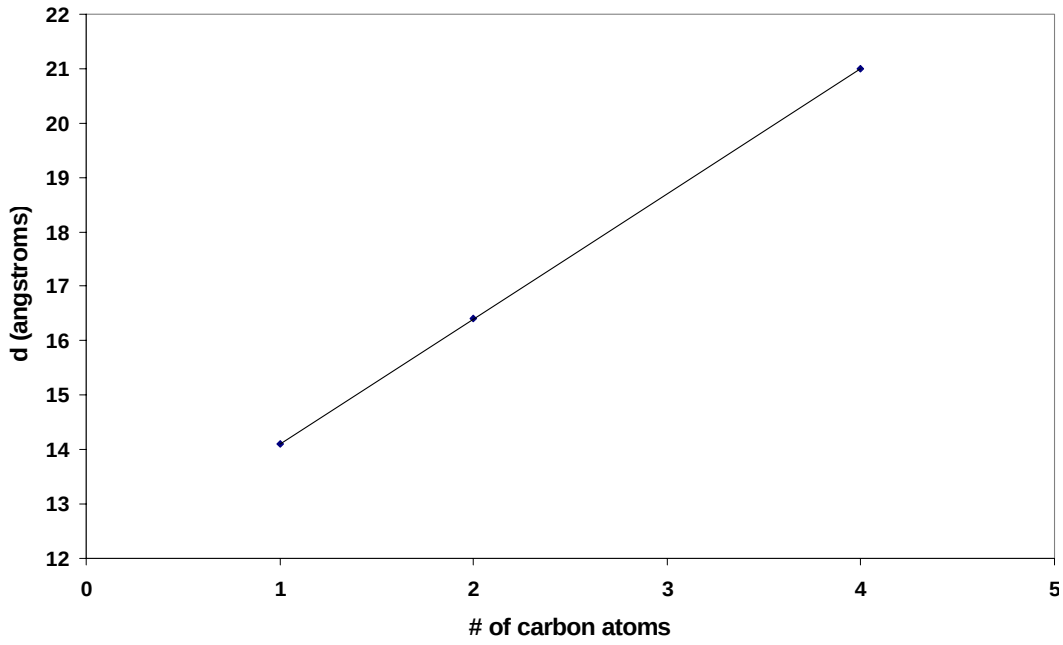

Figure 4.15. Interlayer distances of zirconium nitride alkoxide derivatives as a function of the number of carbon atoms in the alkoxide chains.

$$d\ (Å) = 2.3n_c + 11.8 \qquad \text{eq. 4.5.}$$

Although only three data points are available, the trendline fit is quite good. By comparing this trendline to equation 4.4 and assuming similar van der Waals gaps for each analogue, the calculated angle is $\alpha = 65^o$. This angle can be compared to that calculated (52^o) for layered zirconium phosphate alkoxides.[147] A comparison can also be made with the angle calculated (55^o) when the alkoxy chains are in an all-trans conformation with the first Zr – O bond perpendicular to the plane of the layers. A variation in the relative chain to layer angle (α) between this and previous work is reasonable. In this work, each oxygen is presumably coordinated to three zirconium

atoms (similar to the Zr – Cl bonding in the ZrNCl parent) and these Zr – O bonds are not perpendicular to the layers. In the case of the zirconium phosphate alkoxide materials, the average interlayer spacing per carbon atom addition to the alkoxide chain (2.0 Å per carbon atom) is slightly less than in the materials reported here (2.3 Å) due to the differences in angle (α). This model very effectively describes the observed trends in interlayer dependence on alkoxide chain length in both the zirconium phosphate alkoxides as well as the zirconium nitride alkoxide compounds presented here.

4.3.3. Methanol Exchange of ZrN(OEt)

Interestingly, the ZrN(OEt) phase can undergo a solution exchange to give ZrN(OMe) upon washing with methanol. Powder XRD analysis (Figure 4.16) shows the appropriate interlayer spacing change from 16.4 Å to 15.1 Å. The inset in this figure illustrates a change from the typical (IR) ethoxy C-H stretching pattern to that of a methoxy stretching pattern. In this case, the (methoxy) C-H stretching modes range from 2811 to 2956 cm^{-1}, very similar to that of the compound made by solvothermal methods (2822 - 2954 cm^{-1}).

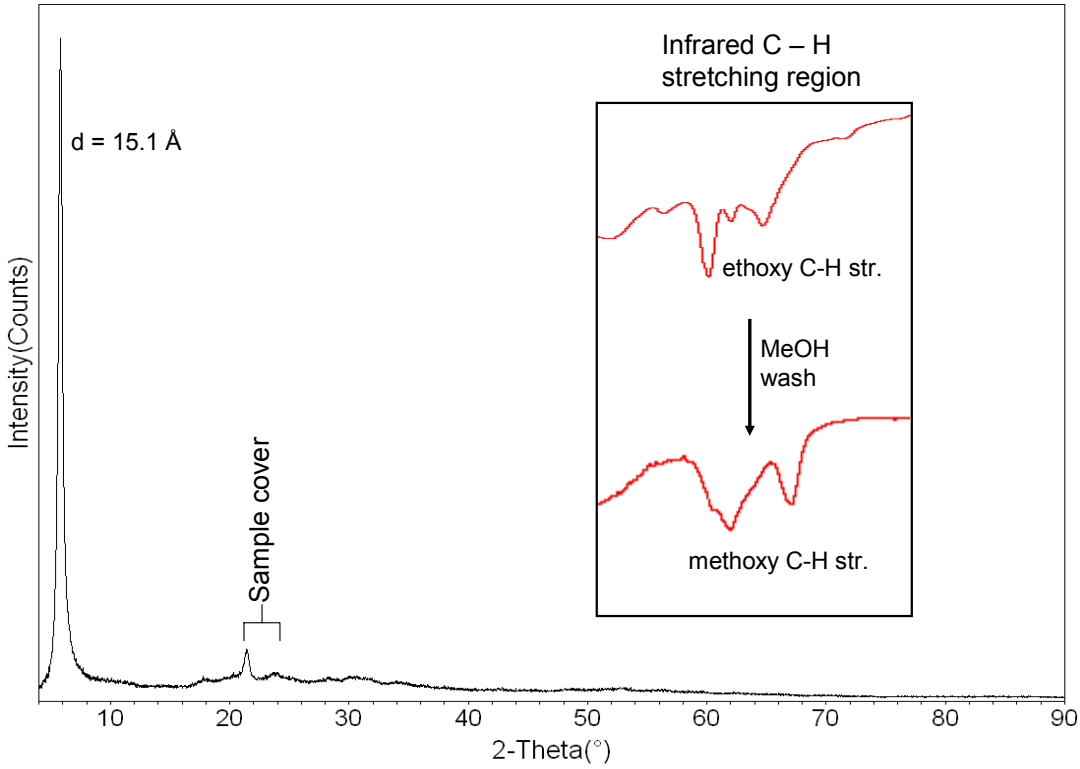

Figure 4.16. Powder XRD of ZrN(OMe) by methanol exhange. The inset shows the change from the ethoxy to methoxy type C-H stretching region.

The 15.1 Å d-spacing obtained with this methanol exchange reaction possibly indicates a slighty different layer packing by this synthetic method compared to the methoxide material produced from solvothermal methods (14.2 Å). This alternate layer packing in the materials made by solvothermal methods is likely due to the high solvothermal reaction pressures. The decrease in interlayer spacing (XRD) and change in the C-H stretching region in the IR spectra strongly indicate ethoxy for methoxy exchange, illustrating functionality in these materials.

4.3.4. THF insertion into ZrN(OEt)

The ZrNOEt compound can also exist as a THF-intercalated phase. When eq. 4.1 is carried out, followed by washing only with THF, this intercalated material is obtained. Figure 4.17 shows the increase in the interlayer spacing due to intercalation of THF in between the layers. The interlayer distance is increased to 22.8 Å, compared to 16.4 Å of the unintercalated compound.

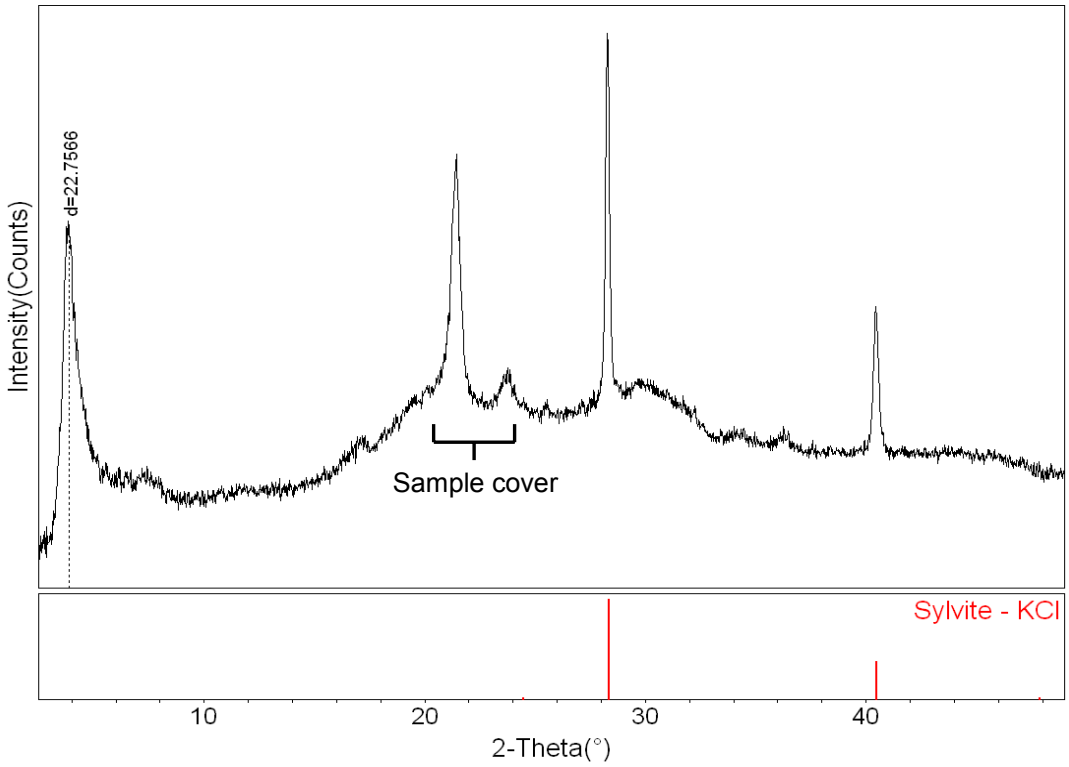

Figure 4.17. Powder XRD of THF intercalated ZrN(OEt). The sample cover is indicated in addition to the KCl byproduct (JC-PDF: 04-0587).

TGA studies suggest approximately 2 % uptake of THF into the structure by comparing with the weight loss of the un-intercalated material. The THF presumably

resides in the van der Waals gap, between the interlayer ethoxy groups, as indicated by the considerable increase in interlayer separation (6.4 Å). This interlayer distance increase is typical of other THF-intercalated materials.[152-154]

4.4. Discussion

This new class of zirconium nitride alkoxide materials provides a unique example of using soft chemical means to obtain new metastable products. Similar to the organic oxides,[110,143] these compounds require kinetic control not possible by traditional solid state synthetic methods. Although difficult synthetic conditions and extreme sensitivity to air make characterization challenging, the presented XRD, analytical, and spectroscopic data show clear chloride for alkoxide exchange with reasonable interlayer van der Waals spaces.

The zirconium nitride ethoxide compound appears to be the most readily accessible phase under these solvothermal conditions, requiring lower temperatures, smaller starting material stoichiometric ratios and shorter reaction times. This is possibly due to an interplay between size and solubility of the alkoxide starting materials. As the alkoxy chain length decreases, the solubility also decreases. In the methoxy case, although the small size is suitable for exchange, the low solubility in THF may retard the reaction. In the *n*-butoxy case, the solubility increases, but the large size makes the exchange reaction unfavorable.

The methoxide phase is accessible by direct solvothermal methods and by a simple solution exchange reaction. Although this material seems to form a single phase only by the solution exchange method, the data shows that this material can be

produced via solvothermal anion metathesis. The difficulty in producing a pure methoxide metathesis product is presumably due to partial decomposition of $KOCH_3$ under these synthetic conditions. XRD analysis shows that the unwashed methoxide metathesis product contains a considerable amount of potassium carbonate, likely formed simultaneously with the metathesis reaction. A decomposition species such as carbonate may be responsible for the second low angle peak observed in the XRD profile of the ZrN(OMe) metathesis compound. Ironically, the higher temperatures required to force the chloride for methoxide metathesis reaction to proceed are potentially responsible for the decomposition product observed.

In the case of the butoxide metathesis product, more forceful reaction conditions were required. A second grinding and heating cycle, a common technique in traditional solid state chemistry, was required with large stoichiometric excess and higher temperatures to obtain a chloride-free product. The ZrN(O*n*-Bu) phase also provides the best example of the extreme air sensitive nature of these new alkoxide materials. This instability proved to be quite problematic, especially for obtaining TGA data. Rapid decomposition also complicated IR analysis and prevented complete removal of the alkali halide salt products prior to analysis in certain cases.

Also notable is that a very recent study has shown very similar chloride for alkoxide exchange in layered zirconium phosphate derivatives.[147] Although these materials show structural similarities, the synthetic methods that produce them are fundamentally different.[155,156] The chemistry presented in this work is true topochemical synthesis performed on a very refractory solid state material, while the zirconium phosphate materials can easily be manipulated in solution. The practical

functionality of this type of material is shown by the ability to readily exchange ethoxy for methoxy groups in solution, while the THF intercalation may provide insight into the reaction mechanism itself. The THF intercalated material was only washed with THF, however if ZrN(OEt) is first washed with ethanol, it does not intercalate THF. This finding suggests that THF possibly holds the ZrNCl layers apart in a manner that allows the larger organic anions to exchange, similar to known ZrNCl – THF intercalated materials.[152,153]

These compounds and synthetic methods potentially provide the first step in obtaining new functional nitride based materials such as nanotubes. The methods presented here again show that anion metathesis in the solid state can be a powerful tool used to obtain materials that cannot be made by traditional means.

Chapter 5:
Conclusions

As shown by the success of the experiments described in this work, anion metathesis in the solid state can undeniably be added to our "toolbox" of soft chemical synthetic techniques. Similar to the previously described soft chemical methods, solid state anion exchange provides very effective kinetic control, affording desired products that cannot be obtained with thermodynamic control. Although the exchange of anions is common in molecular chemistry, this work provides examples of such metathesis in truly refractory, solid state systems.

These refractory systems separate this work from known anion exchange in solid state materials. For example, the layered zirconium phosphate compounds[155,156] (discussed in Chapter 4) are well known for exchanging anions in and out of the layered host structure. However, these are not truly refractory solids. They can easily be manipulated in solution, allowing exchange to occur under very mild conditions. In contrast, systems such as the MNX derivatives (M = Zr, Hf; X = Cl, Br, I) used as precursors in this work are true refractory solids which are relatively unaffected by solvents and very difficult to manipulate.

This work also presents the first instance of using these MNX compounds as precursors to new materials. Intercalation, de-intercalation and electron-doping have been accomplished with compounds such as Zr/HfNCl. However, until this work no

other derivatives have been reported which contain this novel double Zr-N hexagonal net backbone. Potentially, methods such as described here can lead to even more useful and interesting zirconium nitride derivatives.

Another significant aspect of all of the materials described here is an interesting "self-nanosizing" effect. Each of the TEM images taken of these anion metathesis products shows nano-sized particles. While "as prepared" ZrNCl may exist as a nanopowder, the recrystallized ZrNCl starting materials are much larger, more crystalline particles than those observed in the products. It seems that these reaction mechanisms force the product particles into a nanoscale size regime. This phenomenon is reasonable, considering that we are forcing anions to move through large 2-dimensional frameworks. During metathesis, the reaction can presumably minimize the energetic barrier to the product by minimizing the particle size. With much smaller nanoparticles, moving anions through the layered host would require less energy. This effect is evident when comparing the Na_xZrNF_{1+x} products from Chapter 3. When the reaction is carried out with recrystallized ZrNCl, much higher temperatures are required to push the reaction to completion. If "as-prepared" ZrNCl starting material is used, not as much energy is required to complete the reaction, due to the already nano-sized host particles.

In addition to zirconium nitride derivative materials as mentioned above, techniques such as anion metathesis could be used to design numerous solid state materials. For instance, the superconducting rare earth – carbide – halide systems could provide such an example.[157] Similar to ZrNCl, they are lamellar with interlayer halides that should be exchangeable and could lead to other rare earth – carbide

derivative materials. Ideally, this work will pave the way for more solid state exchange chemistry and will aid the rational design of new and interesting solid state systems.

Bibliography

(1) Bestaoui, N.; Prouzet, E. *Chemistry of Materials* **1997**, *9*, 1036-1041.

(2) Koinuma, H.; Takeuchi, I. *Nature Materials* **2004**, *3*, 429-438.

(3) Mallouk, T. E. *Science* **2001**, *291*, 443-444.

(4) Gopalakrishnan, J. *Chemistry of Materials* **1995**, *7*, 1265-1275.

(5) Zhao, Q.; Hou, L.; Huang, R.; Li, S. *Materials Chemistry and Physics* **2004**, *85*, 180-183.

(6) Prabaharan, S. R. S.; Michael, M. S.; Ikuta, H.; Uchimoto, Y.; Wakihara, M. *Solid State Ionics* **2004**, *172*, 39-45.

(7) Yu, A.-s.; Kumagai, N.; Lee, J.-y. *Fudan Xuebao, Ziran Kexueban* **2004**, *43*, 530-536.

(8) Niederberger, M.; Pinna, N.; Polleux, J.; Antonietti, M. *Angewandte Chemie, International Edition* **2004**, *43*, 2270-2273.

(9) Fix, R.; Gordon, R. G.; Hoffman, D. M. *Chemistry of Materials* **1991**, *3*, 1138-1148.

(10) Sim, G. Y.; Yoon, S. Y. In *Repub. Korean Kongkae Taeho Kongbo*; (Samsung SDI Co., Ltd., S. Korea). Kr, 2002, p No pp. given.

(11) Sanchette, F.; Ducros, C. In *Fr. Demande*; (Commissariat a l'Energie Atomique, Fr.; Mecachrome). Fr, 2004, p 44 pp.

(12) Liu, Y.; Matsumura, T.; Imanishi, N.; Ichikawa, T.; Hirano, A.; Takeda, Y. *Electrochemistry Communications* **2004**, *6*, 632-636.

(13) Yokosawa, K.; Kawamoto, J. In *Jpn. Kokai Tokkyo Koho*; (Sumitomo Metal Mining Co., Ltd., Japan). Jp, 2004, p 16 pp.

(14) Gillan, E. G.; Kaner, R. B. *Inorganic Chemistry* **1994**, *33*, 5693-5700.

(15) Lengauer, W. *Surface and Interface Analysis* **1990**, *15*, 377-382.

(16) Kaner, R. B.; Cumberland, R. W.; Weinberger, M. M.; Tolbert, S. H.; Gilman, J. J.; Clark, S. M. *Abstracts of Papers, 228th ACS National Meeting, Philadelphia, PA, United States, August 22-26, 2004* **2004**, INOR-416.

(17) Janes, R. A.; Aldissi, M.; Kaner, R. B. *Chemistry of Materials* **2003**, *15*, 4431-4435.

(18) Juza, R.; Friedrichsen, H. *Zeitschrift fuer Anorganische und Allgemeine Chemie* **1964**, *332*, 173-178.

(19) Vlassov, M.; Palacin, M. R.; Beltran-Porter, D.; Oro-Sole, J.; Canadell, E.; Alemany, P.; Fuertes, A. *Inorganic Chemistry* **1999**, *38*, 4530-4538.

(20) Turnbull, D. *Metallurgical Transactions a-Physical Metallurgy and Materials Science* **1981**, *12*, 695-708.

(21) Sleight, A. W. *Physics Today* **1991**, *44*, 24-30.

(22) Cheetham, A. K. *Science* **1994**, *264*, 794-795.

(23) Ollivier, P. J.; Mallouk, T. E. *Chemistry of Materials* **1998**, *10*, 2585-2587.

(24) Dulieu, B.; Bullot, J.; Wery, J. *Physical Review B* **1996**, *53*, 10641-10650.

(25) Rao, C. N. R. a. G., J. *New Directions in Solid State Chemistry*; second ed.; Cambridge University Press: Cambridge, 1997.

(26) West, A. R. *Solid State Chemistry and its Applications*; John Wiley & Sons, Ltd.: Singapore, 1989.

(27) Wiley, J. B.; Kaner, R. B. *Science* **1992**, *255*, 1093-1097.

(28) Bonneau, P. R.; Shibao, R. K.; Kaner, R. B. *Inorganic Chemistry* **1990**, *29*, 2511-2514.

(29) Bonneau, P. R.; Jarvis, R. F.; Kaner, R. B. *Nature* **1991**, *349*, 510-512.

(30) Hilpert, S. a. W., A. *Z. Physical Chemistry* **1932**, *18B*, 291.

(31) Durand, B. a. P., J.M. *Inorganic Synthesis.* **1980**, 50.

(32) Bonneau, P. R.; Kaner, R. B. *Inorganic Chemistry* **1993**, *32*, 6084-6087.

(33) Miremadi, B. K.; Morrison, S. R. *Journal of Applied Physics* **1990**, *67*, 1515-1520.

(34) Clauss, F. L. *Solid Lubricants and Self-Lubricating Solids*; Academic Press: New York, 1972.

(35) Rouxel, J.; Brec, R. *Annual Review of Materials Science* **1986**, *16*, 137-162.

(36) Pecoraro, T. A.; Chianelli, R. R. *Journal of Catalysis* **1981**, *67*, 430-445.

(37) Lewerenz, H. J.; Tributsch, H.; Spiesser, M. *Journal of the Electrochemical Society* **1985**, *132*, 700-703.

(38) Gillan, E. G.; Kaner, R. B. *Chemistry of Materials* **1996**, *8*, 333-343.

(39) Treece, R. E.; Macala, G. S.; Rao, L.; Franke, D.; Eckert, H.; Kaner, R. B. *Inorganic Chemistry* **1993**, *32*, 2745-2752.

(40) Wallace, C. H.; Reynolds, T. K.; Kaner, R. B. *Chemistry of Materials* **1999**, *11*, 2299-+.

(41) O'Loughlin, J. L.; Wallace, C. H.; Knox, M.; Kaner, R. B. *Inorganic Chemistry* **2001**, *40*, 2240-2245.

(42) Poeppelmeier, K. R.; Kipp, D. O. *Inorganic Chemistry* **1988**, *27*, 766-767.

(43) Tournoux, M.; Marchand, R.; Brohan, L. *Progress in Solid State Chemistry* **1986**, *17*, 33-52.

(44) Feist, T. P.; Davies, P. K. *Journal of Solid State Chemistry* **1992**, *101*, 275-295.

(45) Dronskowski, R. *Inorganic Chemistry* **1993**, *32*, 1-9.

(46) Dronskowski, R. *Journal of the American Chemical Society* **1992**, *114*, 7230-7244.

(47) Gopalakrishnan, J.; Sivakumar, T.; Ramesha, K.; Thangadurai, V.; Subbanna, G. N. *Journal of the American Chemical Society* **2000**, *122*, 6237-6241.

(48) Kodenkandath, T. A.; Lalena, J. N.; Zhou, W. L. L.; Carpenter, E. E.; Sangregorio, C.; Falster, A. U.; Simmons, W. B.; O'Connor, C. J.; Wiley, J. B. *Journal of the American Chemical Society* **1999**, *121*, 10743-10746.

(49) Li, W.; Dahn, J. R.; Wainwright, D. S. *Science* **1994**, *264*, 1115-1118.

(50) Ramesha, K.; Gopalakrishnan, J. *Solid State Sciences* **2001**, *3*, 113-119.

(51) Yamanaka, S.; Kawaji, H.; Hotehama, K.; Ohashi, M. *Advanced Matererials (Weinheim, Ger.)* **1996**, *8*, 771-774.

(52) Yamanaka, S.; Hotehama, K.-i.; Kawaji, H. *Nature (London)* **1998**, *392*, 580-582.

(53) Oro-Sole, J.; Caldes, M. T.; Palacin, M. R.; Vlassov, M.; Beltran-Porter, D.; Martinez, B.; Fuertes, A. *Solid State Sciences* **2000**, *2*, 77-86.

(54) Felser, C.; Seshadri, R. *Journal of Materials Chemistry* **1999**, *9*, 459-464.

(55) Kaschak, D. M.; Johnson, S. A.; Hooks, D. E.; Kim, H. N.; Ward, M. D.; Mallouk, T. E. *Journal of the American Chemical Society* **1998**, *120*, 10887-10894.

(56) Jacobson, A. *Journal of Materials Science Forum* **1994**, 152-153.

(57) Divigalpitiya, W. M. R.; Frindt, R. F.; Morrison, S. R. *Science* **1989**, *246*, 369-371.

(58) Krishnamoorti, R.; Vaia, R. A.; Giannelis, E. P. *Chemistry of Materials* **1996**, *8*, 1728-1734.

(59) Kleinfeld, E. R.; Ferguson, G. S. *Science* **1994**, *265*, 370-373.

(60) Levin, D.; Soled, S. L.; Ying, J. Y. *Chemistry of Materials* **1996**, *8*, 836-843.

(61) Brindley, G. W.; Sempels, R. E. *Clay Minerals* **1977**, *12*, 229-237.

(62) Ebelmen, M. *C. R. Academy of Science Forum* **1845**, 502.

(63) Wu, S. G.; Ellerby, L. M.; Cohan, J. S.; Dunn, B.; Elsayed, M. A.; Valentine, J. S.; Zink, J. I. *Chemistry of Materials* **1993**, *5*, 115-120.

(64) Gopalakrishnan, J.; Ramesha, K.; Rangan, K. K.; Pandey, S. *Journal of Solid State Chemistry* **1999**, *148*, 75-80.

(65) Roberts, M. A.; Sankar, G.; Thomas, J. M.; Jones, R. H.; Du, H.; Chen, J.; Pang, W.; Xu, R. *Nature* **1996**, *381*, 401-404.

(66) Sze, S. M. *Physics of Semiconductor Devices*; second ed.; John Wiley & Sons: New York, 1981.

(67) Treece, R. E.; Conklin, J. A.; Kaner, R. B. *Inorganic Chemistry* **1994**, *33*, 5701-5707.

(68) Toth, L. E. *Transition Metal Carbides and Nitrides*; Academic Press: New York, 1971.

(69) Wallace, C. H.; Kim, S. H.; Rose, G. A.; Rao, L.; Heath, J. R.; Nicol, M.; Kaner, R. B. *Applied Physics Letters* **1998**, *72*, 596-598.

(70) Cross, J. B.; Smith, S. M.; Schlegel, H. B. *Chemistry of Materials* **2001**, *13*, 1095-1100.

(71) Narula, C. K.; Allison, J. E.; Bauer, D. R.; Gandhi, H. S. *Chemistry of Materials* **1996**, *8*, 984-1003.

(72) Brown, S. N. *Journal of the American Chemical Society* **1999**, *121*, 9752-9753.

(73) Addamiano, A. *Journal of the American Chemical Society* **1960**, *82*, 1537-1540.

(74) Antell, G. R.; Effer, D. *Journal of the Electrochemical Society* **1959**, *106*, 509-511.

(75) Byrne, E. K.; Parkanyi, L.; Theopold, K. H. *Science* **1988**, *241*, 332-334.

(76) Wells, R. L.; Hallock, R. B.; McPhail, A. T.; Pitt, C. G.; Johansen, J. D. *Chemistry of Materials* **1991**, *3*, 381-382.

(77) Fix, R.; Gordon, R. G.; Hoffman, D. M. *Chemistry of Materials* **1993**, *5*, 614-619.

(78) Hintermann, H. E. *Thin Solid Films* **1981**, *84*, 215-243.

(79) Wade, T.; Crooks, R. M. *Chemistry of Materials* **1996**, *8*, 832-835.

(80) Jarvis, R. F.; Jacubinas, R. M.; Kaner, R. B. *Inorganic Chemistry* **2000**, *39*, 3243-3246.

(81) Harrison, J. F. *Journal of Physical Chemistry* **1996**, *100*, 3513-3519.

(82) Ohashi, M.; Yamanaka, S.; Sumihara, M.; Hattori, M. *J. Solid State Chem.* **1988**, *75*, 99-104.

(83) Ohashi, M.; Yamanaka, S.; Hattori, M. *Journal of Solid State Chemistry* **1988**, *77*, 342-347.

(84) Zhu, L.-P.; Ye, Z.-Z. *Huaxue Xuebao* **2003**, *61*, 1844-1848.

(85) Zhu, L.; Ohashi, M.; Yamanaka, S. *Chemistry of Materials* **2002**, *14*, 4517-4521.

(86) Oro-Sole, J.; Caldes, M. T.; Palacin, M. R.; Vlassov, M.; Beltran-Porter, D.; Fuertes, A. *Chemistry of Materials* **1999**, *11*, 3425-3429.

(87) Tou, H.; Maniwa, Y.; Koiwasaki, T.; Yamanaka, S. *Physical Review B: Condensed Matter Materials Physics* **2001**, *63*, 020508/020501-020508/020504.

(88) Chen, X.; Zhu, L.; Yamanaka, S. *Journal of Solid State Chemistry* **2002**, *169*, 149-154.

(89) Chen, X.; Koiwasaki, T.; Yamanaka, S. *Journal of Solid State Chemistry* **2001**, *159*, 80-86.

(90) Chen, X.; Koiwasaki, T.; Yamanaka, S. *Journal of Physics: Condensed Matter* **2002**, *14*, 11209-11212.

(91) Yamanaka, S. *Annual Review of Materials Science* **2000**, *30*, 53-82.

(92) Pietronero, L.; Tosatti, E.; Editors *Springer Series in Solid-State Sciences, Vol. 38: Physics of Intercalation Compounds [Proceedings of an International Conference, Trieste, Italy, July 6-10, 1981]*, 1981.

(93) Whittingham, M. S.; Jacobson, A. J.; Editors *Intercalation Chemistry*, 1982.

(94) Jacobson, A. J. In *Solid State Chemistry Compounds*; Cheetham, A. D., P., Ed.; Oxford University Press: New York, 1992, p 182.

(95) Kawaji, H.; Hotehama, K.-i.; Yamanaka, S. *Chemistry of Materials* **1997**, *9*, 2127-2130.

(96) Clarke, S. J.; Michie, C. W.; Rosseinsky, M. J. *Journal of Solid State Chemistry* **1999**, *146*, 399-405.

(97) Fueglein, E.; Hock, R.; Lerch, M. *Zeitschrift fuer Anorganische und Allgemeine Chemie* **1997**, *623*, 304-308.

(98) Yamanaka, S.; Itoh, K.; Fukuoka, H.; Yasukawa, M. *Inorganic Chemistry* **2000**, *39*, 806-809.

(99) Yamanaka, S.; Ohashi, M.; Sumihara, M.; Hattori, M. *Chemistry Letters* **1984**, 1403-1406.

(100) Yamanaka, S. *Oyo Butsuri* **1999**, *68*, 384-390.

(101) Lissner, F.; Schleid, T. *Zeitschrift fuer Anorganische und Allgemeine Chemie* **1999**, *625*, 195-196.

(102) Lissner, F.; Schleid, T. *Zeitschrift fuer Anorganische und Allgemeine Chemie* **2001**, *627*, 2307-2309.

(103) Morosin, B. *Acta Crystallographica, Section B: Structural Crystallography and Crystal Chemistry* **1973**, *29*, 2647-2648.

(104) 5.0 ed.; Materials Data, Inc.: Livermore, CA, 1999.

(105) Bruker AXS: Karlsruhe, Germany, 2000.

(106) Chen, B.-H. E., B.; Fanwick, P. *Inorganic Chemistry* **1992**, 1788.

(107) Hung, Y.-C.; Fettinger, J. C.; Eichhorn, B. W. *Acta Crystallographica, Section C: Crystal Structure Communications* **1997**, *C53*, 827-829.

(108) Fogg, A. M.; Evans, J. S. O.; O'Hare, D. *Chemical Communications (Cambridge)* **1998**, 2269-2270.

(109) Urban, J. J.; Yun, W. S.; Gu, Q.; Park, H. *Journal of the American Chemical Society* **2002**, *124*, 1186-1187.

(110) Schaak, R. E.; Mallouk, T. E. *Chemistry of Materials* **2000**, *12*, 3427-3434.

(111) Ohashi, M.; Yamanaka, S.; Hattori, M. *Nippon Seramikkusu Kyokai Gakujutsu Ronbunshi* **1989**, *97*, 1181-1188.

(112) Yamanaka, S. *Kotai Butsuri* **1998**, *33*, 711-716.

(113) Shamoto, S.; Kato, T.; Ono, Y.; Kajitani, T.; Ohoyama, K.; Ohashi, M.; Yamaguchi, Y. "Structure study on novel layered superconductor Li0.16ZrNCl and its parent b-ZrNCl," Dept. of Applied Physics,Tohoku University,Sendai,Japan. FIELD URL:, 1999.

(114) Fogg, A. M.; Green, V. M.; O'Hare, D. *Chemistry of Materials* **1999**, *11*, 216-217.

(115) Enyashin, A. N.; Makurin, Y. N.; Ivanovskii, A. L. *Chemical Physics Letters* **2004**, *387*, 85-90.

(116) Yamanaka, S.; Ohashi, M.; Sumihara, M.; Hattori, M. *Chemistry Letters* **1984**, 1403-1406.

(117) Martin, N.; Boutinaud, P.; Malinowski, M.; Mahiou, R.; Cousseins, J. C. *J. Alloy. Compd.* **1998**, *275-277*, 304-306.

(118) Burkhalter, R.; Dohnke, I.; Hulliger, J. *Progress in Crystal Growth and Characterization of Materials* **2001**, *42*, 1-64.

(119) Foord, E. E.; O'Connor, J. T.; Hughes, J. M.; Sutley, S. J.; Falster, A. U.; Soregaroli, A. E.; Lichte, F. E.; Kile, D. E. *American Mineralogist* **1999**, *84*, 769-772.

(120) Ross, K. C.; Mitchell, R. H.; Chakhmouradian, A. R. *Journal of Solid State Chemistry* **2003**, *172*, 95-101.

(121) Jung, W.; Juza, R. *Zeitschrift fuer Anorganische und Allgemeine Chemie* **1973**, *399*, 129-147.

(122) Schlichenmaier, R.; Schweda, E.; Straehle, J.; Vogt, T. *Zeitschrift fuer Anorganische und Allgemeine Chemie* **1993**, *619*, 367-373.

(123) Schmid, S.; Withers, R. L. *Journal of Solid State Chemistry* **1994**, *109*, 391-400.

(124) Whithers, R. L.; Schmid, S.; Thompson, J. G. *Acta Crystallographica, Section B: Structural Science* **1993**, *B49*, 941-951.

(125) Stoltz, C.; Ramesha, K.; Sirchio, S. A.; Goenen, Z. S.; Eichhorn, B. W.; Salamanca-Riba, L.; Gopalakrishnan, J. *Journal of the American Chemical Society* **2003**, *125*, 4285-4292.

(126) Larson, A. C. a. V. D., R.B.: Los Alamos National Laboratory Report LAUR 86-748, 2000.

(127) Toby, B. H. *Journal of Applied Crystallography* **2001**, *34*, 210-213.

(128) Tikhonravov, A. V.; Trubetskov, M. K.; Amotchkina, T. V.; Tikhonravov, A. A.; Ristau, D.; Gunster, S. *Proceedings of SPIE-The International Society for Optical Engineering* **2003**, *5188*, 331-342.

(129) Kashin, G. N.; Makhnjuk, V. I.; Rumjantseva, S. M.; Shchekochihin, J. M. *Applied Surface Science* **1993**, *70-71*, 85-88.

(130) Brese, N. E.; O'Keeffe, M. *Acta Crystallographica, Section B: Structural Science* **1991**, *B47*, 192-197.

(131) O'Keefe, M.; Brese, N. E. *Journal of the American Chemical Society* **1991**, *113*, 3226-3229.

(132) Gektin, A. V.; Smushkova, V. I.; Shiran, N. V. *Optika i Spektroskopiya* **1987**, *63*, 314-317.

(133) Cook, J. S.; Dryden, J. S. *Journal of Physics C: Solid State Physics* **1981**, *14*, 1133-1136.

(134) Mandal, T. K.; Gopalakrishnan, J. *Journal of Materials Chemistry* **2004**, *14*, 1273-1280.

(135) Sivakumar, T.; Lofland, S. E.; Ramanujachary, K. V.; Ramesha, K.; Subbanna, G. N.; Gopalakrishnan, J. *Journal of Solid State Chemistry* **2004**, *177*, 2635-2638.

(136) Sivakumar, T.; Ramesha, K.; Lofland, S. E.; Ramanujachary, K. V.; Subbanna, G. N.; Gopalakrishnan, J. *Inorganic Chemistry* **2004**, *43*, 1857-1864.

(137) Roberson, L. B.; Poggi, M. A.; Kowalik, J.; Smestad, G. P.; Bottomley, L. A.; Tolbert, L. M. *Coordination Chemistry Reviews* **2004**, *248*, 1491-1499.

(138) Reisfeld, R.; Weiss, A.; Saraidarov, T.; Yariv, E.; Ishchenko, A. A. *Polymers for Advanced Technologies* **2004**, *15*, 291-301.

(139) Costela, A.; Garcia-Moreno, I.; Gomez, C.; Garcia, O.; Garrido, L.; Sastre, R. *Chemical Physics Letters* **2004**, *387*, 496-501.

(140) Gomez-Romero, P.; Chojak, M.; Cuentas-Gallegos, K.; Asensio, J. A.; Kulesza, P. J.; Casan-Pastor, N.; Lira-Cantu, M. *Electrochemistry Communications* **2003**, *5*, 149-153.

(141) Sanchez, C.; Lebeau, B.; Chaput, F.; Boilot, J.-P. *Advanced Materials (Weinheim, Germany)* **2003**, *15*, 1969-1994.

(142) Kang, Z.; Wang, E.; Wang, Y.; You, W.; Hu, C.; Huang, B.; Wu, Y.; Li, X.; Jiao, M. *Dongbei Shida Xuebao, Ziran Kexueban* **2001**, *33*, 60-63.

(143) Schaak, R. E.; Mallouk, T. E. *Abstracts of Papers, 220th ACS National Meeting, Washington, DC, United States, August 20-24, 2000* **2000**, INOR-533.

(144) Schaak, R. E.; Mallouk, T. E. *Chemical Communications (Cambridge, United Kingdom)* **2002**, 706-707.

(145) Saupe, G. B.; Waraksa, C. C.; Kim, H.-N.; Han, Y. J.; Kaschak, D. M.; Skinner, D. M.; Mallouk, T. E. *Chemistry of Materials* **2000**, *12*, 1556-1562.

(146) Woodward, P. M.; Vogt, T. *Journal of Solid State Chemistry* **1998**, *138*, 207-219.

(147) Vivani, R.; Masci, S.; Alberti, G. *Inorganic Chemistry* **2004**, *43*, 368-374.

(148) Stoltz, C. A.; Eichhorn, B. W. *Abstracts of Papers, 227th ACS National Meeting, Anaheim, CA, United States, March 28-April 1, 2004* **2004**, INOR-836.

(149) Jung, V. W. a. J., R.Z. *Zeitschrift fuer Anorganische und Allgemeine Chemie* **1993**, 367-373.

(150) Huheey, J., Keiter, A. and Keiter, R. *Inorganic Chemistry 4th ed.*; HarperCollins College Publishers: New York, NY, 1993.

(151) Costantino, U.; Vivani, R.; Zima, V.; Benes, L.; Melanova, K. *Langmuir* **2002**, *18*, 1211-1217.

(152) Ohashi, M.; Uyeoka, K.; Yamanaka, S.; Hattori, M. *Chemistry Letters* **1990**, 93-96.

(153) Ohashi, M.; Uyeoka, K.; Yamanaka, S.; Hattori, M. *Bulletin Chemical Society of Japan* **1991**, *64*, 2814-2818.

(154) Cario, L.; Delagrange, S.; Boucher, F.; Faulques, E.; Palvadeau, P. *Chemistry of Materials* **2003**, *15*, 4325-4331.

(155) Clearfield, A.; Costantino, U. *Comprehensive Supramolecular Chemistry* **1996**, *7*, 107-149.

(156) Alberti, G.; Murcia-Mascaros, S.; Vivani, R. *Journal of the American Chemical Society* **1998**, *120*, 9291-9295.

(157) Ahn, K.; Gibson, B. J.; Kremer, R. K.; Mattausch, H.; Stolovits, A.; Simon, A. *Journal Physical Chemistry B* **1999**, *103*, 5446-5453.